Stony Brook University

OFFICIAL COPY

The official electronic file of this thesis or dissertation is maintained by the University Libraries on behalf of The Graduate School at Stony Brook University.

© All Rights Reserved by Author.

Effective Lagrangians for Higgs Physics

A Dissertation Presented

by

Tyler Corbett

to

The Graduate School

in Partial Fulfillment of the Requirements

for the Degree of

Doctor of Philosophy

in

Physics

Stony Brook University

August 2015

Stony Brook University

The Graduate School

Tyler Corbett

We, the dissertation committee for the above candidate for the Doctor of Philosophy degree, hereby recommend acceptance of this dissertation.

Maria Concepcion Gonzalez-Garcia - Advisor
Professor, Department of Physics and Astronomy

George Sterman - Committee Chair
Professor, Department of Physics and Astronomy

Thomas Weinacht
Professor, Department of Physics and Astronomy

Oscar JP Éboli
Professor
Instituto de Fisica Universidade de Sao Paulo

This dissertation is accepted by the Graduate School

Charles Taber
Dean of the Graduate School

Abstract of the Dissertation

Effective Lagrangians for Higgs Physics

by

Tyler Corbett

Doctor of Philosophy

in

Physics

Stony Brook University

2015

The Large Hadron Collider has found an exciting excess at around 125 GeV. This excess appeared early on to behave as the long sought Higgs boson and with the 7 and 8 TeV data sets has been shown to behave very much like the Higgs boson responsible for the mass of the fundamental particles of the Standard Model. As the data continued to converge to the Standard Model predictions it became important to try and classify possible small deviations from the expected behavior. A manner of doing so, consistent with the symmetries of the Standard Model, is the use of effective field theories. Effective field theories are able to constrain the presence of new physics without directly probing the new physics energy scale. They are valid both for scenarios with new fundamental physics such as supersymmetry or new gauge sectors, as well as new strongly interacting scenarios where the degrees of freedom may present as pseudo Goldstone bosons of some new global symmetry such as composite Higgs models.

In this dissertation we work in the effective field theory framework and using the available experimental data we place bounds on the coefficients of the relevant effective operators for Higgs physics. We consider two complementary realizations of the effective field theory: the linear realization, appropriate for a fundamental Higgs and new fundamental particles such as those predicted by supersymmetry, and the chiral or nonlinear realization, appropriate for composite Higgs scenarios. Additionally, by considering the effects of the new operators on other sectors, like triple gauge coupling data and electroweak precision data, we are able to further test the framework and devise signatures with potential to discriminate between the realizations. Finally we look at constraints on the operator coefficients from perturbative unitarity considerations, allowing us to then apply the results from our data analysis to predict the lowest energies at which perturbative unitarity may be violated signaling the possibility of new physics at energies consistent with those which will be probed during the impending Run 2 of the Large Hadron Collider.

This thesis is mainly based on the following publications:

1. T. Corbett, O. J. P. Éboli and M. C. Gonzalez-Garcia, Phys. Rev. D **91**, no. 3, 035014 (2015) [arXiv:1411.5026 [hep-ph]].

2. I. Brivio, T. Corbett, O. J. P. Éboli, M. B. Gavela, J. Gonzalez-Fraile, M. C. Gonzalez-Garcia, L. Merlo and S. Rigolin, JHEP **1403**, 024 (2014) [arXiv:1311.1823 [hep-ph]].

3. T. Corbett, O. J. P. Éboli, J. Gonzalez-Fraile and M. C. Gonzalez-Garcia, Phys. Rev. Lett. **111**, 011801 (2013) [arXiv:1304.1151 [hep-ph]].

4. T. Corbett, O. J. P. Éboli, J. Gonzalez-Fraile and M. C. Gonzalez-Garcia, Phys. Rev. D **87**, 015022 (2013) [arXiv:1211.4580 [hep-ph]].

5. T. Corbett, O. J. P. Éboli, J. Gonzalez-Fraile and M. C. Gonzalez-Garcia, Phys. Rev. D **86**, 075013 (2012) [arXiv:1207.1344 [hep-ph]].

Additional work completed in the duration of the author's PhD career:

1. M. Baak, A. Blondel, A. Bodek, R. Caputo, T. Corbett, C. Degrande, O. Eboli and J. Erler *et al.*, arXiv:1310.6708 [hep-ph].

2. T. Corbett, O. J. P. boli, J. Gonzalez-Fraile and M. C. Gonzalez-Garcia, arXiv:1306.0006 [hep-ph].

To my mother and father.

Contents

List of Figures

List of Tables

Acknowledgements

This work would not have been possible without all of the positive influences in my life. I would like to begin by thanking all of my friends and family who have been my support base throughout my studies.

I must also thank all of my mentors in my academic career starting with Roger Loucks who helped me build a solid foundation in physics at the undergraduate level and worked so hard to be the best possible educator he could for myself and all of his students. Additionally, I am indebted to all the other professors who have taught me and taken the time to help me to better understand physics both in and out of the classroom.

I thank Juan Gonzalez–Fraile for helping me work through the first steps of becoming a researcher and each step thereafter, for being a friend and colleague. I would also like to thank all of my collaborators for allowing me the opportunity to work with them. In particular Oscar Éboli with whom I have worked on so many projects in the last three years.

Of course this dissertation would never have occurred without the help of my advisor Concha Gonzalez–Garcia who has helped me to grow from a student to a researcher. Thank you for all of your time and commitment to my research and understanding, for bringing me to to Spain each year to continue our work and grow my network of colleagues and friends in physics, and thank you for so patiently working through every detail of this dissertation to make sure it is in the best possible form.

Finally, I thank my parents who have sacrificed so much to help me get where I am today. They have always set an example through hard work and love, and have given me every opportunity within their power to help me accomplish my goals.

Chapter 1

Introduction

March 2010 marked the beginning of the Large Hadron Collider (LHC) era with the first recorded 7 TeV collisions. After just over two years of taking data, the experiments, ATLAS and CMS, announced an approximately 5σ signal for the observation of a new particle [4, 5]. This particle appears to behave as the long sought Higgs boson. The Higgs boson is the excitation of the Higgs field which, through the Higgs mechanism, allows for the generation of masses for the Standard Model (SM) gauge bosons and fermions [6–11]. These masses are, without some symmetry breaking mechanism, forbidden by the $SU(3)_C \times SU(2)_L \times U(1)_{Y/2}$ SM gauge symmetry. Additionally, the Higgs mechanism allows for the careful cancellation of the center of mass energy ($\sqrt{s}$) divergent amplitudes of longitudinal gauge boson scattering thereby ensuring perturbative unitarity for the SM.

Since the announcement, where the combination of all decay channels was approximately the 5σ required to achieve the status of discovery in particle physics, a vast improvement in the measurements of the properties of the Higgs has occurred. Consistent with the SM, spin and CP measurements favor spin zero and CP even properties for the observed particle [12, 13]. Additionally the decays of the Higgs are consistent with the SM: the Higgs decays to $\gamma\gamma$, ZZ, and WW are now measured above the 5σ threshold individually[1], with their current values at 5.7σ (5.2σ) [3, 14], 4.3σ (6.1σ) [15, 16], and 6.8σ (8.1σ) [17, 18] respectively for the CMS (ATLAS) experiment at the LHC with respect to the null, or no Higgs, hypothesis. Each channel is consistent with the SM

[1] In the highest resolution channels, excepting the CMS $WW \to \ell\nu\ell\nu$.

prediction at around the 1σ level suggesting that the observed resonance is in fact related to electroweak symmetry breaking (EWSB).

In the fermionic channels, where the signal is smaller or diluted by large SM backgrounds, the picture is less clear. However, the $H \to \tau\tau$ decay is observed with an about 3.2σ (4.5σ) [19, 20] excess above the null hypothesis and for $H \to bb$ there is an observed 2.1σ (1.4σ) excess for the CMS (ATLAS) experiment. Again these decay rates are consistent with the SM prediction at the 1σ level indicating the observed resonance may be responsible for fermion mass generation as well.

Many other decay channels remain to be measured with higher precision as well as identifying the significance of the production cross sections. With the impending start of the LHC Run 2 (injection tests are currently underway) these measurements are among the most exciting and anticipated for the coming three year run.

The Higgs mechanism is not the only scenario in which EWSB may be realized. In fact many theorists use the concept of "fine tuning," or the hierarchy problem, to motivate extensions of the SM. The hierarchy problem is based in the aesthetics of the Higgs mechanism, in particular because of large corrections to the Higgs mass from the heavier fields in the theory its mass receives large corrections proportional to the cut–off scale squared of the theory which is frequently taken to the be Planck or grand unified scale. This large mass correction then indicates that the Higgs mass, a parameter of the SM, must be adjusted to an extraordinary number of decimal places. While rooted in aesthetics this principle is a reasonable guide in the absence of new physics (NP) signals before and after the discovery of the Higgs boson. This principle has led to the formulation of a plethora of beyond the Standard Model (BSM) theories such as, for example, supersymmetric (SUSY) models and strongly interacting theories to break the electroweak symmetry and potentially generate composite Higgses. At present no new states associated with these extensions have been found.

In lieu of the direct observation of NP to guide theoretical discourse, it becomes necessary to introduce a system for quantifying divergences from the SM in a systematic manner. In this dissertation we make use of the framework of Effective Field Theories (EFTs), where the behavior of potential NP is

assumed to be realized at some high energy scale which is not directly probed by experiment, and which allow us to quantify these divergences and guide future experimental searches and design.

1.1 The Standard Model and the Higgs Mechanism of Electroweak Symmetry Breaking

Here we briefly review the formulation of the SM, focusing on the Higgs mechanism for spontaneous symmetry breaking. We begin with the gauge group of the SM, $U(1)_{Y/2} \times SU(2)_L \times SU(3)_C$. Here $U(1)_{Y/2} \times SU(2)_L$ is associated with the Weinberg–Salam–Glashow model of the electroweak interactions. It describes the $W^{\pm}$, Z, and photon of the SM. All fermions interact with the $U(1)_{Y/2}$ gauge field, while only left handed fermions interact via the $SU(2)_L$ gauge fields indicated by the subscript L. $SU(3)_C$ is distinguished from the other gauge groups in that only the quarks experience the "color force" indicated by the subscript C.

In order to write all the charges for the fermionic content of the SM we group the left handed fields into lepton and quark doublets:

$$L_L = \begin{pmatrix} \nu_L \\ e_L \end{pmatrix} \qquad \text{and} \qquad Q_L = \begin{pmatrix} u_L \\ d_L \end{pmatrix} \tag{1.1}$$

Where ν_L, e_L, u_L, and d_L are the left handed part of the Dirac spinors corresponding to the neutrino, electron, up–quark, and down–quark. With this in mind we collect the charges for the fermionic field content in Tab. 1.1. We

Field	$U(1)_Y$	$SU(2)_L$	$SU(3)_C$
L_L	-1	2	1
Q_L	1/3	2	3
e_R	-2	1	1
u_R	4/3	1	3
d_R	-2/3	1	3

Table 1.1: Fermion fields of the SM with their charges under the $U(1)_Y$, $SU(2)_L$, and $SU(3)_C$ gauge symmetries of the SM.

note that in Tab. 1.1 there is no mention of a possible ν_R. This is a reflection

that, at the time of the conception of the SM, neutrinos were believed to be massless and only produced in a left handed helicity which would therefore be preserved. Current bounds placing the absolute neutrino mass scale at less than or at the order of 1 eV make this a justified treatment for the purpose of this dissertation.

In the SM there are three generations for each type of fermion mentioned above. These are distinguished only by mass, i.e. they have the same charges under the SM. Therefore we refrain from further discussion of the three generations until our discussion of the Yukawa couplings and mass generation via the Higgs mechanism.

The kinetic and gauge interaction terms of the fermions are given by:

$$\mathcal{L}_{\text{fermion}} = i\bar{e}_R \not{D} e_R + i\bar{L}_L \not{D} L_L + i\bar{u}_R \not{D} u_R + i\bar{d}_R \not{D} d_R + i\bar{Q}_L \not{D} Q_L, \tag{1.2}$$

where $\not{D} = \gamma^\mu D_\mu$, D_μ is the covariant derivative, and γ^μ are the Dirac gamma matrices. The covariant derivative acting on each fermion is given by:

$$\begin{aligned}
D_\mu e_R &= \left(\partial_\mu + i\tfrac{g'}{2} Y_e B_\mu\right) e_R, \\
D_\mu L_L &= \left(\partial_\mu + i\tfrac{g'}{2} Y_L B_\mu + i\tfrac{g}{2} W_\mu\right) L_L, \\
D_\mu u_R &= \left(\partial_\mu + i\tfrac{g'}{2} Y_u B_\mu + i\tfrac{g_s}{2} G_\mu\right) u_R, \\
D_\mu d_R &= \left(\partial_\mu + i\tfrac{g'}{2} Y_d B_\mu + i\tfrac{g_s}{2} G_\mu\right) d_R, \\
D_\mu Q_L &= \left(\partial_\mu + i\tfrac{g'}{2} Y_Q B_\mu + i\tfrac{g}{2} W_\mu + i\tfrac{g_s}{2} G_\mu\right) Q_L.
\end{aligned} \tag{1.3}$$

Here we have written the hypercharges from Tab. 1.1 as Y_f, and have used the abbreviations W_μ and G_μ in the place of $\frac{\tau^a}{2} W^a_\mu$ and $\frac{\lambda^a}{2} G^a_\mu$ where τ_a with $a = 1, 3$ and λ_a with $a = 1, 8$ are the Pauli and Gell–Mann matrices respectively, and an implicit color index is assumed for the quark fields. g, g', and g_s are the gauge couplings of $SU(2)_L$, $U(1)_{Y/2}$, and $SU(3)_C$ respectively.

The pure gauge part of the SM Lagrangian reads:

$$\mathcal{L}_{\text{Gauge}} = -\frac{1}{4} B_{\mu\nu} B^{\mu\nu} - \frac{1}{4} W^i_{\mu\nu} W^{i\mu\nu} - \frac{1}{4} G^c_{\mu\nu} G^{c\mu\nu}, \tag{1.4}$$

with the stress tensors given by

$$\begin{aligned} B_{\mu\nu} &= \partial_\mu B_\nu - \partial_\nu B_\mu \ , \\ W^i_{\mu\nu} &= \partial_\mu W^i_\nu - \partial_\nu W^i_\mu - g\epsilon^{ijk} W^j_\mu W^k_\nu \ , \\ G^a_{\mu\nu} &= \partial_\mu G^a_\nu - \partial_\nu G^a_\mu - g_s f^{abc} G^b_\mu G^c_\nu \ . \end{aligned} \tag{1.5}$$

Here (ϵ^{ijk}) and (f^{abc}) are the structure constants of $SU(2)_L$ and $SU(3)_C$ respectively.

Lagragians Eq. (1.2) and Eq. (1.4) are invariant under local $U(1)_{Y/2} \times SU(2)_L \times SU(3)_C$ which transform the fermion fields, ψ, as

$$\psi \to \exp\left[-i\left(\frac{g'}{2} Y_\psi \theta_Y(x) + g\frac{\tau_a}{2}\theta^a_w(x) + g_s\frac{\lambda_a}{2}\theta^a_s(x)\right)\right]\psi \tag{1.6}$$

provided the gauge fields transform as

$$\begin{aligned} &B_\mu(x) \to B_\mu(x) + \partial_\mu \theta_Y(x) \\ &W^a_\mu(x) \to W^a_\mu(x) + \partial_\mu \theta^a_w(x) + g\epsilon^{abc}\theta^b_w(x) W^c_\mu(x) \\ &G^a_\mu(x) \to G^a_\mu(x) + \partial_\mu \theta^a_s(x) + g_s f^{abc}\theta^b_s(x) G^c_\mu(x) \end{aligned} \tag{1.7}$$

From here we change our basis of gauge bosons by defining the $W^\pm$ in terms of the W^1 and W^2 along with mixing the W^3 and B to form the Z and photon of the SM. In order to do so we use the definitions:

$$\begin{aligned} W^\pm_\mu &= \tfrac{1}{\sqrt{2}}(W^1_\mu \mp i W^2_\mu) \ , \\ Z_\mu &= \tfrac{1}{\sqrt{g^2+g'^2}}(gW^3_\mu - g'B_\mu) \ , \\ A_\mu &= \tfrac{1}{\sqrt{g^2+g'^2}}(g'W^3_\mu + gB_\mu). \end{aligned} \tag{1.8}$$

We now have constructed the electroweak theory as well as the QCD interactions in the quark sector. After the formulation of this model the only missing components were the observed masses for the W and Z gauge bosons and the masses for the fermions forbidden by the gauge symmetry. Clearly a mass term for the gauge bosons, $m_V^2 V_\mu V^\mu$ will not be invariant under the gauge transformation of Eq. (1.7). As for fermions, looking at a potential fermion mass Lagrangian,

$$\mathcal{L}_{\text{Mass}} = -m\bar{f}f = -m\left(\bar{f}_L f_R + \bar{f}_R f_L\right), \tag{1.9}$$

we see that the mass terms mix the left–handed doublet with the singlet right–handed fields. This explicitly violates $SU(2)_L$ gauge symmetry, thus rendering the theory non–renormalizable.

The well–known solution allowing for mass generation for the W and Z gauge bosons, and the fermions is the Higgs mechanism. For that we introduce another field, a complex scalar doublet Φ. This field is charged under both $SU(2)_L$ and $U(1)_{Y/2}$ (with $Y_\Phi = 1$). Therefore the covariant derivative of Φ takes the form:

$$D_\mu \Phi = \left(\partial_\mu + i\frac{g'}{2} Y_\Phi B_\mu + i\frac{g}{2} W_\mu \right) \Phi \tag{1.10}$$

Then we may write a gauge kinetic term for the new scalar doublet with an arbitrary potential, $V(\Phi)$, as,

$$\mathcal{L}_S = (D^\mu \Phi)^\dagger (D_\mu \Phi) - V(\Phi), \tag{1.11}$$

where for the complex scalar doublet we assume a form,

$$\Phi = \begin{pmatrix} \Phi^+ \\ \Phi^0 \end{pmatrix}. \tag{1.12}$$

The most general form of a renormalizable scalar potential compatible with the gauge symmetries is:

$$V(\Phi) = \mu^2 \Phi^\dagger \Phi + \lambda (\Phi^\dagger \Phi)^2. \tag{1.13}$$

For $\mu^2 < 0$ the state with minimum energy is not located at $\Phi = 0$, but at some value satisfying

$$\langle |\Phi^\dagger \Phi| \rangle \equiv \frac{v^2}{2} = \frac{-\mu^2}{2\lambda}, \tag{1.14}$$

where v is called the vacuum expectation value (vev) of Φ. Only the absolute value but not the direction of the mininum in the $SU(2)_L$ space is determined by the minimum condition. By choosing a direction for the ground state Φ_0 we will spontaneously break the global $SU(2)_L$ symmetry of the Lagrangian. We make the choice of direction for the minimum as

$$\Phi_0 = \frac{1}{\sqrt{2}} \begin{pmatrix} 0 \\ v \end{pmatrix}. \tag{1.15}$$

The electromagnetic charge is defined by the operator $Q = (\tau_3 + Y)/2$. Applying this operator to Φ_0 we obtain $Q\Phi_0 = 0$. Therefore, given this choice for the direction of the ground state, the vacuum remains uncharged or equivalently electromagnetism is unbroken by the scalar vev and we have achieved the symmetry breaking pattern

$$SU(2)_L \times U(1)_{Y/2} \to U(1)_{EM}. \tag{1.16}$$

In full generality we can write the complex scalar doublet in terms of the vev and the other components of the doublet as

$$\Phi = \frac{1}{\sqrt{2}} \exp\left[\frac{i\pi(x)\cdot\tau}{v}\right] \begin{pmatrix} 0 \\ v + h(x) \end{pmatrix} \tag{1.17}$$

where h and π^a are four real fields. In the absence of the gauge symmetry π^a would be the goldstone boson fields of the broken global $SU(2)_L$ symmetry. Instead because of gauge invariance, plugging Eq. (1.17) in Eq. (1.11) one finds that all the dependence in the $\pi^a(x)$ fields can be reabsorved in a redefinition of the gauge fields as in Eq. (1.7) with

$$\frac{g}{2}\theta_w^a(x) = \frac{\pi^a(x)}{v}\,. \tag{1.18}$$

In this gauge (referred to as the unitary gauge) the electroweak gauge bosons acquire a longitudinal component proportional to $\pi^a(x)$ and masses from the pure vev part of Eq. (1.11)

$$\mathcal{L}_\Phi = \frac{1}{2}(0, v)\left(\frac{g}{2}W_\mu + \frac{g'}{2}B_\mu\right)^2 \begin{pmatrix} 0 \\ v \end{pmatrix}, \tag{1.19}$$

which read:

$$\begin{aligned} M_W^2 &= \tfrac{g^2 v^2}{4}, \\ M_Z^2 &= \tfrac{(g^2+g'^2)v^2}{4}, \\ M_A &= 0. \end{aligned} \tag{1.20}$$

We note that the photon remains massless as expected from the breaking pattern Eq. (1.16) and required by observation. It is also important to note that the Higgs–vector interactions are completely determined from the h and

hh terms in $\mathcal{L}_S$, which will be a point of interest throughout this dissertation as we will be looking for deviations from this behavior.

Also in this gauge the h-field acquires a mass,

$$M_H^2 = -2\mu^2 = 2\lambda v^2 \tag{1.21}$$

The same mechanism allows the generation of fermion masses. As Φ is charged under $SU(2)_L$ we may use the forms:

$$\bar{f}_L\Phi = (\bar{f}_1, \bar{f}_2)\begin{pmatrix} 0 \\ v+h \end{pmatrix} = \bar{f}_2(v+h), \tag{1.22}$$

and

$$\bar{f}_L\tilde{\Phi} = i\bar{f}_L\tau_2\Phi^* = (\bar{f}_1, \bar{f}_2)\begin{pmatrix} v+h \\ 0 \end{pmatrix} = \bar{f}_1(v+h). \tag{1.23}$$

We first note that these two expressions are singlets of $SU(2)_L$, this allows us to multiply each by the corresponding right handed quarks and leptons to generate masses when we select the part of the expanded complex doublet corresponding to the vev. For example, if in Eq. (1.22) we associate f_L with L_L or Q_L we may generate masses for the charged leptons or down–like quarks along with inducing Higgs–fermion interactions. Similarly associating f_L with Q_L in Eq. (1.23) allows for the generation of masses for the up–like quark along with Higgs–fermion interactions. Altogether we write the Yukawa terms of the SM Lagrangian responsible for fermion masses as:

$$\mathcal{L}_Y = -y^d\bar{Q}_L\Phi d_R - y^e\bar{L}_L\Phi e_L - y^u\bar{Q}_L\tilde{\Phi}u_L + \text{h.c.}\ . \tag{1.24}$$

As in the case of the gauge bosons, $\mathcal{L}_Y$ completely determines the Higgs–fermion couplings, a prediction we will be testing throughout this dissertation. Thus we have shown that with the Higgs mechanism we are able to generate masses for the SM gauge bosons, $W^\pm$ and Z, along with the SM fermions while simultaneously predicting its couplings to these fields. This dissertation, however, will deal with quantifying deviations from these predictions of the SM Higgs mechanism.

We finish this section by rewriting the scalar and Yukawa sectors of the Standard Model Lagrangian in a non–linear representation. In order to do so

we introduce a matrix, $\mathbf{\Sigma}$, for the scalar field

$$\mathbf{\Sigma(x)} = \sigma(x)\,\mathbf{U(x)} \equiv \sigma(x)\exp\left[\frac{i\pi(x)\cdot\tau}{v}\right] . \tag{1.25}$$

where $\sigma(x)$ and $\pi^a(x)$ are four real fields. In terms of $\mathbf{\Sigma}$ we can write $\mathcal{L}_S + \mathcal{L}_Y$ as:

$$\begin{aligned}\mathcal{L}_S + \mathcal{L}_Y &= \frac{1}{4}\mathrm{Tr}\left[(\boldsymbol{D}_\mu\mathbf{\Sigma})(\boldsymbol{D}^\mu\mathbf{\Sigma})^\dagger\right] - \frac{\mu^2}{4}\mathrm{Tr}\left[\mathbf{\Sigma\Sigma}^\dagger\right] - \frac{\lambda}{8}\mathrm{Tr}\left[\mathbf{\Sigma\Sigma}^\dagger\right]^2 \\ &\quad -\frac{1}{\sqrt{2}}\left(\bar{Q}_L\mathbf{\Sigma}\boldsymbol{y}_Q Q_R + \mathrm{h.c.}\right) - \frac{1}{\sqrt{2}}\left(\bar{L}_L\mathbf{\Sigma}\boldsymbol{y}_L L_R + \mathrm{h.c.}\right) ,\end{aligned} \tag{1.26}$$

where the covariant derivative of $\mathbf{\Sigma}$ takes the form:

$$\boldsymbol{D}_\mu\mathbf{\Sigma}(x) \equiv \partial_\mu\mathbf{\Sigma}(x) + \frac{i}{2}gW^a_\mu(x)\tau_a\mathbf{\Sigma}(x) - \frac{ig'}{2}B_\mu(x)\mathbf{\Sigma}(x)\tau_3 , \tag{1.27}$$

and we have used a compact notation for the right–handed fields by using doublets Q_R and L_R thus placing $\boldsymbol{y}_Q$ and $\boldsymbol{y}_L$ in two 6×6 block-diagonal matrices containing the usual Yukawa couplings, $\boldsymbol{y}_Q \equiv \mathrm{diag}(y^u, y^d)$ and $\boldsymbol{y}_L \equiv \mathrm{diag}(0, y^e)$. Notice that in defining the L_R doublet we have introduced a spurious right-handed neutrino field which, however, does not appear in the Lagrangian in the unitary gauge.

Written in the form in Eq. (1.26) and in the limit of $g' = 0$ it is explicit that $\mathcal{L}_S$ is invariant under chiral $SU(2)_L \times SU(2)_R$ transformations,

$$F_L \to L\,F_L, \qquad F_R \to R\,F_R, \qquad \text{and} \qquad \mathbf{\Sigma} \to L\,\mathbf{\Sigma}\,R^\dagger, \tag{1.28}$$

where $F_{L,R} = L_{L,R}, Q_{L,R}$. In Eq. (1.28) L and R are $SU(2)_{L,R}$ global transformations respectively. This symmetry is explictly broken by g' and the Yukawa matrices which are not proportional to the identity.

After spontaneous symmetry breaking $\sigma(x) = v + h(x)$ and

$$\begin{aligned}\mathcal{L}_S + \mathcal{L}_Y &= \frac{1}{2}\left[(\partial_\mu h)(\partial^\mu h) + 2\mu^2 h^2\right] - \lambda v h^3 - \frac{\lambda}{4}h^4 \\ &\quad +\frac{(v+h)^2}{4}\mathrm{Tr}\left[(\boldsymbol{D}_\mu\boldsymbol{U})(\boldsymbol{D}^\mu\boldsymbol{U})^\dagger\right] \\ &\quad -\frac{v+h}{\sqrt{2}}\left[\left(\bar{Q}_L\boldsymbol{U}\boldsymbol{y}_Q Q_R + \mathrm{h.c.}\right) + \left(\bar{L}_L\boldsymbol{U}\boldsymbol{y}_L L_R + \mathrm{h.c.}\right)\right] .\end{aligned} \tag{1.29}$$

with $\boldsymbol{D}_\mu \boldsymbol{U}$ given by Eq. (1.27) with the exchange of $\boldsymbol{\Sigma}$ to $\boldsymbol{U}$.

The $\boldsymbol{U}$ matrix contains the would–be Goldstone boson fields $\pi^a(x)$. In the unitary gauge $\boldsymbol{U} = I$, and $\pi^a(x)$ become the longitudinal components of the massive weak gauge bosons. In this gauge the $W^a_\mu W^{\mu a}$ part of the second line in Eq. (1.29) gives precisely the mass terms for the gauge bosons in Eq. (1.20).

After spontaneous symmetry breaking (still in the limit of vanishing g' and Yukawa couplings) the global chiral symmetry $SU(2)_L \times SU(2)_R$ of the Lagrangian is broken to $SU(2)_V$. It is this remaining symmetry, referred to as custodial symmetry, that it is responsible for the electroweak parameter T which we will introduced in Sec. 2.3 to be equal to one at tree–level.

1.2 Effective Field Theories

Effective Lagrangians are a useful method to represent in a simple way the dynamical content of a theory in the low energy limit where the effects of high energy dynamics can be systematically incorporated into a few constants. The basic approach is to write out the most general set of Lagrangians consistent with the symmetries of the theory. The important key ingredient is to identify which are the relevant symmetries as they clearly depend on the assumptions about the high-energy dynamics.

Effective field theories have been applied in areas throughout the SM the most famous of which being the examples of the Fermi theory of weak interactions and of chiral perturbation theory of strong interactions. Both of these theories are formed by considering new effective operators respecting the symmetries of the underlying dynamics and identifying their corresponding operator coefficients, commonly referred to as low energy constants, through experimental analyses. Eventually the Fermi theory of weak interactions transformed into the electroweak part of the SM describing the low energy effects of the exchange of the massive gauge bosons, the Ws and Zs. Chiral perturbation theory is considered to be the low energy description of quantum chromodynamics, the renormalizable theory of the quarks and gluons. Still these effective theories resulted in predictive power when no complete underlying dynamics had yet been formulated or when, even if formulated, cannot be treated perturbatively.

1.2.1 Integrating Out Heavy Fields

When one is addressing the physics at some energy scale, one must explicitly take into account all particles which can be produced at that energy. The question is what is the effect of those states which are too heavy to be produced at that energy.

To answer this question, we begin by postulating a theory containing light degrees of freedom, ℓ_i, as well as a heavy degree of freedom which we will denote by S. We may then write the general Lagrangian for such a theory as,

$$\mathcal{L} = \mathcal{L}_\ell + \mathcal{L}_S + \mathcal{L}_{\ell S}, \tag{1.30}$$

where $\mathcal{L}_\ell$ contains the kinetic and interaction terms which only depend on the light degrees of freedom. $\mathcal{L}_S$ contains the kinetic terms for the heavy field, S, and $\mathcal{L}_{\ell S}$ contains all terms in the Lagrangian containing both the light degrees of freedom and the heavy S.

For simplicity we choose the heavy degree of freedom to be connected to the light degrees of freedom only via a term linear in S. We also choose S to have no self–interactions. Therefore we may write the parts of the Lagrangian containing S as:

$$\mathcal{L}(S, J) = \mathcal{L}_S + \mathcal{L}_{\ell S} = \frac{1}{2}\left[(\partial^\mu S)(\partial_\mu S) - M_S^2 S^2\right] + JS. \tag{1.31}$$

Here we have chosen J to represent some combination of the light fields, ℓ_i. We may now write the effective action $Z_{\text{eff}}[\ell_i]$ where we have integrated out the heavy degrees of freedom as:

$$\exp(iZ_{\text{eff}}[\ell_i]) \equiv \frac{\int [dS] \exp\left[i \int d^4x \mathcal{L}(S(x), \ell_i(x))\right]}{\int [dS] \exp\left[i \int d^4x \mathcal{L}(S(x), 0)\right]}. \tag{1.32}$$

In order to calculate this integral we will complete the square, allowing us to cancel the S dependent integrals, leaving only light degrees of freedom in our effective action. In order to do so we first define some shorthand notations,

$$\begin{aligned} \mathcal{D}_x &= \Box_x + M_S^2, \\ \mathcal{D}_x^{-1} J &= -\int d^4y \, \triangle_F (x-y) J(y), \\ \mathcal{D}_x \, \triangle_F (x-y) &= -\delta^4(x-y), \end{aligned} \tag{1.33}$$

where $\triangle_F$ is the propagator. From here we use integration by parts to rewrite the action as

$$\int d^4x \mathcal{L}(S,J) = \int d^4x \left[-\frac{1}{2} S\mathcal{D}S + JS \right]. \tag{1.34}$$

Pulling out the factor of $1/2$ and adding $0 = J\mathcal{D}^{-1}J - J\mathcal{D}^{-1}J$ we obtain:

$$\begin{aligned} \int d^4x \mathcal{L}(S,J) &= -\int d^4x \tfrac{1}{2} \left[S\mathcal{D}S - SJ - SJ + J\mathcal{D}^{-1}J - J\mathcal{D}^{-1}J \right] \\ &= -\int d^4x \tfrac{1}{2} \left[S\mathcal{D}S - S\mathcal{D}\mathcal{D}^{-1}J - \mathcal{D}^{-1}J\mathcal{D}S \right. \\ &\qquad \left. + \mathcal{D}^{-1}J\mathcal{D}\mathcal{D}^{-1}J - J\mathcal{D}^{-1}J \right] \\ &= -\int d^4x \tfrac{1}{2} \left[(S - \mathcal{D}^{-1}J)\mathcal{D}(S - \mathcal{D}^{-1}J) - J\mathcal{D}^{-1}J \right] \\ &= -\int d^4x \tfrac{1}{2} \left[S'\mathcal{D}S' - J\mathcal{D}^{-1}J \right], \end{aligned} \tag{1.35}$$

where in the second line we have integrated by parts resulting in the relation,

$$\int d^4x (JS) = \int d^4x \left[(\mathcal{D}\mathcal{D}^{-1}J)S \right] = \int d^4x (\mathcal{D}S)(\mathcal{D}^{-1}J), \tag{1.36}$$

in the subsequent line we simply collected like terms, and in the final line we have made the field redefinition $S' = S - \mathcal{D}^{-1}J$.

From here we may now rewrite the effective action as,

$$\exp\left(iZ_{\text{eff}}[\ell_i]\right) = \frac{\int [dS'] \exp\left[-\frac{i}{2} \int d^4x \left(S'\mathcal{D}S' - J\mathcal{D}^{-1}J \right) \right]}{\int [dS] \exp\left[-\frac{i}{2} \int d^4x \left(S\mathcal{D}S \right) \right]}. \tag{1.37}$$

As we are integrating over all values of the field at each point of spacetime we may take $[dS] = [dS']$ and cancel the S dependent parts, leaving us with:

$$\exp\left(iZ_{\text{eff}}[\ell_i]\right) = \exp\left[\frac{i}{2} \int d^4x J\mathcal{D}^{-1}J \right]. \tag{1.38}$$

Or equivalently,

$$Z_{\text{eff}}[J] = -\frac{1}{2} \int d^4x d^4y J(x) \triangle_F (x-y) J(y), \tag{1.39}$$

where we have written out the form of $\mathcal{D}^{-1}J$ from Eq. (1.33). Therefore we have integrated out the S dependence for the low energy theory. Noting J is peaked at small distances we may expand J as,

$$J(y) = J(x) + (y-x)^\mu [\partial_\mu J(y)]_{y=x} + \cdots \ , \tag{1.40}$$

allowing us to then write the integral over x as:

$$Z_{\text{eff}}[J] = -\frac{1}{2}\int d^4x d^4y J(x) \triangle_F (x-y) J(x) + \cdots = \int d^4x \frac{1}{2M_S^2} J(x)J(x) + \cdots \,. \tag{1.41}$$

Therefore we have successfully integrated out the heavy field dependence and see that the remaining effects from the full theory appear in inverse powers of the heavy mass and any couplings appearing in J, the combination of light fields, dictating the interaction of the light degrees of freedom with S. The resulting effective low energy theory then presents itself as that of $\mathcal{L}_\ell$ plus a series of higher dimension operators formed with the light degrees of freedom, suppressed by powers of the new physics scale (i.e. the heavy mass), and respecting the symmetries of the theory. When $\mathcal{L}_\ell$ is gauge invariant this construction is an example of a decoupling theory, as in the absence of S the theory described by $\mathcal{L}_\ell$ is renormalizable.

An archetype of an EFT of the type described here is the Fermi model of beta decay where the heavy degree of freedom has been identified with the fundamental particle now known as the W boson. In the SM beta decay describes the process $n \to pe^-\bar{\nu}_e$ (or leptonic β decays like $\mu^- \to e^-\nu_\mu\bar{\nu}_e$) via an intermediate fundamental W–boson. For example from Eq. (1.41) we see that given the following interactions from electroweak theory,

$$\begin{aligned} \mathcal{L}_{W\mu\nu_\mu} &= \tfrac{g}{\sqrt{2}}\bar{\nu}_\mu\gamma^\alpha\tfrac{1}{2}(1-\gamma_5)\mu W^-_\alpha, \\ \mathcal{L}_{We\nu} &= \tfrac{g}{\sqrt{2}}\bar{e}\gamma^\alpha\tfrac{1}{2}(1-\gamma_5)\nu_e W^+_\alpha, \end{aligned} \tag{1.42}$$

the resulting Fermi four fermion interaction, after integrating out the W field, is given by:

$$\begin{aligned} \mathcal{L}_{\text{eff}} &= \tfrac{g^2}{8m_W^2}\left[\bar{\nu}_\mu\gamma^\mu(1-\gamma_5)\mu\right]\left[\bar{e}\gamma_\mu(1-\gamma_5)\nu_e\right] \\ &= \tfrac{G_F}{\sqrt{2}}\left[\bar{\nu}_\mu\gamma^\mu(1-\gamma_5)\mu\right]\left[\bar{e}\gamma_\mu(1-\gamma_5)\nu_e\right], \end{aligned} \tag{1.43}$$

with $G_F \equiv \sqrt{2}g^2/8m_W^2$.

This is the form of the four-fermion interaction describing muon decay. We note that the operator coefficient G_F, known as the Fermi constant, has mass dimension $1/M^2$, consistent with our previous discussion. Eq. (1.43) is referred to as a dimension–six operator as the mass dimension of the field

content of the operator adds to six. Measurements using muon decay indicate $G_F \sim 1.17 \cdot 10^{-5}$ GeV^{-2}. Using the relation between G_F and g yields a W mass of $m_W \sim 80$ GeV consistent with direct measurements of the W mass.

In Chapter 2 we will discuss the implications of this type of EFT expansion for characterizing deviations from the SM prediction for Higgs physics.

1.2.2 Electroweak Chiral Lagrangian

Alternatively we may consider NP theories for which the new dynamics cannot be treated perturbatively. In this case, as we do for strong interactions in the SM, we may still attempt to build an effective Lagrangian for the light degrees of freedom using as guidance the assumed global symmetries of the theory.

For example, let us take the SM Lagrangian written in the chiral form of Eq. (1.29) but without the light scalar h degree of freedom (either because it is heavy or just nonexistent). In this case the lagrangian for the pure would–be Goldstone bosons reads

$$\frac{v^2}{4}\mathrm{Tr}\left[(\boldsymbol{D}_\mu \boldsymbol{U})(\boldsymbol{D}^\mu \boldsymbol{U})^\dagger\right] \tag{1.44}$$

which is invariant under the chiral symmetry $SU(2)_L \times SU(2)_R$ in the limit of vanishing g'. One may think of this as the lowest order term of an infinite series of operators constructed from $\boldsymbol{U}$ and $\boldsymbol{D}_\mu \boldsymbol{U}$ and respecting the same global symmetry. As $\boldsymbol{U}$ is dimensionless, any higher dimensional operator will arise with higher numbers of derivatives, the lowest order shown above being quadratic and the next order being quartic. In this case the general chiral Lagrangian can be organized by the dimensionality of the operators in number of derivatives. At low energy, the higher the number of derivatives in the operator the more suppressed its effect, and therefore the derivative expansion becomes consistent.

In Ref. [21] and [22] the full list of operators which can be built in this approach up to four derivatives including also the electroweak gauge field strengths was systematically constructed. These works were motivated by the possibility of the Higgs being very heavy, in some cases as a consequence of its possible composite nature and therefore it was integrated out from the low energy Lagrangian.

In recent years renewed interest has grown in the construction of composite models for the EWSB sector, but containing a light Higgs–like particle. In these constructions the Higgs appears light as it is a pseudo–Goldstone boson of a global symmetry of the new strongly interacting dynamics. Therefore, contrary to the above discussion, the Higgs is present in the low energy EFT, but the assumption of strongly interacting new physics still implies that we build the EFT as a derivative expansion. Concrete examples of these types of theories are Composite Higgs Models (CHMs) [23–32], for different strong groups and symmetry breaking patterns, generically "little Higgs" models [33] (see [34] for a review), and some higher dimensional scenarios can also be considered in the category of constructions in which the Higgs is a Goldstone boson.

In Chapter 3 we will present the basis of operators appropriate for such a light composite Higgs originally derived in Ref. [35] and we will look at its implications for Higgs physics.

1.3 Outline

In this dissertation we make use of the framework of EFTs for EWSB for which NP related to the EWSB sector is assumed to be accessible at some high energy scale which is not directly probed by experiment. EFTs will allow us to characterize in a systematic way any divergences from the SM predictions. The presentation is divided into five chapters in addition to this introduction. Following the approach outlined in Sec. 1.2.1 in Chapter 2 we develop the linear EFT appropriate for the physics of an elementary Higgs doublet. In Chapter 3 we discuss the possibility of the Higgs as a pseudo–Goldstone boson of some new strongly interacting sector and introduce an appropriate chiral EFT for such a scenario following the approached outlined in Sec. 1.2.2. We also discuss possible signals which can discriminate between both expansions.

Subsequently in Chapter 4 we develop an analysis framework for constraining these two EFTs' operator expansions from the recent LHC collider Higgs data, the Tevatron collider Higgs data, and the triple gauge boson scattering data from the LEP experiment. Chapter 5 proceeds to apply this framework to both the linear and chiral expansions. We also discuss the possibility of

using the correlations between the Higgs and triple gauge couplings (TGCs) in the linear realization to constrain the TGCs from the Higgs data. Finally we quantify possible discriminators between the two expansions.

In Chapter 6 we study unitarity in the gauge boson scattering sector and consider the implications the effective operators of the linear expansion have on perturbative unitarity. In doing so we are able to constrain the coefficients of the operators as a function of the scattering energy. Then by using the experimental constraints obtained in Chapter 5 we place lower bounds on the scale at which perturbative unitarity may be violated signaling the expectation of NP or the breakdown of the perturbative approach.

The dissertation is complemented by two appendices. In the first, Appendix A, we expand the operators of the linear expansion, completing the discussion begun in Chapter 2. The latter, Appendix B, includes projections for the 14 TeV LHC analysis regarding the linear expansion and the related TGV projections. Chapter 7 contains the conclusions of this dissertation.

Chapter 2

Effective Lagrangian with an Elementary Higgs: The Linear Realization

We begin by extending the SM by the use of an EFT construction with the assumption of the SM electroweak symmetry being linearly realized. As described in the previous chapter EFTs have been identified as useful perturbative tools for quantifying divergences from the behavior predicted by low energy models. In order to form an EFT one assumes new physics (NP) occurring at some new energy scale, $\Lambda_{\rm NP}$, and a linear EFT quantifies the divergences from the low energy theory in a series expansion in $1/\Lambda_{\rm NP}$ as briefly sketched in Sec. 1.2.1. For a sufficiently high NP scale relative to the energy scale being probed this implies a well defined perturbative expansion. The Lagrangian is then identified as the low energy theory with the addition of new operators satisfying the symmetries of the underlying ultraviolet (UV) model of the NP. For sufficiently low momenta relative to $\Lambda_{\rm NP}$ the series can be truncated at some order determined by the level of accuracy one desires in calculations.

For our purposes an EFT with a linear realization of the electroweak symmetry describes a NP theory where the Higgs boson is still treated as a fundamental field transforming as a doublet under the electroweak gauge symmetry. Additionally we make the assumption that it is a pure CP even scalar. We begin by describing the Lagrangian appropriate for such a fundamental Higgs

in Sec. 2.1 and we derive the relevant triple vertices generated after accounting for finite renormalization effects (Sec. 2.2). We discuss the contributions of these operators to the electroweak precision parameters in Sec. 2.3. Subsequently in Sec. 2.4 we reduce the basis to that which is relevant for the Higgs analysis performed in Chapter 5 by use of the equations of motion (EOM) and the consideration of precision data.

2.1 The Effective Lagrangian

In this chapter we employ the operator basis introduced by Hagiwara, Ishihara, Szalapski, and Zeppenfeld (HISZ) [36, 37] to parameterize deviations from the SM. This basis contains 59 independent dimension–six (i.e. suppressed by $1/\Lambda_{\rm NP}^2$) operators up to flavor, Hermition conjugation, and assuming baryon and lepton numbers are not violated by the NP [38, 39]. Note that we begin at dimension–six as the only dimension–five operator formed of the SM field content is a Majorana mass term which explicitly violates Lepton number, in contradiction with our assumption that Lepton number is not violated. We also assume that dimension–eight operators' effects are negligible at the current level of precision available. Thus we start by adding the dimension–six operators to the low energy, here the SM, Lagrangian:

$$\mathcal{L}_{\rm eff} = \mathcal{L}_{\rm SM} + \sum_n \frac{f_n}{\Lambda^2}\mathcal{O}_n. \tag{2.1}$$

Where the $\mathcal{O}_n$ represent the HISZ operator basis composed of the SM field content, i.e. gauge bosons, Higgs doublets, and fermionic fields, and (covariant–) derivatives of these fields. In addition to the assumptions mentioned above we will also impose on the HISZ basis that the operators be C– and P–even. This leaves us with ten gauge–Higgs operators (nine electroweak and one gluon–H), with an additional eleven operators when including fermions (up to flavor considerations), that are relevant to Higgs processes. Additionally as we will see there is one extra pure gauge operator relevant to gauge boson scattering in the discussion of unitarity in Chapter 6. Thus the relevant operators involving

bosonic fields include:

$$\begin{aligned}
\mathcal{O}_B &= (D_\mu\Phi)^\dagger \hat{B}^{\mu\nu}(D_\nu\Phi) & \mathcal{O}_{\Phi,1} &= (D_\mu\Phi)^\dagger\Phi\Phi^\dagger(D^\mu\Phi)\\
\mathcal{O}_W &= (D_\mu\Phi)^\dagger \hat{W}^{\mu\nu}(D_\nu\Phi) & \mathcal{O}_{\Phi,2} &= \tfrac{1}{2}\partial_\mu(\Phi^\dagger\Phi)\partial^\mu(\Phi^\dagger\Phi)\\
\mathcal{O}_{BB} &= \Phi^\dagger \hat{B}_{\mu\nu}\hat{B}^{\mu\nu}\Phi & \mathcal{O}_{\Phi,3} &= \tfrac{1}{3}(\Phi^\dagger\Phi)^3\\
\mathcal{O}_{WW} &= \Phi^\dagger \hat{W}_{\mu\nu}\hat{W}^{\mu\nu}\Phi & \mathcal{O}_{\Phi,4} &= (D_\mu\Phi)^\dagger(D^\mu\Phi)(\Phi^\dagger\Phi)\\
\mathcal{O}_{BW} &= \Phi^\dagger \hat{B}_{\mu\nu}\hat{W}^{\mu\nu}\Phi\\
\mathcal{O}_{GG} &= \Phi^\dagger\Phi G^a_{\mu\nu}G^{a\mu\nu} & \mathcal{O}_{WWW} &= \mathrm{Tr}[\hat{W}_\mu{}^\nu\hat{W}_\nu{}^\rho\hat{W}_\rho{}^\mu]
\end{aligned} \tag{2.2}$$

Where the Higgs doublet is denoted by Φ. The covariant derivative is given by $D_\mu\Phi = (\partial_\mu + i\frac{1}{2}g'B_\mu + ig\frac{\tau_a}{2}W^a_\mu)\Phi$. The hatted field strength tensors are $\hat{B}_{\mu\nu} = i\frac{g'}{2}B_{\mu\nu}$ and $\hat{W}_{\mu\nu} = i\frac{g}{2}\tau_a W^a_{\mu\nu}$, while the fields strengths are given by:

$$\begin{aligned}
B_{\mu\nu} &= \partial_\mu B_\nu - \partial_\nu B_\mu\ ,\\
W^a_{\mu\nu} &= \partial_\mu W^a_\nu - \partial_\nu W^a_\mu - g\epsilon^{abc}W^b_\mu W^c_\nu\ ,\\
G^a_{\mu\nu} &= \partial_\mu G^a_\nu - \partial_\nu G^a_\mu - g_s f^{abc}G^b_\mu G^c_\nu\ .
\end{aligned} \tag{2.3}$$

The couplings, g, g', and g_s denote the $SU(2)_L$, $U(1)_Y$, and $SU(3)_C$ gauge couplings, and τ_a are the Pauli matrices.

The SM EW gauge fields are given by:

$$\begin{aligned}
W^\pm_\mu &= \tfrac{1}{\sqrt{2}}(W^1_\mu \mp iW^2_\mu)\ ,\\
Z^{\mathrm{SM}}_\mu &= \tfrac{1}{\sqrt{g^2+g'^2}}(gW^3_\mu - g'B_\mu)\ ,\\
A^{\mathrm{SM}}_\mu &= \tfrac{1}{\sqrt{g^2+g'^2}}(g'W^3_\mu + gB_\mu).
\end{aligned} \tag{2.4}$$

There is an additional operator not considered in our work as it may be removed via the EOM, but it is relevant to the discussions in Chapter 3 where it will be used to help identify the relation between chiral operators and those of the linear expansion. Details relating to this operator and a similar operator in the chiral expansion are discussed in [40]. It has the form:

$$\mathcal{O}_{\Box\Phi} = (D_\mu D^\mu\Phi)^\dagger(D_\nu D^\nu\Phi). \tag{2.5}$$

For completeness we also list an additional set of four operators made up of only EW and strong gauge fields. They do not contribute to the Higgs interactions nor to triple electroweak gauge boson vertices and therefore do

not generate effects in the observables discussed in this dissertation:

$$\begin{aligned}
&\mathcal{O}_{GGG} = i f_{abc} G_{\mu}^{a\,\nu} G_{\nu}^{b\,\rho} G_{\rho}^{c\,\mu}\,, \\
&\mathcal{O}_{DW} = \left(D^{\mu}\,\hat{W}_{\mu\nu}\right)^{i} \left(D_{\rho}\hat{W}^{\rho\nu}\right)^{i}, \quad \mathcal{O}_{DB} = \left(\partial^{\mu}\hat{B}_{\mu\nu}\right)\left(\partial_{\rho}\hat{B}^{\rho\nu}\right)\,, \\
&\mathcal{O}_{DG} = \left(D^{\mu}\,G_{\mu\nu}\right)^{a}\left(D_{\rho}G^{\rho\nu}\right)^{a}\,,
\end{aligned} \tag{2.6}$$

where $\left(D^{\mu}\,W_{\mu\nu}\right)^{i} = \partial^{\mu}W^{i}_{\mu\nu} - g\epsilon^{ijk}W^{\mu j}W^{k}_{\mu\nu}$ and where, in $\mathcal{O}_{DG}$, D^{μ} denotes the covariant derivative acting on a field transforming in the adjoint of $SU(3)_C$, $\left(D^{\mu}\,G_{\mu\nu}\right)^{a} = \partial^{\mu}G^{a}_{\mu\nu} - g_s f^{abc}G^{\mu b}G^{c}_{\mu\nu}$. It is worth noting this set is not minimal as the operators $\mathcal{O}_{DW}$, $\mathcal{O}_{DB}$ and $\mathcal{O}_{DG}$ are usually traded using the EOM for $\mathcal{O}_{WWW}$ and $\mathcal{O}_{GGG}$ and fermionic operators.

Next we also list the dimension–six operators which couple fermions to the Higgs boson [39]:

$$\begin{aligned}
&\mathcal{O}_{e\Phi,ij} = (\Phi^{\dagger}\Phi)(\bar{L}_{Li}\Phi e_{R_j}), \quad \mathcal{O}^{(1)}_{\Phi L,ij} = \Phi^{\dagger}(i\overleftrightarrow{D}_{\mu}\Phi)(\bar{L}_{Li}\gamma^{\mu}L_{Lj}), \\
&\mathcal{O}_{u\Phi,ij} = (\Phi^{\dagger}\Phi)(\bar{Q}_{Li}\tilde{\Phi}u_{R_j}), \quad \mathcal{O}^{(1)}_{\Phi Q,ij} = \Phi^{\dagger}(i\overleftrightarrow{D}_{\mu}\Phi)(\bar{Q}_{Li}\gamma^{\mu}Q_{Lj}), \\
&\mathcal{O}_{d\Phi,ij} = (\Phi^{\dagger}\Phi)(\bar{Q}_{Li}\Phi d_{Rj}), \quad \mathcal{O}^{(1)}_{\Phi e,ij} = \Phi^{\dagger}(i\overleftrightarrow{D}_{\mu}\Phi)(\bar{e}_{R_i}\gamma^{\mu}e_{R_j}), \\
&\qquad\qquad\qquad\quad \mathcal{O}^{(1)}_{\Phi u,ij} = \Phi^{\dagger}(i\overleftrightarrow{D}_{\mu}\Phi)(\bar{u}_{R_i}\gamma^{\mu}u_{R_j}), \\
&\qquad\qquad\qquad\quad \mathcal{O}^{(1)}_{\Phi d,ij} = \Phi^{\dagger}(i\overleftrightarrow{D}_{\mu}\Phi)(\bar{d}_{R_i}\gamma^{\mu}d_{R_j}), \\
&\qquad\qquad\qquad\quad \mathcal{O}^{(1)}_{\Phi ud,ij} = \tilde{\Phi}^{\dagger}(i\overleftrightarrow{D}_{\mu}\Phi)(\bar{u}_{R_i}\gamma^{\mu}d_{R_j}), \\
&\qquad\qquad\qquad\quad \mathcal{O}^{(3)}_{\Phi L,ij} = \Phi^{\dagger}(i\overleftrightarrow{D}^{a}_{\mu}\Phi)(\bar{L}_{Li}\gamma^{\mu}\tau_a L_{Lj}), \\
&\qquad\qquad\qquad\quad \mathcal{O}^{(3)}_{\Phi Q,ij} = \Phi^{\dagger}(i\overleftrightarrow{D}^{a}_{\mu}\Phi)(\bar{Q}_{Li}\gamma^{\mu}\tau_a Q_{Lj}),
\end{aligned} \tag{2.7}$$

where we have used $\tilde{\Phi} = i\tau_2\Phi^{*}$, L_L is the lepton doublet, Q_L the quark doublet, f_R the $SU(2)_L$ singlet fermions, and i, j are family indices. As well as:

$$\begin{aligned}
\Phi^{\dagger}\overleftrightarrow{D}_{\mu}\Phi &= \Phi^{\dagger}D_{\mu}\Phi - (D_{\mu}\Phi)^{\dagger}\Phi \\
\Phi^{\dagger}\overleftrightarrow{D}^{a}{}_{\mu}\Phi &= \Phi^{\dagger}\tau^{a}D_{\mu}\Phi - (D_{\mu}\Phi)^{\dagger}\tau^{a}\Phi
\end{aligned} \tag{2.8}$$

The dimension–six operators in Eq. (2.7) have been classified according to the number of Higgs fields that they contain. In the first column, the operators are denoted by $\mathcal{O}_{f\Phi,ij}$ and they contain three Higgs doublets. After spontaneous symmetry breaking these operators lead to modifications of the SM Higgs Yukawa couplings as we will see below. The second column, $\mathcal{O}^{(1)}_{\Phi f,ij}$,

contains operators with two Higgs doublets and one covariant derivative acting on them. Consequently, they contribute to the Higgs couplings to fermion pairs, but also modify the neutral current weak interactions of the corresponding fermions, with the exception of $\mathcal{O}^{(1)}_{\Phi ud,ij}$ that also changes the charged weak interactions. $\mathcal{O}^{(3)}_{\Phi f,ij}$, besides contributing to the Higgs couplings to fermion pairs, also lead to modifications of the fermionic neutral and charged current interactions.

2.2 Effective Vertices

Next we consider the finite wavefunction and coupling renormalization due to the effective operators. We proceed by expanding the operators to obtain the three– and four–vertex Lorentz forms relevant to our analysis. Here we only include the Lorentz forms relevant to Higgs–vector (HVV), triple gauge vertex (TGV), and Higgs–fermion (Hff) interactions leaving other forms which will be relevant to the discussions in Chapter 6, for Appendix A.

Working in the unitary gauge the Higgs doublet is given by:

$$\Phi = \frac{1}{\sqrt{2}} \begin{pmatrix} 0 \\ v + h(x) \end{pmatrix}. \tag{2.9}$$

Many of the operators induce finite field renormalization requiring us to expand the operators to identify their impacts. First we note there is an induced shift to the Higgs potential from $\mathcal{O}_{\Phi,3}$:

$$V(\Phi) = \mu_0^2(\Phi^\dagger\Phi) + \lambda_0(\Phi^\dagger\Phi)^2 - \frac{f_{\Phi,3}}{3\Lambda^2}(\Phi^\dagger\Phi)^3. \tag{2.10}$$

Leading to a shift in the minimum of the potential with respect to the SM,

$$v^2 = -\frac{\mu_0^2}{\lambda_0}\left(1 + \frac{v^2}{4\Lambda^2}\frac{f_{\Phi,3}}{\lambda_0}\right) \equiv v_0^2\left(1 + \frac{v^2}{4\Lambda^2}\frac{f_{\Phi,3}}{\lambda_0}\right), \tag{2.11}$$

where the subscript "0" denotes the SM value. As $\mathcal{O}_{\Phi,1}$, $\mathcal{O}_{\Phi,2}$, and $\mathcal{O}_{\Phi,4}$ contain derivatives of the Higgs field they therefore induce a finite wavefunction renormalization for the Higgs field, so that the field with a canonical kinetic

term is H:

$$H = h\left[1 + \frac{v^2}{2\Lambda^2}(f_{\phi,1} + 2f_{\phi,2} + f_{\phi,4})\right]^{1/2}. \tag{2.12}$$

To linear order this leads to a shift of the Higgs mass:

$$M_H^2 = 2\lambda_0 v^2\left[1 - \frac{v^2}{2\Lambda^2}\left(f_{\phi,1} + 2f_{\phi,2} + f_{\phi,4} + \frac{f_{\phi,3}}{\lambda_0}\right)\right]. \tag{2.13}$$

Next we consider similar effects on the gauge fields. We note that $\mathcal{O}_{BW}$ affects $Z\gamma$ mixing shifting the mass eigenstates from those in the SM:

$$\begin{aligned} Z_\mu &= \left[1 - \tfrac{g^2 g'^2}{2(g^2+g'^2)}\tfrac{v^2}{\Lambda^2} f_{BW}\right]^{-1/2} Z_\mu^{\rm SM}, \\ A_\mu &= \left[1 + \tfrac{g^2 g'^2}{2(g^2+g'^2)}\tfrac{v^2}{\Lambda^2} f_{BW}\right]^{-1/2} A_\mu^{\rm SM} - \left[\tfrac{gg'(g^2-g'^2)}{4(g^2+g'^2)}\tfrac{v^2}{\Lambda^2} f_{BW}\right] Z_\mu^{\rm SM}, \end{aligned} \tag{2.14}$$

and, additionally, that there are effects on the gauge boson masses:

$$\begin{aligned} M_Z^2 &= \tfrac{g^2+g'^2}{4} v^2\left[1 + \tfrac{v^2}{2\Lambda^2}\left(f_{\Phi,1} + f_{\Phi,4} - \tfrac{g^2 g'^2}{(g^2+g'^2)} f_{BW}\right)\right], \\ M_W^2 &= \tfrac{g^2}{4} v^2\left[1 + \tfrac{v^2}{2\Lambda^2} f_{\Phi,4}\right]. \end{aligned} \tag{2.15}$$

Notice that $\mathcal{O}_{BW}$ and $\mathcal{O}_{\Phi,1}$ contribute to the Z mass, but not the W mass, therefore violating the custodial $SU(2)$ symmetry and contributing to the T parameter as will be discussed in more detail in Sec. 2.3 and 2.4.

We use for our calculations the inputs G_F, M_Z, $\alpha_{\rm EM}$, α_s, and M_H with the electromagnetic coupling evaluated at zero momentum, the so–called Z–scheme. In addition when convenient we can also absorb part of the tree level factors by using the measured value of M_W via the relation

$$\frac{G_F}{\sqrt{2}} = \frac{g^2}{8M_W^2}, \tag{2.16}$$

in combination with Eq. (2.15), so we can express the shift of the vacuum expectation value and M_Z^2 as:

$$\begin{aligned} v &= \left(\sqrt{2}G_F\right)^{-1/2}\left(1 - \tfrac{v^2}{4\Lambda^2} f_{\Phi,4}\right), \\ M_Z^2 &= \left(\sqrt{2}G_F\right)^{-1} \tfrac{g^2}{4c_{\rm W}^2}\left(1 + \tfrac{v^2}{2\Lambda^2} f_{\Phi,1} - \tfrac{g^2 g'^2}{2(g^2+g'^2)}\tfrac{v^2}{\Lambda^2} f_{BW}\right), \end{aligned} \tag{2.17}$$

where we have used $c_{\rm W} \equiv g/\sqrt{g^2+g'^2} = \cos\theta_{\rm W}$, the tree level cosine of the SM

weak mixing angle. Expanding the operators relevant to HVV interactions we define $\mathcal{L}_{HVV}$ with corresponding couplings $g^{(i)}_{HVV}$, where i indicates different Lorentz structures:

$$\begin{aligned}
\mathcal{L}^{HVV}_{\rm eff} &= g_{Hgg} H G^a_{\mu\nu} G^{a\mu\nu} + g_{H\gamma\gamma} H A_{\mu\nu} A^{\mu\nu} + g^{(1)}_{HZ\gamma} A_{\mu\nu} Z^\mu \partial^\nu H \\
&+ g^{(2)}_{HZ\gamma} H A_{\mu\nu} Z^{\mu\nu} + g^{(1)}_{HZZ} Z_{\mu\nu} Z^\mu \partial^\nu H + g^{(2)}_{HZZ} H Z_{\mu\nu} Z^{\mu\nu} \\
&+ g^{(3)}_{HZZ} H Z_\mu Z^\mu + g^{(1)}_{HWW} (W^+_{\mu\nu} W^{-\mu} \partial^\nu H + \text{h.c.}) \\
&+ g^{(2)}_{HWW} H W^+_{\mu\nu} W^{-\mu\nu} + g^{(3)}_{HWW} H W^+_\mu W^{-\mu} \, . \qquad (2.18)
\end{aligned}$$

In Eq. (2.18) we have defined $V_{\mu\nu} = \partial_\mu V_\nu - \partial_\nu V_\mu$, for $V = A, Z, W$ and

$$\begin{aligned}
g_{Hgg} &= \tfrac{f_{GG} v}{\Lambda^2} \equiv -\tfrac{\alpha_s}{8\pi} \tfrac{f_g v}{\Lambda^2} \\
g_{H\gamma\gamma} &= -\left(\tfrac{g^2 v s^2_{\rm W}}{2\Lambda^2}\right) \tfrac{f_{BB}+f_{WW}-f_{BW}}{2} \\
g^{(1)}_{HZ\gamma} &= \left(\tfrac{g^2 v}{2\Lambda^2}\right) \tfrac{s_{\rm W}(f_W - f_B)}{2c_{\rm W}} \\
g^{(2)}_{HZ\gamma} &= \left(\tfrac{g^2 v}{2\Lambda^2}\right) \tfrac{s_{\rm W}[2s^2_{\rm W} f_{BB} - 2c^2_{\rm W} f_{WW} + (c^2_{\rm W} - s^2_{\rm W}) f_{BW}]}{2c_{\rm W}} \\
g^{(1)}_{HZZ} &= \left(\tfrac{g^2 v}{2\Lambda^2}\right) \tfrac{c^2_{\rm W} f_W + s^2_{\rm W} f_B}{2c^2_{\rm W}} \\
g^{(2)}_{HZZ} &= -\left(\tfrac{g^2 v}{2\Lambda^2}\right) \tfrac{s^4_{\rm W} f_{BB} + c^4_{\rm W} f_{WW} + c^2_{\rm W} s^2_{\rm W} f_{BW}}{2c^2_{\rm W}} \\
g^{(3)}_{HZZ} &= \left(\tfrac{g^2 v}{4c^2_{\rm W}}\right) \left[1 + \tfrac{v^2}{4\Lambda^2} \left(3 f_{\Phi,1} + 3 f_{\Phi,4} - 2 f_{\Phi,2} - \tfrac{2 g^2 g'^2}{(g^2+g'^2)} f_{BW}\right)\right] \qquad (2.19) \\
&= M^2_Z (\sqrt{2} G_F)^{1/2} \left[1 + \tfrac{v^2}{4\Lambda^2} (f_{\Phi,1} + 2 f_{\Phi,4} - 2 f_{\Phi,2})\right] \\
g^{(1)}_{HWW} &= \left(\tfrac{g^2 v}{2\Lambda^2}\right) \tfrac{f_W}{2} \\
g^{(2)}_{HWW} &= -\left(\tfrac{g^2 v}{2\Lambda^2}\right) f_{WW} \\
g^{(3)}_{HWW} &= \left(\tfrac{g^2 v}{2}\right) \left[1 + \tfrac{v^2}{4\Lambda^2} (3 f_{\Phi,4} - f_{\Phi,1} - 2 f_{\Phi,2})\right] \\
&= 2 M^2_W (\sqrt{2} G_F)^{1/2} \left[1 + \tfrac{v^2}{4\Lambda^2} (2 f_{\Phi,4} - f_{\Phi,1} - 2 f_{\Phi,2})\right]
\end{aligned}$$

where, as previously, we have expanded to linear order in the f_i coefficients. Also, for convenience, we have rescaled the coefficient of the gluonic operator, f_{GG}, by a loop factor $-\alpha_s/(8\pi)$. This way an anomalous gluonic coupling of order $f_g \sim \mathcal{O}(1-10)$ gives a contribution comparable to the SM top loop, which is the main loop contributing to the coupling of the Higgs boson to gluons in the SM. For the rest of the dimension–six operators involving EW gauge bosons we have decided to keep the same normalization commonly used in all the pre-LHC studies for an easier comparison with the existing literature. Notice that the general expressions above reproduce in the different cases considered those

of [41–48].

Concerning TGVs the relevant couplings are:

$$\begin{aligned}\mathcal{L}_{\rm eff}^{WWV} &= g^{(1)}_{WWZ}(W^+_\nu W^-_\mu - \text{h.c.})Z^{\mu\nu} + g^{(2)}_{WWZ}(W^+_{\mu\nu}W^{-\mu}Z^\nu - \text{h.c.}) \\ &+ g^{(3)}_{WWZ}(W^+_{\mu\nu}W^{-\nu}_\rho - \text{h.c.})Z^{\rho\mu} + g^{(1)}_{WWA}(W^+_\nu W^-_\mu - \text{h.c.})A^{\mu\nu} \\ &+ g^{(2)}_{WWA}(W^+_{\mu\nu}W^{-\nu}_\rho - \text{h.c.})A^{\rho\mu}\ , \end{aligned} \tag{2.20}$$

where

$$\begin{aligned} g^{(1)}_{WWZ} &= \tfrac{ig^3v^2c_{\rm W}}{16\Lambda^2}(f_W + \tfrac{s^2_{\rm W}}{c^2_{\rm W}}f_B + \tfrac{4s^2_{\rm W}}{c_{2\rm W}}f_{BW} - \tfrac{2s^2_{\rm W}}{e^2c_{2\rm W}}f_{\Phi,1}) \\ g^{(2)}_{WWZ} &= -\tfrac{ig^3v^2}{8c_{\rm W}\Lambda^2}(f_W + \tfrac{2s^2_{\rm W}}{c_{2\rm W}}f_{BW} - \tfrac{s^2_{2\rm W}}{2e^2c_{2\rm W}}f_{\Phi,1}) \\ g^{(3)}_{WWZ} &= -\tfrac{3ig^3c_{\rm W}}{2\Lambda^2}f_{WWW} \\ g^{(1)}_{WWA} &= \tfrac{ig^3v^2s_{\rm W}}{16\Lambda^2}(f_W + f_B - 2f_{BW}) \\ g^{(2)}_{WWA} &= -\tfrac{3ig^3s_{\rm W}}{2\Lambda^2}f_{WWW} \end{aligned} \tag{2.21}$$

and we have defined $c_{2\rm W} = \cos(2\theta_W)$ and $s_{2\rm W} = \sin(2\theta_W)$. We note that the coefficients f_W and f_B contribute to both Higgs-vector and TGVs. This correlation is due to the fact the Higgs is a doublet charged under $SU(2)_L$ and will prove important in our future discussions. We will see this correlation is absent in the chiral EFT presented in Chapter 3 and that it will also allow us to make projections of the Higgs data onto the space of TGCs at a competitive level with the current best measurements in Chapter 5. As mentioned above we save other vertices generated by the operators for Appendix A.

Changing to the effective operators concerning the couplings of the Higgs boson to fermions the form of the effective Lagrangian for the fermionic operators in Eq. (2.7) (noticing that generically these operators are not Hermitian) is then given by:

$$\mathcal{L}_{\rm eff}^{Hff} = \frac{f_{d\Phi,ij}}{\Lambda^2}\mathcal{O}_{d\Phi,ij} + \frac{f_{u\Phi,ij}}{\Lambda^2}\mathcal{O}_{u\Phi,ij} + \frac{f_{e\Phi,ij}}{\Lambda^2}\mathcal{O}_{e\Phi,ij} + \text{h.c.} \tag{2.22}$$

Recalling that in the SM the Yukawa interactions take the form (see Eq. (1.24))

$$\mathcal{L}_{\rm Yuk} = -y^e_{ij}\bar{L}_{Li}\Phi e_{Rj} - y^d_{ij}\bar{Q}_{Li}\Phi d_{R,j} - y^u_{ij}\bar{Q}_{Li}\tilde{\Phi}u_{Rj} + \text{h.c.}\ \ , \tag{2.23}$$

we see that the operators $\mathcal{O}_{f\Phi,ij}$ renormalize fermion masses and mixing, and then modify the Yukawa interactions as well.

After spontaneous symmetry breaking and prior to Higgs wave function renormalization we can decompose $\mathcal{L}_{\text{eff}}^{Hqq}$ into two pieces, $\mathcal{L}_0$ and $\mathcal{L}_1$:

$$\begin{aligned}\mathcal{L}_0 &= \tfrac{1}{\sqrt{2}}\bar{d}_L\left(-y^d+\tfrac{v^2}{2\Lambda^2}f_{d\Phi}\right)d_R(v+h)+\tfrac{1}{\sqrt{2}}\bar{u}_L\left(-y^u+\tfrac{v^2}{2\Lambda^2}f_{u\Phi}\right)u_R(v+h)\\ &+ \tfrac{1}{\sqrt{2}}\bar{e}_L\left(-y^e+\tfrac{v^2}{2\Lambda^2}f_{e\Phi}\right)e_R(v+h)+\text{h.c.}\\ \\ \mathcal{L}_1 &= \tfrac{1}{\sqrt{2}}\tfrac{v^2}{\Lambda^2}\bar{d}_L f_{d\Phi}d_R h+\tfrac{1}{\sqrt{2}}\tfrac{v^2}{\Lambda^2}\bar{u}_L f_{u\Phi}u_R h+\tfrac{1}{\sqrt{2}}\tfrac{v^2}{\Lambda^2}\bar{e}_L f_{e\Phi}e_R h+\text{h.c.}\end{aligned} \tag{2.24}$$

We can see that $\mathcal{L}_0$ then corresponds to the mass term of the fermions with Higgs-fermion interactions subject to renormalized fermion masses and quark mixing. The new interactions, contained in $\mathcal{L}_1$, are not generically flavor diagonal in the mass basis unless $f_{f\Phi} \propto y^f$, where here $f_{f\Phi}$ and y^f are the 3×3 matrices in generation space whose components are $f_{f\Phi,ij}$ and y^f_{ij} with $f = u$, or d or e.

Altogether in the physical fermion mass basis and after renormalization of the Higgs wave function from Eq. (2.12) the $H\bar{f}f$ couplings may be written as:

$$\mathcal{L}^{Hff} = g^f_{Hij}\bar{f}'_L f'_R H + \text{h.c.} \tag{2.25}$$

with

$$g^f_{Hij} = -\frac{m^f_i}{v}\delta_{ij}\left[1-\frac{v^2}{4\Lambda^2}(f_{\Phi,1}+2f_{\Phi,2}+f_{\Phi,4})\right]+\frac{v^2}{\sqrt{2}\Lambda^2}f'_{f\Phi,ij}, \tag{2.26}$$

where the physical masses are denoted by m^f_j and the coefficients of the corresponding operators in the mass basis are given by $f'_{q\Phi,ij}$. In what follows, for the sake of simplicity, we will drop the primes in these fields and coefficients.

2.3 Electroweak Parameters: S, T, U

In this dissertation we will make use of and refer to electroweak precision data (EWPD) with great frequency. In this section we present a short introduction to the S, T, and U parameters the most common parameterization of universal (also referred to as oblique) contributions to electroweak precision data [49]. These parameters are also frequently referred to as ϵ_1, ϵ_2, and ϵ_3 [50].

As a result of the great success of electroweak theory it was realized that

deviations from the SM predictions had to be considered at loop level. The strongest constraints come from LEP, where the processes $e^+e^- \to Z \to \bar{f}f$ were measured with high accuracy. In order to quantify divergences from the SM predictions related to these processes in a gauge covariant manner we must consider corrections to the two point function of all gauge vectors, V, along with vertex corrections to $V \to \bar{f}f'$. For both we restrict ourselves to the electroweak sector as that is the focus of in this dissertation. Our discussion in this section will closely follow that of [51].

We begin by considering the corrections to the two point functions of the electroweak vectors (projected into their longitudinal and transverse components),

$$-i\Pi^{\mu\nu}_{V_1V_2}(q^2) = -i\Pi^{V_1V_2}_T(q^2)\left(g^{\mu\nu} - \frac{q^\mu q^\nu}{q^2}\right) - i\Pi^{V_1V_2}_L(q^2)\left(\frac{q^\mu q^\nu}{q^2}\right), \qquad (2.27)$$

where $\Pi^{\mu\nu}$ is the correction to the $V_1^\mu V_2^\nu$ two-point functions, the sub– and super–scripts V_1 and V_2 indicate the vectors under consideration, and the subscripts T and L indicate the transverse and longitudinal projections of the tensor respectively. The corrections to the Vff vertex, neglecting fermion masses, are:

$$\begin{aligned} -i\Gamma^{\gamma f_1 f_2}_\mu(q) &= -i\gamma_\mu \tfrac{1}{2}(1-\gamma_5) g I_3^f \Gamma^\gamma_L(q^2), \\ -i\Gamma^{Z f_1 f_2}_\mu(q) &= -i\gamma_\mu \tfrac{1}{2}(1-\gamma_5) g I_3^f \Gamma^Z_L(q^2), \\ -i\Gamma^{W f_1 f_2}_\mu(q) &= -i\gamma_\mu \tfrac{1}{2}(1-\gamma_5) \tfrac{g}{\sqrt{2}} \Gamma^W_L(q^2), \end{aligned} \qquad (2.28)$$

where the superscripts Vf_1f_2 indicate the vector, V, and two fermions, f_1 and f_2, under consideration, γ_μ and γ_5 are the usual gamma matrices, and I_3^f is the third component of weak isospin for the external fermion.

We are interested in NP signals so we split the SM and anomalous parts via

$$\Pi = \Pi_{\rm SM} + \Delta\Pi \qquad \text{and} \qquad \Gamma = \Gamma_{\rm SM} + \Delta\Gamma, \qquad (2.29)$$

and define the (gauge invariant) quantities:

$$\begin{aligned}
\Delta\bar{\Pi}_T^{\gamma\gamma}(q^2) &= \Delta\Pi_T^{\gamma\gamma}(q^2) - 2s_{\rm W}q^2\Delta\Gamma_L^{\gamma}(q^2), \\
\Delta\bar{\Pi}_T^{\gamma Z}(q^2) &= \Delta\Pi_T^{\gamma Z}(q^2) - s_{\rm W}q^2\Delta\Gamma_L^{Z}(q^2) - c_{\rm W}(q^2-m_Z^2)\Delta\Gamma_L^{\gamma}(q^2), \\
\Delta\bar{\Pi}_T^{ZZ}(q^2) &= \Delta\Pi_T^{ZZ}(q^2) - 2c_{\rm W}(q^2-m_Z^2)\Delta\Gamma_L^{Z}(q^2), \\
\Delta\bar{\Pi}_T^{WW}(q^2) &= \Delta\Pi_T^{WW}(q^2) - 2(q^2-m_W^2)\Delta\Gamma_L^{W}(q^2).
\end{aligned} \tag{2.30}$$

Allowing us to then define

$$\Delta\bar{\Pi}_{T,V_3}^{V_1V_2}(q^2) = \frac{\Delta\bar{\Pi}_T^{V_1V_2}(q^2) - \Delta\bar{\Pi}_T^{V_1V_2}(m_{V_3}^2)}{q^2-m_{V_3}^2}, \tag{2.31}$$

and we finally arrive at the S, T, and U parameters:

$$\begin{aligned}
\alpha_{\rm EM}\Delta S &= 4s_{\rm W}^2c_{\rm W}^2\left(-\Delta\bar{\Pi}_{T,Z}^{ZZ}(0) + \tfrac{c_{\rm W}^2-s_{\rm W}^2}{s_{\rm W}c_{\rm W}}\Delta\bar{\Pi}_{T,\gamma}^{\gamma Z}(m_Z^2) + \Delta\bar{\Pi}_{T,\gamma}^{\gamma\gamma}(m_Z^2)\right), \\
\alpha_{\rm EM}\Delta T &= \left(\tfrac{\Delta\bar{\Pi}_T^{ZZ}(0)}{m_Z^2} - \tfrac{\Delta\bar{\Pi}_T^{WW}(0)}{m_W^2}\right), \\
\alpha_{\rm EM}\Delta U &= 4s_{\rm W}\left(c_{\rm W}^2\Delta\bar{\Pi}_{T,Z}^{ZZ}(0) - \Delta\bar{\Pi}_{T,W}^{WW}(0)\right. \\
&\quad \left. + s_{\rm W}^2\Delta\bar{\Pi}_{T,\gamma}^{\gamma\gamma}(m_Z^2) + 2s_{\rm W}c_{\rm W}\Delta\bar{\Pi}_{T,\gamma}^{\gamma Z}(m_Z^2)\right).
\end{aligned} \tag{2.32}$$

By inspection we can see that T is the difference between corrections to W and Z interactions/propagators. Therefore any operators which induce different behavior for the Z from that of the W, i.e. violate custodial symmetry, will induce corrections to the T parameter. Recalling from Eq. (2.15) that the operator $\mathcal{O}_{\Phi,1}$ induces a shift to the Z propagator (and to its mass), but not that of the W, we expect that $\mathcal{O}_{\Phi,1}$ contributes to the T parameter. In fact it does at tree-level, with its contribution given by:

$$\alpha_{\rm EM}\Delta T = \frac{1}{2}\frac{v^2}{\Lambda^2}f_{\Phi,1}. \tag{2.33}$$

The S parameter contains new physics contributions to the neutral currents at different energies. Hence $\mathcal{O}_{BW}$ which gives a tree-level contribution to the $Z\gamma$ two-point function, gives a correction to S that reads:

$$\alpha_{\rm EM}\Delta S = e^2\frac{v^2}{\Lambda^2}f_{BW}. \tag{2.34}$$

We note that despite its contribution to the Z mass and not that of the W,

$\mathcal{O}_{BW}$ does not contribute directly to the T parameter because it does not modify the Z propagator. The correction to the Z mass is induced by the redefinition of the neutral gauge boson fields after the mixing induced by this operator, an effect which is accounted for in the S parameter.

Operators $\mathcal{O}_B$, $\mathcal{O}_W$, $\mathcal{O}_{BB}$, $\mathcal{O}_{WW}$, and $\mathcal{O}_{\Phi,2}$ give contributions at the one loop level:

$$\begin{aligned}
\alpha_{\rm EM}\Delta S &= \tfrac{1}{6}\tfrac{e^2}{16\pi^2}\left\{3(f_W+f_B)\tfrac{m_H^2}{\Lambda^2}\log\left(\tfrac{\Lambda^2}{m_H^2}\right)\right. \\
&\quad + 2\left[(5c_{\rm W}^2-2)\,f_W-(5c_{\rm W}^2-3)\,f_B\right]\tfrac{m_Z^2}{\Lambda^2}\log\left(\tfrac{\Lambda^2}{m_H^2}\right) \\
&\quad - \left[(22c_{\rm W}^2-1)\,f_W-(30c_{\rm W}^2+1)\,f_B\right]\tfrac{m_Z^2}{\Lambda^2}\log\left(\tfrac{\Lambda^2}{m_Z^2}\right) \\
&\quad -24\left(c_{\rm W}^2 f_{WW}+s_{\rm W}^2 f_{BB}\right)\tfrac{m_Z^2}{\Lambda^2}\log\left(\tfrac{\Lambda^2}{m_H^2}\right) \\
&\quad \left.+2f_{\Phi,2}\tfrac{v^2}{\Lambda^2}\log\left(\tfrac{\Lambda^2}{m_H^2}\right)\right\}, \\
\alpha_{\rm EM}\Delta T &= \tfrac{3}{4c_{\rm W}^2}\tfrac{e^2}{16\pi^2}\left\{f_B\tfrac{m_H^2}{\Lambda^2}\log\left(\tfrac{\Lambda^2}{m_H^2}\right)+(c_{\rm W}^2 f_W+f_B)\tfrac{m_Z^2}{\Lambda^2}\log\left(\tfrac{\Lambda^2}{m_H^2}\right)\right. \\
&\quad + \left[2c_{\rm W}^2 f_W+(3c_{\rm W}^2-1)\,f_B\right]\tfrac{m_Z^2}{\Lambda^2}\log\left(\tfrac{\Lambda^2}{m_Z^2}\right) \\
&\quad \left.- f_{\Phi,2}\tfrac{v^2}{\Lambda^2}\log\left(\tfrac{\Lambda^2}{m_H^2}\right)\right\}, \\
\alpha_{\rm EM}\Delta U &= -\tfrac{1}{3}\tfrac{e^2 s_{\rm W}^2}{16\pi^2}\left\{(-4f_W+5f_B)\tfrac{m_Z^2}{\Lambda^2}\log\left(\tfrac{\Lambda^2}{m_H^2}\right)\right. \\
&\quad \left.+(2f_W-5f_B)\tfrac{m_Z^2}{\Lambda^2}\log\left(\tfrac{\Lambda^2}{m_Z^2}\right)\right\},
\end{aligned} \tag{2.35}$$

where the calculations have been performed using dimensional regularization with $d=4-2\epsilon$. The logarithms result from identifying the poles with logarithmic divergences, that is:

$$\frac{1}{\epsilon}(4\pi)^{\epsilon}\Gamma(1+\epsilon)\to\log\left(\frac{\Lambda^2}{\mu^2}\right). \tag{2.36}$$

In these expressions we have also neglected the finite parts as the logarithms are meant to capture the running of the couplings which is the only information from the loops of the ultraviolet completion which can be robustly reconstructed with the low energy EFT.

2.4 The Choice of Basis and the Application of Precision Data

In the effective Lagrangian framework not all operators are independent as they can be related by the use of the classical EOM[1]. This is shown by proving that operators connected by the EOM lead to the same S-matrix elements [52–55]. In an approach where the full or UV theory is known one may integrate out heavy degrees of freedom obtaining the operators (a top down approach) thus leading to higher dimension operators whose form is tied to the UV physics and therefore it may be convenient not to choose a minimal set of operators in order to more easily identify the higher dimensional operators at low energy. However, in our approach we use the effective Lagrangian to obtain bounds on generic extensions of the SM (a bottom-up approach). As the NP is not known a priori in this approach it is useful to adjust one's basis via the EOM to choose operators better constrained by low energy physics.

Since we truncate our expansion in effective operators at dimension–six it is only necessary to consider the SM EOM. These EOM relate bosonic operators to fermionic ones and we use those for the Higgs field and electroweak gauge bosons giving three relations between operators:

$$\begin{aligned}
2\mathcal{O}_{\Phi,2}+2\mathcal{O}_{\Phi,4} &= \sum_{ij}\left(y^e_{ij}(\mathcal{O}_{e\Phi,ij})^\dagger + y^u_{ij}\mathcal{O}_{u\Phi,ij} + y^d_{ij}(\mathcal{O}_{d\Phi,ij})^\dagger + \text{h.c.}\right) \\
&\quad - 2(\Phi^\dagger\Phi)\Phi^\dagger\tfrac{\partial V}{\partial\Phi^\dagger}\ , \\
2\mathcal{O}_B+\mathcal{O}_{BW}+\mathcal{O}_{BB}+g'^2\left(\mathcal{O}_{\Phi,1}-\tfrac{1}{2}\mathcal{O}_{\Phi,2}\right) &= -\tfrac{g'^2}{2}\sum_i\Big(-\tfrac{1}{2}\mathcal{O}^{(1)}_{\Phi L,ii}+\tfrac{1}{6}\mathcal{O}^{(1)}_{\Phi Q,ii} \\
&\quad -\mathcal{O}^{(1)}_{\Phi e,ii}+\tfrac{2}{3}\mathcal{O}^{(1)}_{\Phi u,ii}-\tfrac{1}{3}\mathcal{O}^{(1)}_{\Phi d,ii}\Big)\ , \\
2\mathcal{O}_W+\mathcal{O}_{BW}+\mathcal{O}_{WW}+g^2\left(\mathcal{O}_{\Phi,4}-\tfrac{1}{2}\mathcal{O}_{\Phi,2}\right) &= -\tfrac{g^2}{4}\sum_i\left(\mathcal{O}^{(3)}_{\Phi L,ii}+\mathcal{O}^{(3)}_{\Phi Q,ii}\right)\ .
\end{aligned} \tag{2.37}$$

From these three EOM we are able to remove three of the operators listed in Eqs. (2.2) and (2.7). We put off the discussion of which operators we will remove via the EOM until after discussing precision data.

[1]Note our discussion on reducing the basis via the EOM and precision data primarily pertains to Higgs related fits which will be discussed in Chapter 5, and is not directly used in Chapter 6

We wish to use pre–Higgs precision data to reduce the size of the relevant set of operators for our Higgs studies. In particular we notice that the Z and W couplings to fermions as well as the oblique parameters S, T, and U are in agreement with the SM at least at the percent level [56]. These results severely constrain the effects of $\mathcal{O}_{\Phi f}^{(1)}$, $\mathcal{O}_{\Phi f}^{(3)}$, $\mathcal{O}_{BW}$ and $\mathcal{O}_{\Phi,1}$. In particular as described in the previous section the operators $\mathcal{O}_{BW}$ and $\mathcal{O}_{\Phi,1}$ give tree level contributions to the S and T parameters (see Eq. (2.35)).

Precise constraints also exist on triple gauge boson interactions from LEPII and the Tevatron [57]. In order to account for these we begin by putting the relevant terms of $\mathcal{L}_{\rm eff}$ into the parameterization of Ref. [37, 58] which is generically used in experimental searches:

$$\begin{aligned}\mathcal{L}_{WWV} &= -ig_{WWV}\Big[g_1^V(W^+_{\mu\nu}W^{-\mu}V^{\nu} - W^+_{\mu}V_{\nu}W^{-\mu\nu}) + \kappa_V W^+_{\mu}W^-_{\nu}V^{\mu\nu} \\ &\quad + \tfrac{\lambda_V}{m_W^2}W^+_{\mu\nu}W^{-\nu\rho}V_{\rho}^{\mu}\Big] \ ,\end{aligned} \tag{2.38}$$

which, after comparison with Eqs. (2.20) and (2.21) yields the following relations:

$$\begin{aligned}\Delta g_1^Z &= g_1^Z - 1 = \tfrac{g^2v^2}{8c_{\rm W}^2\Lambda^2}\left(f_W + 2\tfrac{s_{\rm W}^2}{c_{\rm W}^2-s_{\rm W}^2}f_{BW}\right) - \tfrac{1}{4(c_{\rm W}^2-s_{\rm W}^2)}f_{\Phi,1}\tfrac{v^2}{\Lambda^2} \ , \\ \Delta\kappa_\gamma &= \kappa_\gamma - 1 = \tfrac{g^2v^2}{8\Lambda^2}\left(f_W + f_B - 2f_{BW}\right) \ , \\ \Delta\kappa_Z &= \kappa_Z - 1 = \tfrac{g^2v^2}{8c_{\rm W}^2\Lambda^2}\left(c_{\rm W}^2 f_W - s_{\rm W}^2 f_B + \tfrac{4s_{\rm W}^2c_{\rm W}^2}{c_{\rm W}^2-s_{\rm W}^2}f_{BW}\right) \\ &\quad - \tfrac{1}{4(c_{\rm W}^2-s_{\rm W}^2)}f_{\Phi,1}\tfrac{v^2}{\Lambda^2} \ , \\ \lambda_\gamma &= \tfrac{3g^2M_W^2}{2\Lambda^2}f_{WWW} \ , \\ \lambda_Z &= \tfrac{3g^2M_W^2}{2\Lambda^2}f_{WWW} \ .\end{aligned} \tag{2.39}$$

LEPII and Tevatron results constrained these effective couplings to be in agreement with the SM expectation with precision ranging from between 10 to 1% [57].

It is important to realize that in applying the constraints from these EWPD we must take care that we do not introduce a combination of the anomalous

operators whose contribution at tree level to the EWPD cancels out – we must avoid "blind directions."

To illustrate this point we consider the dependence on the anomalous couplings of a subset of the EWPD that contains the W mass, W leptonic width, the Z width into charged leptons, the leptonic Z left-right asymmetry, and the invisible Z width (M_W, $\Gamma^W_{\ell\nu}$, $\Gamma_{\ell\ell}, A_\ell$, and $\Gamma_{\rm inv}$ respectively). We can write the departures of these observables (i.e. $\Delta\text{OBS} \equiv \frac{\text{OBS}-\text{OBS}_{\rm SM}}{\text{OBS}_{\rm SM}}$) from the SM predictions as [59, 60]

$$\begin{pmatrix} \Delta\Gamma_{\ell\ell} \\ \Delta\Gamma_{\rm inv} \\ \Delta A_\ell \\ \Delta M_W \\ \Delta\Gamma^W_{\ell\nu} \end{pmatrix} = M \begin{pmatrix} f^{(1)}_{\Phi e} \\ f^{(1)}_{\Phi L} \\ f^{(3)}_{\Phi L} \\ f_{\Phi,1} \\ -\frac{gg'}{4} f_{BW} \end{pmatrix} \frac{v^2}{\Lambda^2}, \tag{2.40}$$

where the matrix M is given by

$$\begin{pmatrix} -\frac{4s^2_{\rm W}}{D} & \frac{2-4s^2_{\rm W}}{D} & \frac{4s^2_{\rm W}(4s^2_{\rm W}-1)}{(c^2_{\rm W}-s^2_{\rm W})D} & -\frac{1-2s^2_{\rm W}-4s^4_{\rm W}}{2(c^2_{\rm W}-s^2_{\rm W})D} & \frac{4c_{\rm W}s_{\rm W}(4s^2_{\rm W}-1)}{(c^2_{\rm W}-s^2_{\rm W})D} \\ 0 & -2 & 0 & -\frac{1}{2} & 0 \\ -\frac{2s^2_{\rm W}(s^2_{\rm W}-1/2)^2}{s^8_{\rm W}-(s^2_{\rm W}-1/2)^4} & \frac{2s^4_{\rm W}(s^2_{\rm W}-1/2)^2}{s^8_{\rm W}-(s^2_{\rm W}-1/2)^4} & \frac{s^4_{\rm W}}{s^8_{\rm W}-(s^2_{\rm W}-1/2)^4} & \frac{c^2_{\rm W}s^4_{\rm W}}{2(s^8_{\rm W}-(s^2_{\rm W}-1/2)^4)} & \frac{c_{\rm W}s^3_{\rm W}}{s^8_{\rm W}-(s^2_{\rm W}-1/2)^4} \\ 0 & 0 & -\frac{s^2_{\rm W}}{c^2_{\rm W}-s^2_{\rm W}} & -\frac{c^2_{\rm W}}{4(c^2_{\rm W}-s^2_{\rm W})} & -\frac{c_{\rm W}s_{\rm W}}{c^2_{\rm W}-s^2_{\rm W}} \\ 0 & 0 & -\frac{3s^2_{\rm W}}{c^2_{\rm W}-s^2_{\rm W}} & -\frac{3c^2_{\rm W}}{4(c^2_{\rm W}-s^2_{\rm W})} & -\frac{3c_{\rm W}s_{\rm W}}{c^2_{\rm W}-s^2_{\rm W}} \end{pmatrix}, \tag{2.41}$$

with $D = 1 - 4s^2_{\rm W} + 8s^4_{\rm W}$.

One can show that M has two zero eigenvalues, indicating that two coupling constant combinations cannot be determined. Considering all LEP observables also results in two blind directions. In this example we find the blind directions to be:

$$f_{\Phi,1} = -4f^{(1)}_{\Phi L} = -2f^{(1)}_{\Phi e} = g'^2 f_{BW} \qquad \text{and} \qquad f^{(3)}_{\Phi L} = \frac{g^2}{4} f_{BW}. \tag{2.42}$$

This then indicates that we cannot simply choose any operators to remove via the EOM, but instead have to choose in such a manner as to prevent

the introduction of blind directions. The two combinations of operators that do not contribute to these example leptonic observables are any two linear combinations of:

$$\begin{aligned} \mathcal{O}_{\text{LEP blind,1}} &= g'^2 \left(\mathcal{O}_{\Phi,1} - \tfrac{1}{4} \sum_i \mathcal{O}^{(1)}_{\Phi L,ii} - \tfrac{1}{2} \sum_i \mathcal{O}^{(1)}_{\Phi e,ii} \right) + \mathcal{O}_{BW}, \\ \mathcal{O}_{\text{LEP blind,2}} &= \mathcal{O}_{BW} + \tfrac{g^2}{4} \sum_i \mathcal{O}^{(3)}_{\Phi L,ii}. \end{aligned} \tag{2.43}$$

We note that there exists a relation between operators that do not lead to a tree–level contribution to the EWPD and blind directions: the elimination of an operator that does not lead to tree–level contributions to EWPD leads to a combination of operators each one apparently contributing to EWPD at tree level. This combination, however, must define a blind direction as it has the same S–matrix element as the original operator which had no impact on the EWPD [61].

For example the bosonic operator $\mathcal{O}_{\Phi,2}$ does not contribute to EWPD at tree level since it modifies only the Higgs couplings, therefore it is a blind operator. We can then rewrite the EOM from Eq. (2.37) to give:

$$\begin{aligned} 3g^2 \mathcal{O}_{\Phi,2} = \Bigg[& 2\mathcal{O}_{BW} + 4\mathcal{O}_W + 2\mathcal{O}_{WW} + \tfrac{g^2}{2} \sum_i \left(\mathcal{O}^{(3)}_{\Phi L,ii} + \mathcal{O}^{(3)}_{\Phi Q,ii} \right) \\ & + g^2 \Big(\sum_{ij} \left(y^e_{ij} \left(\mathcal{O}_{e\Phi,ij} \right)^\dagger + y^u_{ij} \mathcal{O}_{u\Phi,ij} + y^d_{ij} \left(\mathcal{O}_{d\Phi,ij} \right)^\dagger + \text{h.c.} \right) \\ & - 2(\Phi^\dagger \Phi) \Phi^\dagger \tfrac{\partial V}{\partial \Phi^\dagger} \Big) \Bigg]. \end{aligned} \tag{2.44}$$

Then the right hand side of Eq. (2.44) defines a blind direction. However, since we know that only the operators $\mathcal{O}_{BW}$ and $\sum_i \mathcal{O}^{(3)}_{\Phi L,ii}$ contribute to the above leptonic observables at tree level, we find from the equation above that the effect of $\mathcal{O}_{\Phi,2}$ is equivalent to:

$$\frac{2}{3g^2} \left(\mathcal{O}_{BW} + \frac{g^2}{4} \sum_i \mathcal{O}^{(3)}_{\Phi L,ii} \right). \tag{2.45}$$

Which corresponds to our previously given combination of operators $\mathcal{O}_{\text{LEP blind,2}}$ in Eq. (2.43).

In summary the EOM in Eq. (2.37) allow for the elimination of three dimension–six operators from the basis with the caveat that we must avoid blind directions. This is then achieved by removing operators that contribute at tree level to the EWPD in such a way that the new form of the matrix M has a non–vanishing determinant.

We then choose to eliminate $\mathcal{O}^{(1)}_{\Phi L,ii}$, $\mathcal{O}^{(3)}_{\Phi L,ii}$, and $\mathcal{O}_{\Phi,4}$ leaving ourselves with a basis which will allow us to take full advantage of the EWPD as well as TGV data from LEP. Altogether our basis is reduced to:

$$\{\ \mathcal{O}_{GG}\ ,\ \mathcal{O}_{BB}\ ,\ \mathcal{O}_{WW}\ ,\ \mathcal{O}_{BW}\ ,\ \mathcal{O}_{B}\ ,\ \mathcal{O}_{W}\ ,\ \mathcal{O}_{\Phi,2}\ ,\ \mathcal{O}_{\Phi,1}\ ,\ \mathcal{O}_{f\Phi}\ ,\ \mathcal{O}^{(1)}_{\Phi f}\ ,\ \mathcal{O}^{(3)}_{\Phi f}\ \}, \tag{2.46}$$

excepting the operators removed above, $\mathcal{O}^{(1)}_{\Phi L,ii}$ and $\mathcal{O}^{(3)}_{\Phi L,ii}$. Now we are able to apply the available experimental information in order to reduce the number of relevant parameters for our analysis of the Higgs data.

As mentioned above the Z and W couplings to fermions and the S, T, and U parameters agreement with the SM is sufficiently high we can remove from our basis $\mathcal{O}^{(1)}_{\Phi f}$, $\mathcal{O}^{(3)}_{\Phi f}$, $\mathcal{O}_{BW}$, and $\mathcal{O}_{\Phi,1}$. Additionally limits on low–energy flavor–changing interactions impose strong bounds on the off–diagonal Yukawa couplings [62–68]. This allows us to discard the off diagonal part of $\mathcal{O}_{f\Phi}$. We note there is potential for sizeable flavor changing effects in $\bar{\tau}e$ and $\bar{\tau}\mu$ [69, 70] along with recent hints from CMS [71] of a $\tau\mu$ decay with an excess of just over 2σ above the SM prediction. This is however not considered in our current analysis. Finally the effects of flavor diagonal $\mathcal{O}_{f\Phi}$ from the first and second generation have not been directly accessed in current experiments and they only appear in Higgs-g-g and Higgs-γ-γ vertices at one loop. These loop form factors are suppressed for the light fermions and consequently they are entirely negligible. Therefore of the remaining diagonal $\mathcal{O}_{f\Phi}$ we retain only $\mathcal{O}_{e\Phi,33}$, $\mathcal{O}_{u\Phi,33}$, and $\mathcal{O}_{d\Phi,33}$.

After all these constraints are imposed we conclude that the relevant $\mathcal{L}_{\text{eff}}$ for our Higgs analysis in Chapter 5, after reduction of the basis via the EOM

and precision data, is:

$$\begin{aligned}\mathcal{L}_{\text{eff}} &= -\frac{\alpha_s v}{8\pi}\frac{f_g}{\Lambda^2}\mathcal{O}_{GG} + \frac{f_{\Phi,2}}{\Lambda^2}\mathcal{O}_{\Phi,2} + \frac{f_{BB}}{\Lambda^2}\mathcal{O}_{BB} + \frac{f_{WW}}{\Lambda^2}\mathcal{O}_{WW} + \frac{f_B}{\Lambda^2}\mathcal{O}_B + \frac{f_W}{\Lambda^2}\mathcal{O}_W \\ &\quad + \frac{f_\tau}{\Lambda^2}\mathcal{O}_{e\Phi,33} + \frac{f_{\text{bot}}}{\Lambda^2}\mathcal{O}_{d\Phi,33} + \frac{f_{\text{top}}}{\Lambda^2}\mathcal{O}_{u\Phi,33}.\end{aligned} \tag{2.47}$$

Notice that with this choice of basis all of the dimension–six operators considered contribute to the Higgs–gauge boson and Higgs–fermion couplings at tree level. However, a final remark regarding the top Yukawa–like dimension–six operator, $\mathcal{O}_{u\Phi,33}$, is required. The tree–level information on $h\bar{t}t$ from associated production of the Higgs with a top pair still has very large errors. As such, quantitatively, the effects of the parameter f_{top} enter mainly via its contribution to the one–loop Higgs couplings to photon pairs and gluon pairs. These contributions can be absorbed in the redefinition of the rest of the parameters contributing to these vertices, f_g and $f_{WW} + f_{BB}$, and therefore, we set $f_{\text{top}} = 0$ for our Higgs analysis in Chapter 5. In the future, when a larger luminosity is accumulated, and direct information on top associated production is available, it will be necessary to introduce f_{top} as one of the parameters in the analysis.

2.5 Summary and Discussion

In this chapter we have introduced the HISZ basis of dimension–six operators for a CP–even Higgs under the assumptions of baryon and lepton number conservation and a linear realization of the electroweak symmetry which is the relevant expansion for NP theories in which the Higgs is a fundamental state. We have detailed the wavefunction renormalization due to the operators in the basis and after accounting for those we have expanded the operators to find the Lorentz structures generated for the gauge–Higgs, TGV, and Higgs–fermion interactions; in doing so we have found that gauge–Higgs and TGV interactions are correlated as a consequence of the gauge invariance, a relation which will become relevant when trying to discriminate this expansion against that characteristic of a dynamical Higgs which we will introduce in the next Chapter. We continued to introduce the electroweak parameters S, T, and U and their contributions from the operators in our basis. Next, taking care not

to generate blind directions, we used the EOM and precision data to reduce the size of our operator basis to those relevant for the present interpretation of the Higgs results. The final linear basis which will be considered for our analysis of Higgs data is:

$$\begin{aligned}\mathcal{L}_{\text{eff}} &= -\tfrac{\alpha_s v}{8\pi}\tfrac{f_g}{\Lambda^2}\mathcal{O}_{GG} + \tfrac{f_{\Phi,2}}{\Lambda^2}\mathcal{O}_{\Phi,2} + \tfrac{f_{BB}}{\Lambda^2}\mathcal{O}_{BB} + \tfrac{f_{WW}}{\Lambda^2}\mathcal{O}_{WW} + \tfrac{f_B}{\Lambda^2}\mathcal{O}_B + \tfrac{f_W}{\Lambda^2}\mathcal{O}_W \\ &\quad + \tfrac{f_\tau}{\Lambda^2}\mathcal{O}_{e\Phi,33} + \tfrac{f_{\text{bot}}}{\Lambda^2}\mathcal{O}_{d\Phi,33}.\end{aligned} \tag{2.48}$$

We will return to this basis in Chapter 5 when we apply our analysis framework to constrain the parameters of this EFT and look at interesting implications of the correlation between Higgs and triple gauge couplings.

Chapter 3

Effective Lagrangian for a Dynamical Higgs: Chiral Expansion

In Chapter 2 we discussed the effective Lagrangian for an extension of the SM assuming a linear realization of the electroweak symmetry. There we noted that such an expansion is appropriate under the circumstances that the Higgs is a fundamental doublet of $SU(2)_L$ as in the SM. However other possibilities exist. In particular it is an interesting question to consider the possibility of some new strongly interacting sector with a global symmetry spontaneously broken down resulting in new condensates which may result in EWSB and also impart mass to the SM fermions. Among the first such models considered were Technicolor theories which sought to generate masses for the gauge bosons [72] and subsequently the inclusion of fermion masses in Extended Technicolor [73, 74]. However many such attempts induced large corrections to some of the precision electroweak parameters which was in contradiction with the experimental results. Furthermore generically in these models the "would be" Higgs became very heavy and was not present in the light particle spectrum (see Sec. 1.2.2).

In the latest years renewed interest has grown on the construction of composite models, but containing a light Higgs–like particle. In these constructions the Higgs appears light as it is a pseudo–Goldstone boson of a global symmetry of the new strongly interacting dynamics. These types of models are also

typically employed as a partial solution to the hierarchy problem. Concrete examples of this type of theory are Composite Higgs Models (CHMs) [23–32], for different strong groups and symmetry breaking patterns, generically "little Higgs" models [33] (see [34] for a review), and some higher dimensional scenarios can also be considered in the category of constructions in which the Higgs is a Goldstone boson. In the previous chapter we observed that in the linear expansion the Higgs boson is assumed to belong to an $SU(2)_L$ doublet and therefore the leading order operators extending the renormalizable SM are dimension–six operators suppressed by the NP scale Λ^2. Instead, in dynamical Higgs scenarios the Goldstone boson parenthood of the Higgs boson makes a non–linear or chiral expansion suitable [75]: a derivative expansion as corresponds to the Goldstone boson dynamics as sketched in Sec.1.2.2.

In this chapter we discuss the general chiral EFT valid for these realizations as outlined in [76]. In Sec. 3.1 we will present the Lagrangian introduced in Ref. [76], but our purpose will not be to work out the details of the construction which builds on previous works of some of the authors of that paper [35]. In Sec. 3.2 we will relate this chiral Lagrangian to that of the linear basis and the TGV effective parameterization of Eq. (2.38), and formulate possible discriminators between the two expansions. A global fit of Higgs data to the coefficients of the operators is left to Sec. 5.3 where we will also discuss the implications of the global fit on the discriminators developed in this chapter.

3.1 The Chiral Basis

As mentioned above we treat the Higgs as a composite field, in this case a pseudo–Goldstone boson of a new global symmetry which is exact at a high energy scale Λ_s. This new scale corresponds to that at which new resonances should appear, with the relative lightness of the Higgs being explained by its Goldstone−boson−like nature. We relax the requirement that the Higgs belong to a doublet of $SU(2)_L$ and our EFT expansion is no longer in inverse powers of Λ, but instead it is a derivative series (i.e. powers of p/Λ_s). The characteristic scale of the Goldstone bosons is identified as f which is distinguished from the electroweak scale, $v = 2m_W/g$, and the electroweak symmetry breaking scale, $\langle h \rangle$. The scale $\langle h \rangle$ is then associated with the scale

at which the Higgs develops a potential which, generically, at the loop level, breaks $SU(2)_L \times U(1)_Y$ to $U(1)_{\rm EM}$. These scales then respect the relation $\Lambda_s < 4\pi f$ while for particular models one can relate the three scales through a function g via $v = g(f, \langle h \rangle)$ (particular models are discussed in, for example, [77]). We then define the degree of non–linearity of the Higgs dynamics [35] via

$$\xi \equiv (v/f)^2, \tag{3.1}$$

where $\xi \to 1$ represents the technicolor-like scenario. This parameter will prove useful in the comparison of the linear and chiral expansions in Sec. 3.2.

In [35] a complete effective Lagrangian basis for pure gauge and gauge–Higgs operators up to four derivatives was presented. The particle content of the chiral Lagrangian includes all the SM fermions, gauge bosons, and the Higgs field h. The longitudinal degrees of freedom of the electroweak gauge bosons are included in the usual way for chiral theories, that is in a dimensionless unitary matrix transforming as a bi-doublet of the global symmetry:

$$\boldsymbol{U}(x) = \exp\left(i\tau_a \pi(x)^a / v\right), \qquad \boldsymbol{U} \to L\boldsymbol{U}(x)R^\dagger. \tag{3.2}$$

Here L and R are the $SU(2)_{L,R}$ global transformations respectively, and the τ_a the Pauli matrices. After EWSB the $SU(2)_{L,R}$ symmetries are broken down to custodial $SU(2)_C$, and subsequently explicitly broken by the gauge $U(1)_Y$ and by the fermionic masses. We note that the Higgs now transforms as a singlet of $SU(2)_L$ and Higgs insertions are now weighted by f instead of Φ/Λ in the linear case.

Again we assume that the observed 125 GeV boson is a CP-even state and in contrast to the linear case we will restrict ourselves strictly to bosonic operators with the exception of the Yukawa couplings of the SM. We then define the effective Lagrangian to order four derivatives as

$$\mathcal{L} = \mathcal{L}_0 + \mathcal{L}_{\rm eff}, \tag{3.3}$$

where $\mathcal{L}_0$ is the SM Lagrangian and we have chosen in this case to leave the sign of the Yukawa couplings open, which we will indicate by s_Y. Therefore

we write $\mathcal{L}_0$ in the usual chiral form (see Eq. (1.29)):

$$\begin{aligned}\mathcal{L}_0 &= \tfrac{1}{2}(\partial_\mu h)(\partial^\mu h) - \tfrac{1}{4}W^a_{\mu\nu}W^{a\mu\nu} - \tfrac{1}{4}B_{\mu\nu}B^{\mu\nu} - \tfrac{1}{4}G^a_{\mu\nu}G^{a\mu\nu} - V(h) \\ &+\tfrac{(v+h)^2}{4}\mathrm{Tr}\left[\boldsymbol{D}^\mu\boldsymbol{U}(\boldsymbol{D}_\mu\boldsymbol{U})^\dagger\right] + \mathcal{L}_{\text{fermion}} \\ &-\tfrac{v+s_Y h}{\sqrt{2}}\left(\bar{Q}_L\boldsymbol{U}\boldsymbol{y}_Q Q_R + \text{h.c.}\right) - \tfrac{v+s_Y h}{\sqrt{2}}\left(\bar{L}_L\boldsymbol{U}\boldsymbol{y}_L L_R + \text{h.c.}\right),\end{aligned} \tag{3.4}$$

with $\mathcal{L}_{\text{fermion}}$ given in Eq. (1.2).

The covariant derivative then takes the form:

$$\boldsymbol{D}_\mu\boldsymbol{U}(x) \equiv \partial_\mu\boldsymbol{U}(x) + \frac{i}{2}gW^a_\mu(x)\tau_a\boldsymbol{U}(x) - \frac{ig'}{2}B_\mu(x)\boldsymbol{U}(x)\tau_3. \tag{3.5}$$

The first line of Eq. (3.4) shows the Higgs and gauge kinetic terms, along with the Higgs potential which induces spontaneous symmetry breaking. We do not specify the Higgs potential here as it is not relevant to our discussion. The second line then describes the W and Z masses and their interactions with the Higgs as well as the kinetic terms for the Goldstone bosons and the fermions. The third line corresponds to the SM Yukawa interactions with the sign of the Higgs coupling left open and encoded in $s_Y = \pm 1$. Quark mixing is implicitly assumed in the definition of Q_L. Here, as in Eq. (1.29), we have used a compact notation for the right–handed fields by using doublets Q_R and L_R thus placing $\boldsymbol{y}_Q$ and $\boldsymbol{y}_L$ in two 6×6 block-diagonal matrices containing the usual Yukawa couplings, $\boldsymbol{y}_Q \equiv \mathrm{diag}(y^u, y^d)$ and $\boldsymbol{y}_L \equiv \mathrm{diag}(0, y^e)$.

As described in Sec. 1.2.2 the expansion is in number of derivatives, corresponding to powers of p/Λ_s, which in the low momentum limit should correspond to a well defined perturbative series. Then $\mathcal{L}_{\text{eff}}$ to four derivatives takes the form,

$$\begin{aligned}\mathcal{L}_{\text{eff}} &= \xi\left[c_B\mathcal{P}_B(h) + c_W\mathcal{P}_W(h) + c_G\mathcal{P}_G(h) + c_C\mathcal{P}_C(h) + c_T\mathcal{P}_T(h)\right. \\ &\left.+c_H\mathcal{P}_H(h) + c_{\Box H}\mathcal{P}_{\Box H}(h)\right] + \xi\sum_{i=1}^{10}c_i\mathcal{P}_i(h) + \xi^2\sum_{i=11}^{25}c_i\mathcal{P}_i(h) \\ &+\xi^4 c_{26}\mathcal{P}_{26}(h) + \textstyle\sum_i \xi^{n_i}c^i_{HH}\mathcal{P}^i_{HH}(h),\end{aligned} \tag{3.6}$$

where the c_i are the model dependent constant coefficients corresponding to each operator. The last term accounts for the many possible pure Higgs operators weighted by ξ^{n_i} with $n_i \geq 2$. Then the set of pure–gauge and gauge–Higgs operators is defined by [35, 76][1]

Weighted by ξ:

$$\begin{aligned}
\mathcal{P}_C(h) &= -\tfrac{v^2}{4}\mathrm{Tr}(\boldsymbol{V}^\mu \boldsymbol{V}_\mu)\mathcal{F}_C & \mathcal{P}_4 &= ig' B_{\mu\nu}\mathrm{Tr}(\boldsymbol{T}\boldsymbol{V}^\mu)\partial^\nu \mathcal{F}_4 \\
\mathcal{P}_T(h) &= \tfrac{v^2}{4}\mathrm{Tr}(\boldsymbol{T}\boldsymbol{V}_\mu)\mathrm{Tr}(\boldsymbol{T}\boldsymbol{V}^\mu)\mathcal{F}_T & \mathcal{P}_5 &= ig\mathrm{Tr}(W_{\mu\nu}\boldsymbol{V}^\mu)\partial^\nu \mathcal{F}_5 \\
\mathcal{P}_B(h) &= -\tfrac{g'^2}{4}B_{\mu\nu}B^{\mu\nu}\mathcal{F}_B & \mathcal{P}_6 &= (\mathrm{Tr}(\boldsymbol{V}_\mu \boldsymbol{V}^\mu))^2 \mathcal{F}_6 \\
\mathcal{P}_W(h) &= -\tfrac{g^2}{4}W^a_{\mu\nu}W^{a\mu\nu}\mathcal{F}_W & \mathcal{P}_7 &= \mathrm{Tr}(\boldsymbol{V}_\mu \boldsymbol{V}^\mu)\partial_\nu \partial^\nu \mathcal{F}_7 \\
\mathcal{P}_G(h) &= -\tfrac{g_s^2}{4}G^a_{\mu\nu}G^{a\mu\nu}\mathcal{F}_G & \mathcal{P}_8 &= \mathrm{Tr}(\boldsymbol{V}_\mu \boldsymbol{V}_\nu)\partial^\mu \mathcal{F}_8 \partial^\nu \mathcal{F}'_8 \\
\mathcal{P}_1(h) &= gg' B_{\mu\nu}\mathrm{Tr}(\boldsymbol{T}W^{\mu\nu})\mathcal{F}_1 & \mathcal{P}_9 &= \mathrm{Tr}((\mathcal{D}_\mu \boldsymbol{V}^\mu)^2)\mathcal{F}_9 \\
\mathcal{P}_2(h) &= ig' B_{\mu\nu}\mathrm{Tr}(\boldsymbol{T}[\boldsymbol{V}^\mu, \boldsymbol{V}^\nu])\mathcal{F}_2 & \mathcal{P}_{10} &= \mathrm{Tr}(\boldsymbol{V}_\nu \mathcal{D}_\mu \boldsymbol{V}^\mu)\mathcal{F}_{10} \\
\mathcal{P}_3(h) &= ig\mathrm{Tr}(W_{\mu\nu}[\boldsymbol{V}^\mu, \boldsymbol{V}^\nu])\mathcal{F}_3
\end{aligned} \tag{3.7}$$

Weighted by ξ^2:

$$\begin{aligned}
&\mathcal{P}_{11} = (\mathrm{Tr}(\boldsymbol{V}_\mu \boldsymbol{V}_\nu))^2 \mathcal{F}_{11} && \mathcal{P}_{19} = \mathrm{Tr}(\boldsymbol{T}\mathcal{D}_\mu \boldsymbol{V}^\mu)\mathrm{Tr}(\boldsymbol{T}\boldsymbol{V}_\nu)\partial^\nu \mathcal{F}_{19} \\
&\mathcal{P}_{12} = g^2(\mathrm{Tr}(\boldsymbol{T}W_{\mu\nu}))^2 \mathcal{F}_{12} && \mathcal{P}_{20} = \mathrm{Tr}(\boldsymbol{V}_\mu \boldsymbol{V}^\mu)\partial_\nu \mathcal{F}_{20} \partial^\nu \mathcal{F}'_{20} \\
&\mathcal{P}_{13} = ig\mathrm{Tr}(\boldsymbol{T}W_{\mu\nu})\mathrm{Tr}(\boldsymbol{T}[\boldsymbol{V}^\mu, \boldsymbol{V}^\nu])\mathcal{F}_{13} && \mathcal{P}_{21} = (\mathrm{Tr}(\boldsymbol{T}\boldsymbol{V}_\mu))^2 \partial_\nu \mathcal{F}_{21} \partial^\nu \mathcal{F}'_{21} \\
&\mathcal{P}_{14} = g\epsilon^{\mu\nu\rho\lambda}\mathrm{Tr}(\boldsymbol{T}\boldsymbol{V}_\mu)\mathrm{Tr}(\boldsymbol{V}_\nu W_{\rho\lambda})\mathcal{F}_{14} && \mathcal{P}_{22} = \mathrm{Tr}(\boldsymbol{T}\boldsymbol{V}_\mu)\mathrm{Tr}(\boldsymbol{T}\boldsymbol{V}_\nu)\partial^\mu \mathcal{F}_{22} \partial^\nu \mathcal{F}'_{22} \\
&\mathcal{P}_{15} = \mathrm{Tr}(\boldsymbol{T}\mathcal{D}_\mu \boldsymbol{V}^\mu)\mathrm{Tr}(\boldsymbol{T}\mathcal{D}_\nu \boldsymbol{V}^\nu)\mathcal{F}_{15} && \mathcal{P}_{23} = \mathrm{Tr}(\boldsymbol{V}_\mu \boldsymbol{V}^\mu)(\mathrm{Tr}(\boldsymbol{T}\boldsymbol{V}_\nu))^2 \mathcal{F}_{23} \\
&\mathcal{P}_{16} = \mathrm{Tr}([\boldsymbol{T}, \boldsymbol{V}_\nu]\mathcal{D}_\mu \boldsymbol{V}^\mu)\mathrm{Tr}(\boldsymbol{T}\boldsymbol{V}^\nu)\mathcal{F}_{16} && \mathcal{P}_{24} = \mathrm{Tr}(\boldsymbol{V}_\mu \boldsymbol{V}_\nu)\mathrm{Tr}(\boldsymbol{T}\boldsymbol{V}^\mu)\mathrm{Tr}(\boldsymbol{T}\boldsymbol{V}^\nu)\mathcal{F}_{24} \\
&\mathcal{P}_{17} = ig\mathrm{Tr}(\boldsymbol{T}W_{\mu\nu})\mathrm{Tr}(\boldsymbol{T}\boldsymbol{V}^\mu)\partial^\nu \mathcal{F}_{17} && \mathcal{P}_{25} = (\mathrm{Tr}(\boldsymbol{T}\boldsymbol{V}_\mu))^2 \partial_\nu \partial^\nu \mathcal{F}_{25} \\
&\mathcal{P}_{18} = \mathrm{Tr}(\boldsymbol{T}[\boldsymbol{V}_\mu, \boldsymbol{V}_\nu])\mathrm{Tr}(\boldsymbol{T}\boldsymbol{V}^\mu)\partial^\nu \mathcal{F}_{18}
\end{aligned} \tag{3.8}$$

Weighted by ξ^4:

$$\mathcal{P}_{26}(h) = (\mathrm{Tr}(\boldsymbol{T}\boldsymbol{V}_\mu)\mathrm{Tr}(\boldsymbol{T}\boldsymbol{V}_\nu))^2 \mathcal{F}_{26} \tag{3.9}$$

Where we have made use of the covariant derivative,

$$\mathcal{D}_\mu \boldsymbol{V}_\nu \equiv \partial_\mu \boldsymbol{V}_\nu + ig\left[W^a_\mu \frac{\sigma_a}{2}, \boldsymbol{V}_\nu\right], \tag{3.10}$$

and we have introduced $\boldsymbol{V}_\mu \equiv (\boldsymbol{D}_\mu \boldsymbol{U})\boldsymbol{U}^\dagger$, known as the vector chiral field,

[1] Here we have suppressed the h dependence of $\mathcal{F}_i$:, i.e. $\mathcal{F}_i(h) = \mathcal{F}_i$.

and we also define the scalar field $\boldsymbol{T} \equiv \boldsymbol{U}\tau_3\boldsymbol{U}^\dagger$ the scalar chiral field, which transform in the adjoint of $SU(2)_L$. In all cases $\mathcal{F}_i(h)$ is an arbitrary function of h (see Eq. (3.12) below).

Finally the two pure Higgs operators weighted by ξ include:

$$\mathcal{P}_H(h) = \frac{1}{2}(\partial_\mu h)(\partial^\mu h)\mathcal{F}_H(h), \qquad \text{and} \qquad \mathcal{P}_{\Box H} = \frac{1}{v^2}(\partial_\mu\partial^\mu h)^2\mathcal{F}_{\Box H}(h). \quad (3.11)$$

Notice that we have slightly adjusted our power counting in a data–driven manner, that is we have taken $\mathcal{L}_0$ to be leading order, but we allow for two–derivative operators in $\mathcal{L}_{\text{eff}}$: for example $\text{Tr}(\boldsymbol{T}\boldsymbol{V}_\mu)\text{Tr}(\boldsymbol{T}\boldsymbol{V}^\mu)$) is a two derivative operator known to break custodial symmetry, and as such is well constrained by data, therefore we move it to the next order Lagrangian.

There are additional Higgs operators weighted by $\xi \geq 2$, however they will not be relevant to our analysis as their corresponding Feynman rules contain too many Higgs legs. Some are briefly discussed in [76].

As in the linear basis the operator $\mathcal{P}_{\Box H}$ can be removed by the EOM. We include this operator here only for the purpose of identifying at what order in ξ it occurs as neglecting it leads to accidental miscounting for other operators in the basis. For the remainder of this dissertation we neglect to include $\mathcal{P}_{\Box H}$ in our discussion as it has no bearing on our results. Further details may be found in [40, 76].

The reduced symmetry of the Higgs implies more possible invariant operators at any given order. These can be seen in the fact that in the nonlinear realization the chiral symmetry breaking interactions of h now come in the form of arbitrary functions $\mathcal{F}(h)$, instead of powers of $(v + h)$. Additionally there is a shuffling of the order at which operators occur in the chiral Lagrangian relative to that of the linear [35, 78, 79] and consequently a higher number of uncorrelated couplings are present in the leading corrections of the chiral Lagrangian which were subleading in the Linear (i.e. occurring at operator dimension $d \geq 8$).

3.2 Relating the Chiral and Linear Expansions

We begin by stressing that the weights in ξ do not reflect an expansion in terms of ξ. ξ proves useful for relating the chiral and linear expansions. We define

a "sibling" of a chiral operator $\mathcal{P}_i(h)$ as the operator of the linear expansion whose pure gauge interactions coincide with those described by $\mathcal{P}_i(h)$. The canonical dimension d of the sibling is related to the power of ξ^n as $d = 4+2n$ and therefore ξ^n acts as an indicator of to which order in the linear expansion it is necessary and sufficient to expand in order to account for the same gauge interactions of the given chiral operator. More specifically the chiral operator's weight in ξ corresponds to the lowest dimension to which one must expand in linear operators to reproduce the chiral operator's gauge interactions. Therefore it follows the lowest order in the linear expansion to which we must expand to obtain the siblings of the operators in Eqs. (3.7) and (3.11) is $d = 6$, while for Eq. (3.8) we must expand to $d = 8$ and for Eq. (3.9) to dimension $d = 12$. Therefore ξ has no physical meaning in the context of the effective Lagrangian and could be reabsorbed into the definition of the coefficients c_i.

We note that in comparison with the linear basis where the Higgs enters in powers of $(v + h)$, it is now introduced via the functions $\mathcal{F}_i(h)$. Each of these functions can be defined as,

$$\mathcal{F}(h) \equiv g_0(h, v) + \xi g_1(h, v) + \xi^2 g_2(h, v) + \cdots \quad , \tag{3.12}$$

where the g_i are model dependent functions of h and v once $\langle h \rangle$ has been reexpressed in terms of ξ and v. For our current work we will assume a general polynomial form of the g_i taking the general form:

$$\mathcal{F}_i(h) \equiv 1 + 2\tilde{a}_i \frac{h}{v} + \tilde{b}_i \frac{h^2}{v^2} + \cdots \quad . \tag{3.13}$$

We will treat the $\tilde{a}_i$ and $\tilde{b}_i$ as unknown phenomenological parameters for the fit performed in Chapter 5.

In order to compare the two expansions we need to consider the limit in which they should converge. Recalling that ξ helps to parameterize the degree to which the expansion is nonlinear we expect the two expansions to be equivalent for $\xi \to 0$. Therefore we can truncate the chiral expansion at $\mathcal{O}(\xi)$ and compare the operators which contribute to gauge–Higgs interactions with those of the linear expansion at $d = 6$. The linear basis then contains ten independent couplings (see Eq. (2.2) and Eq. (2.5) noting $\mathcal{O}_{WWW}$ and $\mathcal{O}_{\Phi,3}$ do not contribute to gauge–Higgs interactions) while the chiral depends on

seventeen (those of Eqs. (3.7) and (3.11)). For the purpose of comparison we consider $\mathcal{F}_i(h) = (1 + h/v)^2$ for all $\mathcal{P}_i$ which leads to the relations:

$$\begin{aligned}
\mathcal{O}_{BB} &= \tfrac{v^2}{2}\mathcal{P}_B(h), & \mathcal{O}_{WW} &= \tfrac{v^2}{2}\mathcal{P}_W(h), \\
\mathcal{O}_{GG} &= -\tfrac{2v^2}{g_s^2}\mathcal{P}_G(h), & \mathcal{O}_{BW} &= \tfrac{v^2}{8}\mathcal{P}_1(h), \\
\mathcal{O}_{B} &= \tfrac{v^2}{16}\mathcal{P}_2(h) + \tfrac{v^2}{8}\mathcal{P}_4(h), & \mathcal{O}_{W} &= \tfrac{v^2}{8}\mathcal{P}_3(h) - \tfrac{v^2}{4}\mathcal{P}_5(h), \\
\mathcal{O}_{\Phi,1} &= \tfrac{v^2}{2}\mathcal{P}_H(h) - \tfrac{v^2}{4}\mathcal{F}(h)\mathcal{P}_T(h), & \mathcal{O}_{\Phi,2} &= v^2\mathcal{P}_H(h), \\
\mathcal{O}_{\Phi,4} &= \tfrac{v^2}{2}\mathcal{P}_H(h) + \tfrac{v^2}{2}\mathcal{F}(h)\mathcal{P}_C(h), & & \\
\mathcal{O}_{\Box\Phi} &= \tfrac{v^2}{2}\mathcal{P}_{\Box H}(h) + \tfrac{v^2}{8}\mathcal{P}_6(h) + \tfrac{v^2}{4}\mathcal{P}_7(h) - v^2\mathcal{P}_8(h) - \tfrac{v^2}{4}\mathcal{P}_9(h) - \tfrac{v^2}{2}\mathcal{P}_{10}(h)\ . & &
\end{aligned} \tag{3.14}$$

We note that these relations indicate that the five chiral operators $\mathcal{P}_B$, $\mathcal{P}_W$, $\mathcal{P}_G$, $\mathcal{P}_1$, and $\mathcal{P}_H$ are in one−to−one correspondence with the linear operators $\mathcal{O}_{BB}$, $\mathcal{O}_{WW}$, $\mathcal{O}_{GG}$, $\mathcal{O}_{BW}$, and $\mathcal{O}_{\Phi,2}$ respectively. While $\mathcal{P}_T$ ($\mathcal{P}_C$) correspond to linear combinations of $\mathcal{O}_{\Phi,1}$ and $\mathcal{O}_{\Phi,2}$ ($\mathcal{O}_{\Phi,4}$ and $\mathcal{O}_{\Phi,2}$). Conversely we note $\mathcal{O}_B$ ($\mathcal{O}_W$) corresponds to a specific combination of the chiral operators $\mathcal{P}_2$ and $\mathcal{P}_4$ ($\mathcal{P}_3$ and $\mathcal{P}_5$). In order to break these last correlations in the linear expansion we must consider operators at the next order, i.e. $d = 8$, such as:

$$\left((D_\mu\Phi)^\dagger\Phi\right)\hat{B}^{\mu\nu}\left(\Phi^\dagger D_\nu\Phi\right) \qquad \text{and} \qquad \left((D_\mu\Phi)^\dagger\Phi\right)\hat{W}^{\mu\nu}\left(\Phi^\dagger D_\nu\Phi\right). \tag{3.15}$$

In fact we will shortly consider how to use this difference to construct observables which may aid in identifying the underlying dynamics of the observed Higgs–like resonance.

3.3 Effective Vertices

As was the case in Chapter 2, the chiral operators will introduce wave function renormalizations for the various SM field content, along with renormalization of the parameters of the theory. We employ again the Z–scheme taking as input parameters $\alpha_{\rm EM}$, α_s, G_F, M_Z, and M_H. Then in the following expressions if the other parameters, such as g, g', v, e, or the mixing angle, are used they must be expressed in terms of these input parameters. Recalling Eq. (3.13)

we will further simplify the notation by using,

$$a_i \equiv c_i \tilde{a}_i, \qquad \text{and} \qquad b_i \equiv c_i \tilde{b}_i, \tag{3.16}$$

where the c_i are the operator coefficients of Eq. (3.6). Working in the unitary gauge we see that $\mathcal{P}_B$, $\mathcal{P}_W$, $\mathcal{P}_G$, $\mathcal{P}_H$, $\mathcal{P}_1$, and $\mathcal{P}_{12}$ introduce corrections to the SM kinetic terms and require field redefinitions to put the kinetic terms in the canonical form. These operators then affect the input parameters as:

$$\begin{aligned} \tfrac{\delta\alpha_{\rm EM}}{\alpha_{\rm EM}} &\sim 4e^2 c_1 \xi + 4e^2 c_{12} \xi^2, & \tfrac{\delta G_F}{G_F} &\sim 0, \\ \tfrac{\delta M_Z}{M_Z} &\sim -c_T \xi - 2e^2 c_1 \xi + 2e^2 \tfrac{c_{\rm W}^2}{s_{\rm W}^2} c_{12} \xi^2, & \tfrac{\delta M_H}{M_H} &\sim 0. \end{aligned} \tag{3.17}$$

Then the W–mass diverges from that of the SM as:

$$\frac{\Delta M_W^2}{M_W^2} = \frac{4e^2}{c_{2\rm W}} c_1 \xi + \frac{2c_{\rm W}^2}{c_{2\rm W}} c_T \xi - \frac{4e^2}{s_{\rm W}^2} c_{12} \xi^2. \tag{3.18}$$

As we would expect from their relation to $\mathcal{O}_{BW}$ and $\mathcal{O}_{\Phi,1}$, $\mathcal{P}_1$ and $\mathcal{P}_T$ generate tree level contributions to the oblique parameters S and T,

$$\alpha_{\rm EM} \Delta S = -8e^2 c_1 \xi \qquad \text{and} \qquad \alpha_{\rm EM} \Delta T = 2 c_T \xi. \tag{3.19}$$

We note that the operators $\mathcal{P}_7$, $\mathcal{P}_9$, and $\mathcal{P}_{10}$ induce additional terms in the HVV Lagrangian, beyond those in Eq. (2.18), such as:

$$\begin{aligned} \mathcal{L}'_{HVV} \equiv\ & g^{(4)}_{HZZ} Z_\mu Z^\mu \Box h + g^{(5)}_{HZZ} \partial_\mu Z^\mu Z_\nu \partial^\nu h + g^{(6)}_{HZZ} \partial_\mu Z^\mu \partial_\nu Z^\nu h \\ & + g^{(4)}_{HWW} W^+_\mu W^{-\mu} \Box h + g^{(5)}_{HWW} (\partial_\mu W^{+\mu} W^-_\nu \partial^\nu h + \text{h.c.}) \\ & + g^{(6)}_{HWW} \partial_\mu W^{+\mu} \partial_\nu W^{-\nu} h. \end{aligned} \tag{3.20}$$

The operators which are proportional to $\Box h$ become redundant for on shell Higgses and the those proportional to $\partial^\mu V$ vanish for on-shell W or Z or massless fermions. Therefore they will prove irrelevant to our analysis. We include in Tab. 3.1 the values of the coefficients for the HVV operators in Eqs. (2.18) and (3.20) in the chiral basis. We include the effects of the operators $\mathcal{P}_7$, $\mathcal{P}_9$, and $\mathcal{P}_{10}$ for completeness, however they will not be used in our analysis for the reasons above. For the sake of comparison we also include the

coefficients for the linear case as well. To simplify the table we employ the definition,

$$g_i^{(j)} \equiv g_i^{(j)\mathrm{SM}} + \Delta g_i^{(j)}, \tag{3.21}$$

i.e. we remove the SM part and only show in the table the anomalous contributions. TGV related coefficients are saved for the discussion in the next section.

	Coeff.	Chiral		Linear
	$\times e^2/4v$	$\times\xi$	$\times\xi^2$	$\times v^2/\Lambda^2$
Δg_{Hgg}	$\frac{g_s^2}{e^2}$	$-2a_G$	–	$-4f_{GG}$
$\Delta g_{H\gamma\gamma}$	1	$-2(a_B+a_W)+8a_1$	$8a_{12}$	$-(f_{BB}+f_{WW})+f_{BW}$
$\Delta g^{(1)}_{HZ\gamma}$	$\frac{1}{s_{2\mathrm{W}}}$	$-8(a_5+2a_4)$	$-16a_{17}$	$2(f_W-f_B)$
$\Delta g^{(2)}_{HZ\gamma}$	$\frac{c_\mathrm{W}}{s_\mathrm{W}}$	$4\frac{s^2_\mathrm{W}}{c^2_\mathrm{W}}a_B-4a_W+8\frac{c_{2\mathrm{W}}}{c^2_\mathrm{W}}a_1$	$16a_{12}$	$2\frac{s^2_\mathrm{W}}{c^2_\mathrm{W}}f_{BB}-2f_{WW}+\frac{c_{2\mathrm{W}}}{c^2_\mathrm{W}}f_{BW}$
$\Delta g^{(1)}_{HZZ}$	$\frac{1}{c^2_\mathrm{W}}$	$-4\frac{c^2_\mathrm{W}}{s^2_\mathrm{W}}a_5+8a_4$	$-8\frac{c^2_\mathrm{W}}{s^2_\mathrm{W}}a_{17}$	$\frac{c^2_\mathrm{W}}{s^2_\mathrm{W}}f_W+f_B$
$\Delta g^{(2)}_{HZZ}$	$-\frac{c^2_\mathrm{W}}{s^2_\mathrm{W}}$	$2\frac{s^4_\mathrm{W}}{c^4_\mathrm{W}}a_B+2a_W+8\frac{s^2_\mathrm{W}}{c^2_\mathrm{W}}a_1$	$-8a_{12}$	$\frac{s^4_\mathrm{W}}{c^4_\mathrm{W}}f_{BB}+f_{WW}+\frac{s^2_\mathrm{W}}{c^2_\mathrm{W}}f_{BW}$
$\Delta g^{(3)}_{HZZ}$	$\frac{m_Z^2}{e^2}$	$-2c_H+2(2a_C-c_C)-8(a_T-c_T)$	–	$f_{\Phi,1}+2f_{\Phi,4}-2f_{\Phi,2}$
$\Delta g^{(4)}_{HZZ}$	$-\frac{1}{s^2_{2\mathrm{W}}}$	$16a_7$	$32a_{25}$	–
$\Delta g^{(5)}_{HZZ}$	$-\frac{1}{s^2_{2\mathrm{W}}}$	$16a_{10}$	$32a_{19}$	–
$\Delta g_{HZZ}s^{(6)}$	$-\frac{1}{s^2_{2\mathrm{W}}}$	$16a_9$	$32a_{15}$	–
$\Delta g^{(1)}_{HWW}$	$\frac{1}{s^2_\mathrm{W}}$	$-4a_5$	–	f_W
$\Delta g^{(2)}_{HWW}$	$\frac{1}{s^2_\mathrm{W}}$	$-4a_W$	–	$-2f_{WW}$
$\Delta g^{(3)}_{HWW}$	$\frac{m_Z^2c^2_\mathrm{W}}{e^2}$	$-4c_H+4(2a_C-c_C)+32\frac{e^2}{c_{2\mathrm{W}}}c_1+\frac{16c^2_\mathrm{W}}{c_{2\mathrm{W}}}c_T$	$-32\frac{e^2}{s^2_\mathrm{W}}c_{12}$	$-2\frac{(3c^2_\mathrm{W}-s^2_\mathrm{W})}{c_{2\mathrm{W}}}f_{\Phi,1}+4f_{\Phi,4}-4f_{\Phi,2}+4\frac{e^2}{c_{2\mathrm{W}}}f_{BW}$
$\Delta g^{(4)}_{HWW}$	$-\frac{1}{s^2_\mathrm{W}}$	$8a_7$	–	–
$\Delta g^{(5)}_{HWW}$	$-\frac{1}{s^2_\mathrm{W}}$	$4a_{10}$	–	–
$\Delta g^{(6)}_{HWW}$	$-\frac{1}{s^2_\mathrm{W}}$	$8a_9$	–	–

Table 3.1: The trilinear Higgs–gauge boson couplings defined in Eq. (2.18). The coefficients in the second column are common to both the chiral and linear expansions. The contributions from the operators weighted by ξ and ξ^2 are listed in the third and fourth columns respectively. For comparison, the last column shows the corresponding expressions for the linear expansion at order d=6.

In our analysis in Chapter 5 we will consider the constraints on the ξ–weighted operators from the presently available Higgs data. After eliminating operators whose contribution cancels for on–shell Higgs and/or light external fermions, and considering the strong constraints on $\mathcal{P}_T$ and $\mathcal{P}_1$ from the S and T parameters, the basis of 15 operators in Eq. (3.7) is greatly reduced, and the relevant operators for our analysis are:

$$\mathcal{P}_G,\ \ \mathcal{P}_4,\ \ \mathcal{P}_5,\ \ \mathcal{P}_B,\ \ \mathcal{P}_W,\ \ \mathcal{P}_H,\ \ \text{and}\ \ \mathcal{P}_C. \tag{3.22}$$

3.4 Discriminating Signatures

Before we move on to the analysis framework and results we briefly discuss the implications of the chiral basis for TGVs and by considering the relations in Eq. (3.14) we construct discriminants between the two expansions. We begin by parameterizing the effects of the chiral basis on the form of Eq. (2.38) in Tab. 3.2, including two new Lorentz structures for the TGV Lagrangian here:

$$\begin{aligned}\mathcal{L}'_{WWV} &= -ig_{WWV}[-ig_5^V\epsilon^{\mu\nu\rho\sigma}(W^+_\mu\partial_\rho W^-_\nu - W^-_\nu\partial_\rho W^+_\mu)V_\sigma \\ &\qquad + g_6^V(\partial_\mu W^{+\mu}W^{-\nu} - \partial_\mu W^{-\mu}W^{+\nu})V_\nu].\end{aligned} \tag{3.23}$$

In Tab. 3.2 we have used the definitions

$$\begin{gathered}\Delta g_1^Z = g_1^Z - 1, \qquad \Delta\kappa_\gamma = \kappa_\gamma - 1, \qquad \Delta\kappa_Z = \kappa_Z - 1, \\ \Delta g_6^\gamma = g_6^\gamma, \qquad \Delta g_6^Z = g_6^Z, \qquad \Delta g_5^Z = g_5^Z.\end{gathered} \tag{3.24}$$

	Coeff.	Chiral		Linear
	$\times e^2/s^2_{\rm W}$	$\times\xi$	$\times\xi^2$	$\times v^2/\Lambda^2$
$\Delta\kappa_\gamma$	1	$-2c_1+2c_2+c_3$	$-4c_{12}+2c_{13}$	$\frac{1}{8}(f_W+f_B-2f_{BW})$
Δg_6^γ	1	$-c_9$	–	–
Δg_1^Z	$\frac{1}{c^2_{\rm W}}$	$\frac{s^2_{2\rm W}}{4e^2c_{2\rm W}}c_T+2\frac{s^2_{\rm W}}{c_{2\rm W}}c_1+c_3$	–	$\frac{1}{8}f_W+\frac{s^2_{\rm W}}{4c_{2\rm W}}f_{BW}-\frac{s^2_{2\rm W}}{16e^2c_{2\rm W}}f_{\Phi,1}$
$\Delta\kappa_Z$	1	$\frac{s^2_{\rm W}}{e^2c_{2\rm W}}c_T+4\frac{s^2_{\rm W}}{c_{2\rm W}}c_1-2\frac{s^2_{\rm W}}{c^2_{\rm W}}c_2+c_3$	$-4c_{12}+2c_{13}$	$\frac{1}{8}f_W-\frac{s^2_{\rm W}}{8c^2_{\rm W}}f_B+\frac{s^2_{\rm W}}{2c_{2\rm W}}f_{BW}-\frac{s^2_{\rm W}}{4e^2c_{2\rm W}}f_{\Phi,1}$
Δg_5^Z	$\frac{1}{c^2_{\rm W}}$	–	c_{14}	–
Δg_6^Z	$\frac{1}{c^2_{\rm W}}$	$s^2_{\rm W}c_9$	$-c_{16}$	–

Table 3.2: Effective couplings parameterizing the VW^+W^- vertices defined in Eqs. (2.38) and (3.23). The coefficients in the second column are common to both the chiral and linear expansions. In the third and fourth columns the specific contributions from the operators in the chiral Lagrangian are shown. For comparison the last column shows the corresponding contributions from the linear d=6 operators.

There are two main effects which are clearly distinct between the two expansions with respect to TGV and HVV couplings which we discuss next.

3.4.1 Differences in TGV

From the results in Tab. 3.2 we see that there are Lorentz structures in the TGV vertex which appear at leading order in one expansion while subleading in the others. For example $\mathcal{O}_{WWW}$ contributes at the tree level to the

anomalous TGV as parameterized in Eq. (2.38) by λ_V, however this coupling does not receive contributions from any of the non–linear operators up to four derivatives. Consequently the strength of the contributions to λ_V in the non–linear case are expected to be suppressed with respect to the other effective couplings ($\Delta\kappa_{\gamma,Z}$ and Δg_1^Z). On the contrary in the linear case the strength of the λ_V contributions could have the same size as those of all other effective couplings. Therefore, a measurement of an anomalous TGV signal compatible with λ_V, which is the anomalous TGV with the most striking high energy signature as we will see in the following, would point to a fundamental Higgs boson.

Conversely in the chiral expansion and for large ξ all chiral operators weighted by ξ^n with $n \geq 2$ are equally relevant to the ξ–weighted operators. However their siblings require operators of dimension $d \geq 8$ in the linear expansion. A case of special interest is $\mathcal{P}_{14}(h)$ which generates a contribution to the g_5^Z effective vertex in Eq. (3.23) (see Tab. 3.2) which is absent both in the SM Lagrangian and in the linear expansion up to dimension–six. This fact provides a viable strategy to test the nature of the physical Higgs which we quantify in Sec. 5.4.2.

3.4.2 (De)correlation Between HVV and TGV

As we have mentioned briefly before, the relations between HVV and TGV are different in the two expansions. We will recall the relation between $\mathcal{O}_B$ and $\mathcal{O}_W$ and the chiral operators $\mathcal{P}_2$, $\mathcal{P}_3$, $\mathcal{P}_4$, and $\mathcal{P}_5$:

$$\mathcal{O}_B = \frac{v^2}{16}\mathcal{P}_2(h) + \frac{v^2}{8}\mathcal{P}_4(h), \qquad \text{and} \qquad \mathcal{O}_W = \frac{v^2}{8}\mathcal{P}_3(h) - \frac{v^2}{4}\mathcal{P}_5(h). \tag{3.25}$$

Focusing on $\mathcal{O}_B$, in the unitary gauge we may expand $\mathcal{P}_2(h)$ and $\mathcal{P}_4(h)$ finding:

$$\begin{aligned} \mathcal{P}_2(h) &= 2ieg^2 A_{\mu\nu}W^{-\mu}W^{+\nu}\mathcal{F}_2(h) - 2\tfrac{ie^2g}{c_{\mathrm{W}}}Z_{\mu\nu}W^{-\mu}W^{+\nu}\mathcal{F}_2(h), \\ \mathcal{P}_4(h) &= -\tfrac{eg}{c_{\mathrm{W}}}A_{\mu\nu}Z^{\mu}\partial^{\nu}\mathcal{F}_4(h) + \tfrac{e^2}{c_{\mathrm{W}}^2}Z_{\mu\nu}Z^{\mu}\partial^{\nu}\mathcal{F}_4(h). \end{aligned} \tag{3.26}$$

Expanding $\mathcal{O}_B$, their $d=6$ sibling, we find similar Lorentz and field structures:

$$\begin{aligned}\mathcal{O}_B &= \tfrac{ieg^2}{8}A_{\mu\nu}W^{-\mu}W^{+\nu}(v+h)^2 - \tfrac{ie^2g}{8c_{\rm W}}Z_{\mu\nu}W^{-\mu}W^{+\nu}(v+h)^2 \\ &\quad -\tfrac{eg}{4c_{\rm W}}A_{\mu\nu}Z^{\mu}\partial^{\nu}h(v+h) + \tfrac{e^2}{4c_{\rm W}^2}Z_{\mu\nu}Z^{\mu}\partial^{\nu}h(v+h).\end{aligned} \tag{3.27}$$

From this we notice that in the linear case the Lorentz structures present in $\mathcal{P}_2$ and $\mathcal{P}_4$ are correlated, whereas in the chiral case they are independently tuned by the corresponding operator coefficients c_2 and c_4. In particular the Chiral basis allows for the decorrelation of:

- γWW from γZh and ZWW from ZZh vertices, these are examples of interactions involving different numbers of external h legs.
- γWWh from γZh and $ZWWh$ from ZZh; examples of interactions involving the same number of h legs.

While these decorrelations are expected in the leading deviations from the SM in the chiral approach, they require the inclusion of the next order (i.e. $d=8$) operators in the linear approach. This observation allows us to create useful discriminators between the chiral and linear expansions from the relations in Eq. (3.25).

Given that the linear expansion requires the relations:

$$2c_2 = a_4, \qquad \text{and} \qquad 2c_3 = -a_5. \tag{3.28}$$

We define Σ_B and Σ_W such that they quantify the divergence from the SM behavior of the Higgs data considered, and define Δ_B and Δ_W as discriminators between the linear and chiral expansions via the correlation (possible decorrelation) that each one exhibits:

$$\begin{aligned}\Sigma_B &\equiv 4(2c_2+a_4), \qquad \Sigma_W \equiv 2(2c_3-a_5), \\ \Delta_B &\equiv 4(2c_2-a_4), \qquad \Delta_W \equiv 2(2c_3+a_5).\end{aligned} \tag{3.29}$$

Notice that this implies that for a Higgs behaving as a part of the linear expansion $\Sigma_{B(W)} \to f_{B(W)}/\Lambda^2$ and $\Delta_B = \Delta_W \to 0$. We return to these discriminators and the set of operators in Eq. (3.22) in Sec. 5.3, where we will

make use of the relevant Higgs data from the LHC and Tevatron to constrain their allowed values.

3.4.3 Quartic Gauge Boson Couplings

The quartic gauge boson couplings also receive contributions from the operators in Eqs. (3.7)-(3.9). The corresponding effective Lagrangian reads

$$\begin{aligned}\mathcal{L}_{4X} \equiv g^2 \Big\{ & g^{(1)}_{ZZ}(Z_\mu Z^\mu)^2 + g^{(1)}_{WW} W^+_\mu W^{+\mu} W^-_\nu W^{-\nu} - g^{(2)}_{WW}(W^+_\mu W^{-\mu})^2 \\ & + g^{(3)}_{VV'} W^{+\mu} W^{-\nu} \left(V_\mu V'_\nu + V'_\mu V_\nu\right) - g^{(4)}_{VV'} W^+_\nu W^{-\nu} V^\mu V'_\mu \\ & + i g^{(5)}_{VV'} \varepsilon^{\mu\nu\rho\sigma} W^+_\mu W^-_\nu V_\rho V'_\sigma \Big\}, \end{aligned} \tag{3.30}$$

where $VV' = \{\gamma\gamma, \gamma Z, ZZ\}$. Notice that all these couplings are C and P even, except for $g^{(5)}_{VV'}$ that is CP–even but both C– and P–odd. Some of these couplings are nonvanishing at tree-level in the SM:

$$\begin{aligned} g^{(1)SM}_{WW} &= \frac{1}{2}\,, & g^{(2)SM}_{WW} &= \frac{1}{2}\,, & g^{(3)SM}_{ZZ} &= \frac{c^2_{\rm W}}{2}\,, & g^{(3)SM}_{\gamma\gamma} &= \frac{s^2_{\rm W}}{2}\,, \\ g^{(3)SM}_{Z\gamma} &= \frac{s_{2\rm W}}{2}\,, & g^{(4)SM}_{ZZ} &= c^2_{\rm W}\,, & g^{(4)SM}_{\gamma\gamma} &= s^2_{\rm W}\,, & g^{(4)SM}_{Z\gamma} &= s_{2\rm W}\,. \end{aligned} \tag{3.31}$$

Table 3.3 shows the contributions to the effective quartic couplings from the chiral operators and from the linear operators in Eq. (2.2). As can be seen by comparing Tabs. 3.3 and 3.2, in the chiral expansion several operators weighted by ξ or higher powers contribute to quartic gauge boson vertices without inducing any modification to TGVs. Therefore, their coefficients are much less constrained at present, and one can still expect larger deviations on future studies of quartic vertices at LHC for large values of ξ. This is unlike in the linear expansion, in which the modifications of quartic gauge couplings that do not induce changes to TGVs appear only when the $d = 8$ operators are considered [80]. We will discuss in Sec. 5.4.3 the present status on the bounds of these effects.

	Coeff.	Chiral		Linear
	$\times e^2/4s_{\rm W}^2$	$\times\xi$	$\times\xi^2$	$\times v^2/\Lambda^2$
$\Delta g_{WW}^{(1)}$	1	$\frac{s_{2\rm W}^2}{e^2c_{2\rm W}}c_T+8\frac{s_{\rm W}^2}{c_{2\rm W}}c_1+4c_3$	$2c_{11}-16c_{12}+8c_{13}$	$\frac{f_W}{2}+\frac{s_{\rm W}^2}{c_{2\rm W}}f_{BW}-\frac{s_{2\rm W}^2}{4c_{2\rm W}e^2}f_{\Phi 1}$
$\Delta g_{WW}^{(2)}$	1	$\frac{s_{2\rm W}^2}{e^2c_{2\rm W}}c_T+8\frac{s_{\rm W}^2}{c_{2\rm W}}c_1+4c_3-4c_6$	$-2c_{11}-16c_{12}+8c_{13}$	$\frac{f_W}{2}+\frac{s_{\rm W}^2}{c_{2\rm W}}f_{BW}-\frac{s_{2\rm W}^2}{4c_{2\rm W}e^2}f_{\Phi 1}-\frac{1}{2}f_{\Box\Phi}$
$\Delta g_{ZZ}^{(1)}$	$\frac{1}{c_{\rm W}^4}$	c_6	$c_{11}+2c_{23}+2c_{24}+4c_{26}\xi^2$	$\frac{1}{8}f_{\Box\Phi}$
$\Delta g_{ZZ}^{(3)}$	$\frac{1}{c_{\rm W}^2}$	$\frac{s_{2\rm W}^2c_{\rm W}^2}{e^2c_{2\rm W}}c_T+2\frac{s_{2\rm W}^2}{c_{2\rm W}}c_1+4c_{\rm W}^2c_3-2s_{\rm W}^4c_9$	$2c_{11}+4s_{\rm W}^2c_{16}+2c_{24}$	$\frac{f_Wc_{\rm W}^2}{2}+\frac{s_{2\rm W}^2}{4c_{2\rm W}}f_{BW}-\frac{s_{2\rm W}^2c_{\rm W}^2}{4e^2c_{2\rm W}}f_{\Phi 1}+\frac{s_{\rm W}^4}{2}f_{\Box\Phi}$
$\Delta g_{ZZ}^{(4)}$	$\frac{1}{c_{\rm W}^2}$	$2\frac{s_{2\rm W}^2c_{\rm W}^2}{e^2c_{2\rm W}}c_T+4\frac{s_{2\rm W}^2}{c_{2\rm W}}c_1+8c_{\rm W}^2c_3-4c_6$	$-4c_{23}$	$f_Wc_{\rm W}^2+2\frac{s_{2\rm W}^2}{4c_{2\rm W}}f_{BW}-\frac{s_{2\rm W}^2c_{\rm W}^2}{2e^2c_{2\rm W}}f_{\Phi 1}-\frac{1}{2}f_{\Box\Phi}$
$\Delta g_{\gamma\gamma}^{(3)}$	$s_{\rm W}^2$	$-2c_9$	–	$\frac{1}{2}f_{\Box\Phi}$
$\Delta g_{\gamma Z}^{(3)}$	$\frac{s_{\rm W}}{c_{\rm W}}$	$\frac{s_{2\rm W}^2}{e^2c_{2\rm W}}c_T+8\frac{s_{\rm W}^2}{c_{2\rm W}}c_1+4c_3+4s_{\rm W}^2c_9$	$-4c_{16}$	$\frac{f_W}{2}+\frac{s_{\rm W}^2}{c_{2\rm W}}f_{BW}-\frac{s_{2\rm W}^2}{4c_{2\rm W}e^2}f_{\Phi 1}-s_{\rm W}^2f_{\Box\Phi}$
$\Delta g_{\gamma Z}^{(4)}$	$\frac{s_{\rm W}}{c_{\rm W}}$	$2\frac{s_{2\rm W}^2}{e^2c_{2\rm W}}c_T+16\frac{s_{\rm W}^2}{c_{2\rm W}}c_1+8c_3$	–	$f_W+2\frac{s_{\rm W}^2}{c_{2\rm W}}f_{BW}-\frac{s_{2\rm W}^2}{2c_{2\rm W}e^2}f_{\Phi 1}$
$\Delta g_{\gamma Z}^{(5)}$	$\frac{s_{\rm W}}{c_{\rm W}}$	–	$8c_{14}$	–

Table 3.3: Effective couplings parametrizing the vertices of four gauge bosons defined in Eq. (3.30). The contributions from the operators weighted by ξ and $\xi^{\geq 2}$ are listed in the third and fourth columns, respectively. For comparison, the last column exhibits the corresponding expressions for the linear expansion at order $d = 6$ (see Eq. (A.6)).

3.5 Summary and Discussion

In this chapter we have discussed the effective Lagrangian relevant to a Higgs introduced as a pseudo–Goldstone boson which results from the breaking of a global symmetry of some new strong dynamics at a high energy scale. In this case EWSB is assumed to be non–linearly realized at low energies and the more appropriate expansion is that provided by chiral perturbation theory. Hence we have introduced the effective chiral Lagrangian to order four derivatives. Subsequently we have discussed the relation to the dimension–six effective Lagrangian in the linear realization of EWSB by invoking the parameter ξ, defined in Eq. (3.1) which helps to organize the chiral basis in terms of the order at which similar operators are introduced in the linear realization. In doing so we have pointed out the importance of the connection between TGV and HVV couplings, as well as quartic gauge boson couplings in discriminating between these two expansions. We will return to the present experimental constraints on the coefficients of the operators in the chiral basis and the discriminating signals in Chapter 5 when we apply the current Higgs and gauge boson scattering data to these discussions. In the next chapter we will

put together the analysis framework necessary for achieving this goal.

Chapter 4

The Analysis Framework

In this chapter we describe how to impose the constraints on our operator bases from the available data. In particular we discuss how to include information from the Higgs searches at the Tevatron and the Higgs results from the LHC taken in the 7 TeV and 8 TeV runs. Additionally we will include the data on the TGCs from LEP and the one–loop constraints from EWPD. Section 4.1 discusses the analysis framework for collider constraints, Sec. 4.2 discusses the framework for the inclusion of TGC data, and finally Sec. 4.3 puts together the framework for inclusion of EWPD. In Chapter 5 we will apply this analysis framework and give the results for both the linear basis (see Chapter 2) and the chiral basis (see Chapter 3).

4.1 Inclusion of Higgs Collider Data

In order to obtain the quantative information on the coefficients of the new operators from the Higgs data coming from both LHC and Tevatron experimental analyses we will make a chi–square test based on the signal strengths of the different available channels measured by the experiments (See Tabs. 4.1, 4.2 and 4.3). The signal strength for production of a final state F mediated by the Higgs boson is defined as the measured cross section for such a process divided by the expected cross section in the SM:

$$\mu_F = \frac{\sigma^{obs}(pp(p\bar{p}) \to H \to F)}{\sigma^{SM}(pp(p\bar{p}) \to H \to F)} \, . \tag{4.1}$$

In order to form our chi-square test we must predict the expected signal strengths in the presence of the new operators. In doing so we must consider both the effects of the operators on the production channels and the decay branching ratios. To simplify the calculation we will be assuming the narrow width approximation, which holds for Higgs widths sufficiently narrow compared with M_H, a well justified limit in the SM as well as given recent experimental bounds [81, 82]. In this approximation we will assume that for both SM and anomalous contributions,

$$\sigma(pp(p\bar{p}) \to H \to F) = \sigma(pp(p\bar{p}) \to H) \times \mathrm{Br}(H \to F), \tag{4.2}$$

where we have denoted as $\sigma(pp(p\bar{p}) \to H)$ the relevant production processes for a Higgs alone or in association with other particles. The main contributions to the Higgs production cross sections are from the following subprocesses which we label as indicated in parenthesis: gluon-fusion (gg), associate production of a Higgs with a gauge boson $V = Z, W$ (VH), production in gauge-boson fusion (VBF), or associated production with a pair of top quarks ($t\bar{t}H$). For illustration we show in Fig. 4.1 the cross sections for the dominant production processes in the SM at the LHC at 7 TeV. Regarding the decay modes, we show in Fig. 4.2 the SM branching ratios in the different final states.

For our analysis, and given the accessible public data, we assume that the correlations between the different sources of errors for the different channels are negligible except for the theoretical uncertainties which are treated with the pull method [91, 92] in order to account for their correlations. In this approach each source of uncertainty correlated between the different channels, is characterized by a "pull parameter" ξ_{pull} which modifies the corresponding theoretical prediction and which is allowed to vary within the expected range of the uncertainty σ_{pull}. Thus assuming that each such uncertainty is gaussian-distributed, the chi–square can be schematically written as

$$\chi^2 = \min_{\xi_{\mathrm{pull}}} \sum_j \frac{(\mu_j - \mu_j^{\mathrm{exp}})^2}{\sigma_j^2} + \sum_{\mathrm{pull}} \left(\frac{\xi_{\mathrm{pull}}}{\sigma_{\mathrm{pull}}} \right)^2 \quad , \tag{4.3}$$

where j stand for the different experimental channels considered. We present the different Tevatron and LHC (at 7 TeV and 8 TeV) data points in Tabs. 4.1,

Channel	μ^{exp}	comment
$p\bar{p} \to W^+W^-$	$0.94^{+0.85}_{-0.83}$	CDF & D0 [69]
$p\bar{p} \to \tau\bar{\tau}$	$1.68^{+2.28}_{-1.68}$	CDF & D0 [69]
$p\bar{p} \to b\bar{b}$	$1.59^{+0.69}_{-0.72}$	CDF & D0 [69]
$p\bar{p} \to \gamma\gamma$	$5.97^{+3.39}_{-3.12}$	CDF & D0 [69]
$pp \to \tau\bar{\tau}$	$0.7^{+0.7}_{-0.7}$	ATLAS @ 7 and 8 TeV [70]
$pp \to b\bar{b}$	$-2.1^{+1.4}_{-1.4}$	ATLAS @ 7 TeV [83]
$pp \to b\bar{b}$	$0.6^{+0.7}_{-0.7}$	ATLAS @ 8 TeV [83]
$pp \to ZZ^* \to \ell^+\ell^-\ell^+\ell^-$	$1.7^{+0.5}_{-0.4}$	ATLAS @ 7 and 8 TeV [84]
$pp \to WW^* \to \ell^+\nu\ell^-\bar{\nu}$	$0.0^{+0.6}_{-0.6}$	ATLAS @ 7 TeV [85]
$pp \to WW^* \to \ell^+\nu\ell^-\bar{\nu}$	$1.26^{+0.35}_{-0.35}$	ATLAS @ 8 TeV [85]
$pp \to Z\gamma \to \ell^+\ell^-\gamma$	$4.7^{+6.89}_{-6.89}$	ATLAS @ 7 and 8 TeV [86]
$pp \to \tau\bar{\tau}$	$1.1^{+0.4}_{-0.4}$	CMS @ 7 and 8 TeV [19]
$pp \to b\bar{b}$	$1.0^{+0.49}_{-0.49}$	CMS @ 7 and 8 TeV [87]
$pp \to b\bar{b}$ VBF	$0.7^{+1.4}_{-1.4}$	CMS @ 8 TeV [88]
$pp \to ZZ^* \to \ell^+\ell^-\ell^+\ell^-$	$0.91^{+0.30}_{-0.24}$	CMS @ 7 and 8 TeV [18]
$pp \to WW^* \to \ell^+\nu\ell^-\bar{\nu}$	$0.91^{+0.44}_{-0.44}$	CMS @ 7 TeV [89]
$pp \to WW^* \to \ell^+\nu\ell^-\bar{\nu}$	$0.71^{+0.22}_{-0.22}$	CMS @ 8 TeV [89]
$pp \to Z\gamma \to \ell^+\ell^-\gamma$	$-0.5^{+4.87}_{-4.87}$	CMS @ 7 and 8 TeV [90]

Table 4.1: Results included in the analysis for the Higgs decay modes listed except for the $\gamma\gamma$ channels.

	μ^{exp}	
Channel	7 TeV	8 TeV
Unconverted central, low p_{T_t}	$0.52^{+1.45}_{-1.40}$	$0.89^{+0.74}_{-0.71}$
Unconverted central, high p_{T_t}	$0.23^{+1.98}_{-1.98}$	$0.95^{+1.08}_{-0.92}$
Unconverted rest, low p_{T_t}	$2.56^{+1.69}_{-1.69}$	$2.52^{+0.92}_{-0.77}$
Unconverted rest, high p_{T_t}	$10.47^{+3.66}_{-3.72}$	$2.71^{+1.35}_{-1.14}$
Converted central, low p_{T_t}	$6.10^{+2.62}_{-2.62}$	$1.39^{+1.05}_{-0.95}$
Converted central, high p_{T_t}	$-4.36^{+1.80}_{-1.80}$	$2.0^{+1.54}_{-1.26}$
Converted rest, low p_{T_t}	$2.73^{+1.98}_{-1.98}$	$2.22^{+1.17}_{-0.99}$
Converted rest, high p_{T_t}	$-1.57^{+2.91}_{-2.91}$	$1.29^{+1.32}_{-1.26}$
Converted transition	$0.41^{+3.55}_{-3.66}$	$2.83^{+1.69}_{-1.60}$
2-jets / 2-jets high mass tight	$2.73^{+1.92}_{-1.86}$	$1.63^{+0.83}_{-0.68}$
2-jets high mass loose	—	$2.77^{+1.79}_{-1.39}$
2-jets low mass	—	$0.338^{+1.72}_{-1.48}$
E_T^{miss} significance	——	$2.99^{+2.74}_{-2.15}$
One Lepton	——	$2.71^{+2.00}_{-1.66}$

Table 4.2: $H \to \gamma\gamma$ results from ATLAS [1, 2] included in our analysis.

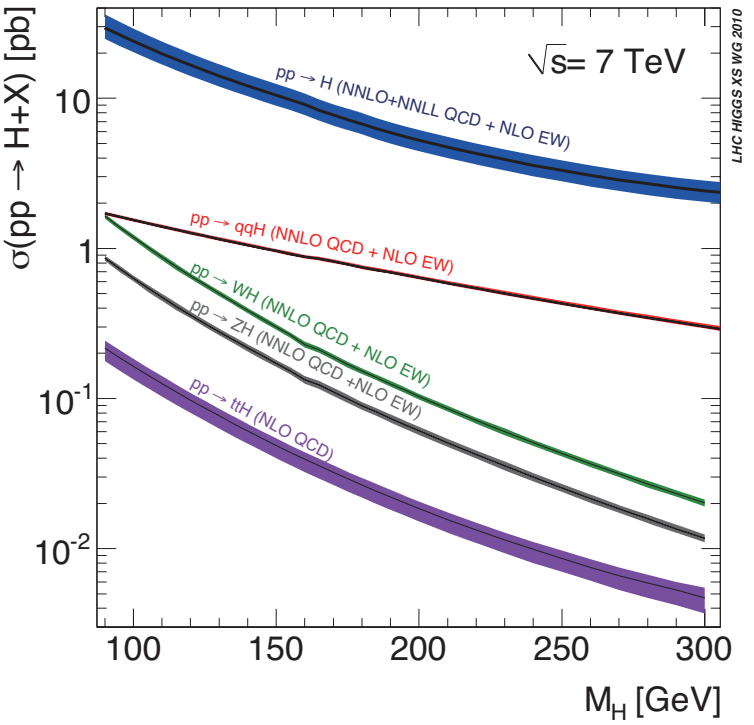

Figure 4.1: Cross sections for the dominant production channels in the SM at the LHC at 7 TeV as a function of M_H.

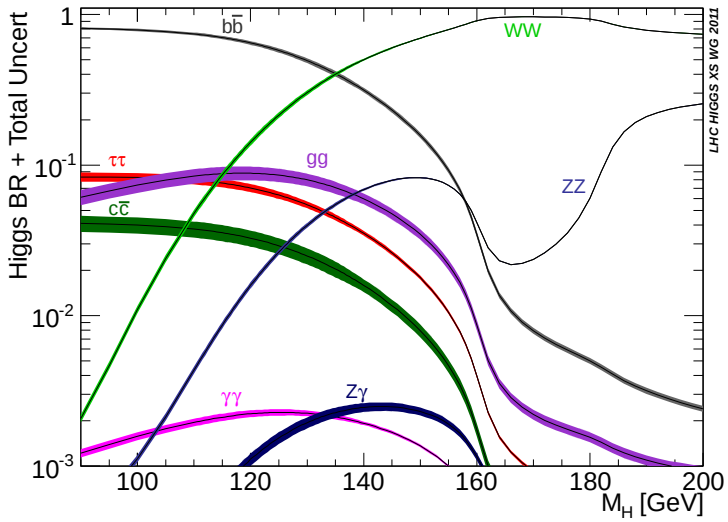

Figure 4.2: Decay branching ratios for the SM Higgs as a function of M_H.

4.2, and 4.3. In Eq. (4.3) we denote the theoretically expected signal as μ_j, the observed best fit values as μ_j^{exp} and the corresponding experimental errors

	μ^{exp}	
Channel	7 TeV	8 TeV
$pp \to \gamma\gamma$ Untagged 3	$1.48^{+1.65}_{-1.60}$	$-0.364^{+0.85}_{-0.82}$
$pp \to \gamma\gamma$ Untagged 2	$0.024^{+1.24}_{-1.24}$	$0.291^{+0.49}_{-0.46}$
$pp \to \gamma\gamma$ Untagged 1	$0.194^{+0.99}_{-0.95}$	$0.024^{+0.703}_{-0.655}$
$pp \to \gamma\gamma$ Untagged 0	$3.83^{+2.01}_{-1.67}$	$2.16^{+0.95}_{-0.75}$
$pp \to \gamma\gamma jj$	$4.19^{+2.30}_{-1.77}$	loose $0.80^{+1.09}_{-0.99}$ tight $0.291^{+0.679}_{-0.606}$
$pp \to \gamma\gamma$ MET	—	$1.89^{+2.62}_{-2.28}$
$pp \to \gamma\gamma$ Electron	—	$-0.655^{+2.76}_{-1.96}$
$pp \to \gamma\gamma$ Muon	—	$0.412^{+1.79}_{-1.38}$

Table 4.3: $H \to \gamma\gamma$ results from CMS [3] included in our analysis.

as σ_j. As we can see from these Tables the experimental errors are not symmetric in some of the channels, showing a deviation from Gaussian behavior as expected from the still low statistics. In our calculations we make the errors in each channel symmetric by taking:

$$\sigma_j = \sqrt{\frac{(\sigma_j^+)^2 + (\sigma_j^-)^2}{2}} \quad . \tag{4.4}$$

Concerning the theoretical uncertainties, the largest ones are associated with the gluon fusion production subprocess and in order to account for these errors we introduce two pull factors, one to account for the Tevatron uncertainty (ξ_g^T), and one for both the LHC at 7 and 8 TeV uncertainties (ξ_g^L). We consider that the errors associated with these pulls are $\sigma_g^T = 0.43$ and $\sigma_g^L = 0.15$ [93]. Additionally we introduce two pull factors to account for the theoretical uncertainties associated with vector boson fusion (VBF) cross section, one for Tevatron (ξ_{VBF}^T) with associated error $\sigma_{VBF}^T = 0.035$, and one for LHC at both 7 and 8 TeV (ξ_{VBF}^L) with associated error $\sigma_{VBF}^L = 0.03$ [93]. Finally theoretical uncertainties from associated production (VH) cross section are included with two more pulls, one for Tevatron (ξ_{VH}^T) with associated error $\sigma_{VH}^T = 0.075$ and one for LHC at both 7 and 8 TeV (ξ_{VH}^L) with associated error $\sigma_{VH}^L = 0.05$ [93]. These pulls modify the corresponding signal strength predictions as we will see below.

From the expressions in the previous chapters it is straight forward to

compute the expected signal strengths at tree-level including the contributions to the new operators. Concerning the higher order corrections we assume that the corresponding "K–factors" (defined as the ratio of the higher order predictions divided by the predictions at the leading order) are the same for the SM as for the new operator contributions. In this approximation we then write:

$$\sigma_Y^{\rm ano} = \left.\frac{\sigma_Y^{\rm ano}}{\sigma_Y^{\rm SM}}\right|_{\rm tree} \sigma_Y^{\rm SM}|_{\rm soa}, \tag{4.5}$$

$$\Gamma^{\rm ano}(h \to F) = \left.\frac{\Gamma^{\rm ano}(h \to F)}{\Gamma^{\rm SM}(h \to F)}\right|_{\rm tree} \Gamma^{\rm SM}(h \to F)|_{\rm soa}. \tag{4.6}$$

Where the superscripts ano (SM) indicate the value of the observable considering the anomalous and SM interactions (SM interactions only). These ratios of the cross sections (where Y indicates the subprocesses, gg, VBF, VH, or $t\bar{t}H$) and decay widths are evaluated at tree level and multiplied by the state of the art SM calculations, $\sigma_Y^{\rm SM}|_{\rm soa}$ and $\Gamma^{\rm SM}(h \to F)|_{\rm soa}$. In our analysis we do not include an invisible decay component, therefore we are assuming the total width is obtained by summing over the decays to the SM particles. In the future it may be insightful to include such analysis as recently developed techniques [94, 95] have allowed for great improvements on indirect measurements of the Higgs width [81, 82]. Calculation of the relevant tree–level cross sections was performed with the package MadGraph5 [96] with anomalous Higgs interactions introduced using FeynRules [97]. Additionally our results were checked against COMPHEP [98, 99] and VBFNLO [100].

With all these considerations, for any final state F listed in Tabs. 4.1, 4.2 and 4.3 we can write the theoretical signal strength as

$$\mu_F = \frac{\epsilon_{gg}^F \sigma_{gg}^{\rm ano}(1+\xi_g) + \epsilon_{\rm VBF}^{\rm ano}\sigma_{\rm VBF}^{\rm ano}(1+\xi_{\rm VBF}) + \epsilon_{WH}^F \sigma_{WH}^{\rm ano}(1+\xi_{VH}) + \epsilon_{ZH}^F \sigma_{ZH}^{\rm ano}(1+\xi_{VH}) + \epsilon_{t\bar{t}H}^F \sigma_{t\bar{t}H}^{\rm ano}}{\epsilon_{gg}^F \sigma_{gg}^{\rm SM} + \epsilon_{\rm VBF}^{\rm SM}\sigma_{\rm VBF}^{SM} + \epsilon_{WH}^F \sigma_{WH}^{\rm SM} + \epsilon_{ZH}^F \sigma_{ZH}^{\rm SM} + \epsilon_{t\bar{t}H}^F \sigma_{t\bar{t}H}^{\rm SM}} \cdot \frac{{\rm BR}_F^{\rm ano}}{{\rm BR}_F^{\rm SM}} \tag{4.7}$$

where we explicitly show how the "pull factors" described above are introduced. ϵ_Y^F denotes the weight of the different production channels $Y = $ VBF, gg, WH , ZH, and $t\bar{t}H$ to each final state F.

Searches for $H \to b\bar{b}$ are performed using only Higgs production via associated production with a W or Z meaning

$$\epsilon_{gg}^{b\bar{b}} = \epsilon_{\rm VBF}^{b\bar{b}} = \epsilon_{t\bar{t}H}^{b\bar{b}} = 0, \qquad \epsilon_{WH}^{b\bar{b}} = \epsilon_{ZH}^{b\bar{b}} = 1, \tag{4.8}$$

with the exception of the analysis by CMS [88] where

$$\epsilon_{gg}^{b\bar{b}} = \epsilon_{WH}^{b\bar{b}} = \epsilon_{ZH}^{b\bar{b}} = \epsilon_{t\bar{t}H}^{b\bar{b}} = 0, \qquad \epsilon_{\rm VBF}^{b\bar{b}} = 1 \tag{4.9}$$

is assumed.

In the case of the $F = \gamma\gamma$ signals both CMS and ATLAS for 7 and 8 TeV data separate the signal into various different categories. For ATLAS we reference Tab. 6 of [1] and Tab. 1 of [2] and for CMS Tab. 2 of [3]. For convenience we summarize this information in Tabs. 4.4 and 4.5.

Excepting those cases all other channels $F = WW^*$, ZZ^*, $\bar{\tau}\tau$, and $Z\gamma$ are treated as inclusive, that is:

$$\epsilon_{gg}^{F} = \epsilon_{WH}^{F} = \epsilon_{ZH}^{F} = \epsilon_{\rm VBF}^{F} = \epsilon_{t\bar{t}H}^{F} = 1. \tag{4.10}$$

Finally, we notice that some data available after the LHC 8 TeV run has been combined with that of the 7 TeV run. In this case we construct the expected theoretical signal strength as an average of the expected signal strengths for the center of mass energies of 7 and 8 TeV by weighting the contributions by the total number of events expected at each energy in the framework of the SM,

$$\mu_F^{\rm comb} = \frac{\mu_F^{\rm 7TeV}\sigma_F^{\rm SM,7TeV}\mathcal{L}^{\rm 7TeV} + \mu_F^{8TeV}\sigma_F^{\rm SM,8TeV}\mathcal{L}^{\rm 8TeV}}{\sigma_F^{\rm SM,7TeV}\mathcal{L}^{\rm 7TeV} + \sigma_F^{\rm SM,8TeV}\mathcal{L}^{\rm 8TeV}}, \tag{4.11}$$

where $\mathcal{L}^{7(8)\rm TeV}$ is the integrated luminosity accumulated at 7 (8) TeV in the given channel F.

It is important to note that our analysis neglects possible effects associated with the distortions of the kinematic distributions of the final states due to the Higgs anomalous couplings arising from their non SM–like Lorentz structure. Therefore we have implicitly assumed that the anomalous contributions have the same detection efficiency as the SM Higgs. A full simulation of the Higgs anomalous operators which considers their special kinematic features may aid to increase both sensitivity to the anomalous couplings and to break degeneracies between operators. However, at the time of this work there was not sufficient public information available to perform such an analysis.

Channel	ϵ_{gg}	ϵ_{VBF}	ϵ_{WH}	ϵ_{ZH}	$\epsilon_{t\bar{t}H}$
Unconverted central, low p_{T_t}	1.06	0.579	0.550	0.555	0.355
	1.07	0.572	0.448	0.452	0.343
Unconverted central, high p_{T_t}	0.760	2.27	3.03	3.16	4.26
	0.906	1.80	1.31	1.41	2.40
Unconverted rest, low p_{T_t}	1.06	0.564	0.612	0.610	0.355
	1.06	0.572	0.512	0.566	0.171
Unconverted rest, high p_{T_t}	0.748	2.33	3.30	3.38	3.19
	0.892	1.90	1.50	1.58	1.88
Converted central, low p_{T_t}	1.06	0.578	0.581	0.555	0.357
	1.07	0.572	0.416	0.509	0.343
Converted central, high p_{T_t}	0.761	2.21	3.06	3.16	4.43
	0.901	1.80	1.38	1.53	2.57
Converted rest, low p_{T_t}	1.06	0.549	0.612	0.610	0.355
	1.06	0.586	0.512	0.566	0.171
Converted rest, high p_{T_t}	0.747	2.31	3.36	3.27	3.19
	0.887	1.86	1.66	1.70	1.88
Converted transition	1.02	0.752	1.01	0.943	0.532
	1.04	0.787	0.704	0.735	0.343
2-jets / 2-jets high mass tight	0.257	11.1	0.122	0.111	0.177
	0.272	10.9	0.032	0.056	0.0
2-jets high mass loose (only 8 TeV)	0.514	7.74	0.160	0.170	0.171
2-jets low mass (only 8 TeV)	0.550	0.429	9.51	9.73	3.25
E_T^{miss} significance (only 8 TeV)	0.047	0.072	11.4	26.9	20.7
One lepton (only 8 TeV)	0.025	0.086	20.2	8.71	31.9

Table 4.4: Weight of each production mechanism for the different $\gamma\gamma$ categories in the ATLAS analyses of the 7 TeV data (upper values) and 8 TeV (lower values). For the 8 TeV analysis three new exclusive categories enriched in vector boson associated production were added with the 2-jets low mass (lepton tagged) [E_T^{miss} significance] category being built to select hadronic (leptonic) [invisible] decays of the associated vector boson.

Channel	ϵ_{gg}	ϵ_{VBF}	ϵ_{VH}	$\epsilon_{t\bar{t}H}$
$pp \to \gamma\gamma$ Untagged 3	1.04	0.637	0.808	0.355
	1.06	0.558	0.675	0.343
$pp \to \gamma\gamma$ Untagged 2	1.04	0.637	0.769	0.532
	1.05	0.629	0.715	0.685
$pp \to \gamma\gamma$ Untagged 1	1.00	0.897	1.10	0.887
	0.954	1.20	1.45	1.71
$pp \to \gamma\gamma$ Untagged 0	0.702	2.43	3.69	5.50
	0.833	1.66	2.66	4.45
$pp \to \gamma\gamma jj$ (7 TeV)	0.306	10.5	0.118	0
$pp \to \gamma\gamma jj$ loose (8 TeV)	0.535	7.31	0.348	0.856
$pp \to \gamma\gamma jj$ tight (8 TeV)	0.236	11.3	0.061	0.171
$pp \to \gamma\gamma$, μ-tag (8 TeV)	0.0	0.029	16.2	35.6
$pp \to \gamma\gamma$, e-tag (8 TeV)	0.013	0.057	16.1	33.7
$pp \to \gamma\gamma$, E_T^{miss}-tag (8 TeV)	0.241	0.358	13.2	20.2

Table 4.5: Weight of each production mechanism for the different $\gamma\gamma$ categories in the CMS analyses of the 7 TeV data (upper values) and 8 TeV (lower values). $\epsilon_{VH} = \epsilon_{ZH} = \epsilon_{WH}$. For the $pp \to \gamma\gamma jj$ category the 8 TeV data was divided in two independent subsamples labeled as "loose" and "tight" according to the requirement on the minimum transverse momentum of the softer jet and the minimum dijet invariant mass. For the 8 TeV analysis three new exclusive categories were added enriched in vector boson associated production: μ–tag, e–tag and E_T^{miss}–tag.

4.2 Inclusion of Triple Gauge Coupling Data

Recalling the Lagrangian of Eq. (2.38) and its relation to the linear basis (see Eq. (2.39)) and the chiral basis (Tab. 3.2) we are able to include experimental information on the TGV measurements in our analysis. We do this by adding a new term to our chi–square test of Eq. (4.3).

We notice that Eq. (2.39) implies that only three of the five relevant TGV couplings are independent. These three can be chosen to be $\Delta\kappa_\gamma$, λ_γ, and Δg_1^Z, while λ_Z and $\Delta\kappa_Z$ remain to be determined by the relations

$$\lambda_Z = \lambda_\gamma \ , \qquad \Delta\kappa_Z = -\frac{s_{\rm W}^2}{c_{\rm W}^2}\Delta\kappa_\gamma + \Delta g_1^Z \ . \tag{4.12}$$

Experimental results, however, are usually given in terms of the effective parametrization in Eq. (2.38) assuming that only some of the couplings $\Delta\kappa_\gamma$, λ_γ, g_1^Z $\Delta\kappa_Z$, λ_Z are not vanishing (usually one) while all others are taken to be zero hence not all can be used in our analysis. For example in the framework of the effective Lagrangians considered here, it is not consistent to use as experimental results those obtained under the assumption that only one of the effective couplings is non–vanishing since for any given operator at least two of the couplings are non–vanishing as seen from the relations in Eq. (4.12).

So for our analyisis we will make use of the results from the LEP collaboration [101] on γW^+W^- and ZW^+W^- TGVs which are the most precise measurements obtained under the assumption that the couplings are related as predicted by Eq. (4.12). In such analysis they present the results in terms of correlated ranges between the parameters κ_γ and g_1^Z:

$$\kappa_\gamma = 0.984^{+0.049}_{-0.049} \qquad g_1^Z = 1.004^{+0.024}_{-0.025} \ , \tag{4.13}$$

with a correlation factor of $\rho = 0.11$. We define the (row) vector

$$\left(\delta g_1^Z,\ \delta\kappa_\gamma\right) \equiv \left(\frac{g_1^Z - g_1^{Z,\rm exp}}{\sigma_{g_1^Z}},\ \frac{\kappa_\gamma - \kappa_\gamma^{\rm exp}}{\sigma_{\kappa_\gamma}}\right), \tag{4.14}$$

where in the expressions above g_1^Z and κ_γ are to be understood as functions

of f_W and f_B as in Eq. (2.39). The correlation matrix is

$$C_{\rm TGV} \equiv \begin{pmatrix} 1 & \rho \\ \rho & 1 \end{pmatrix}. \tag{4.15}$$

This allows us to define the chi square test for the TGV data:

$$\chi^2_{\rm TGV}(f_W, f_B) = \left(\delta g_1^Z,\ \delta\kappa_\gamma\right) C^{-1}_{\rm TGV} \left(\delta g_1^Z,\ \delta\kappa_\gamma\right)^T. \tag{4.16}$$

4.3 Inclusion of Electroweak Precision Data

Next we wish to include the effects of electroweak precision data on our analysis. We remind the reader that we have removed the two operators $\mathcal{O}_{BW}$ and $\mathcal{O}_{\Phi,1}$ because they contribute at tree level to EWPD. Now we consider additional constraints on the dimension–six operators still remaining in our basis, as given in Eq. (2.48), and which give contributions to EWPD at one–loop. As these effects are calculated at loop level they suffer from the usual issues with the interpretation of non–renormalizable operators effects' at loop level.

In order to account for the information from EWPD we use the reduced set of S, T, and U parameters as calculated in Sec. 2.3 and statistically compare them to the current experimental extracted values from the global analysis of LEP and low energy electroweak data [57]:

$$\Delta S = 0.00 \pm 0.10, \qquad \Delta T = 0.02 \pm 0.11, \qquad \text{and} \qquad \Delta U = 0.03 \pm 0.09, \tag{4.17}$$

which are correlated with a correlation matrix given by:

$$C_{\rm EWPD} = \begin{pmatrix} 1 & 0.89 & -0.55 \\ 0.89 & 1 & -0.8 \\ -0.55 & -0.8 & 1 \end{pmatrix}. \tag{4.18}$$

Then, as with the case of TGV (Sec. 5.2), we define a (row) vector corresponding to this data,

$$(\delta S, \delta T, \delta U) \equiv \left(\frac{\Delta S - \Delta S^{\rm exp}}{\sigma_{\Delta S}},\ \frac{\Delta T - \Delta T^{\rm exp}}{\sigma_{\Delta T}},\ \frac{\Delta U - \Delta U^{\rm exp}}{\sigma_{\Delta U}} \right), \tag{4.19}$$

and we form our chi-square test related to the EWPD as:

$$\chi^2_{\rm EWPD}(f_W, f_B, f_{WW}, f_{BB}, f_{\Phi,2}) = (\delta S, \delta T, \delta U)\, C^{-1}_{\rm EWPD}\, (\delta S, \delta T, \delta U)^T\,. \quad (4.20)$$

4.4 Summary

In this chapter we have put together an analysis framework which allows us to place constraints on the operator bases of Eqs. (2.48) and (3.22). In doing so we have presented the available Higgs data from the Tevatron and LHC, introduced the pulls method to account for correlations in theoretical errors, and taken care to properly weight the channels by the appropriate production cross sections which for the $\gamma\gamma$ decay channel are not straightforward. In addition we have formulated a way to incorporate TGV data from LEP where the correlations between TGCs were appropriately handled for our basis of operators, as well as incorporating the implications of EWPD via the loop-level contributions to S, T, and U of the operators in the linear basis.

In the following chapter we will bring together all of the topics discussed in Chapters 2, 3, and 4 to quantify our best determination of the coefficients of the operator in the bases of Eqs. (2.48) and (3.22) and some of the signatures which have the potential to discriminate between the two expansions. In particular we will recall the correlations between the HVV and TGV couplings implied in the linear expansion and compare the data to these correlations searching for signatures (dis)favoring the linear vs chiral expansions. Conversely we will quantify how the assumption that the Higgs is a fundamental scalar doublet of $SU(2)_L$, befitting of the linear expansion, allows for the Higgs data to constrain the TGCs.

Chapter 5

Status After LHC 7 and 8 TeV Runs

In this chapter we apply the framework outlined in Chapter 4 to obtain the best present determination of the coefficients of the operators in our effective Lagrangians. In Sec. 5.1 we find the constraints on the coefficients of the operators in the linear basis (see Chapter 2) and we project the constraints from the linear basis onto limits on triple gauge couplings in Sec. 5.2. The present determination of the coefficients of the operators in the chiral expansion are presented in Sec. 5.3. Finally in Sec. 5.4 we quantify the variables developed in Chapter 3 with potential to discriminate between the two expansions.

5.1 Results in the Linear Expansion

We recall for convenience the final basis of operators we found in Chapter 2 – after reducing the basis via the EOM and precision data – which contains eight operators relevant for the present analysis:

$$\begin{aligned}\mathcal{L}_{\text{eff}} &= -\tfrac{\alpha_s v}{8\pi}\tfrac{f_g}{\Lambda^2}\mathcal{O}_{GG} + \tfrac{f_{\Phi,2}}{\Lambda^2}\mathcal{O}_{\Phi,2} + \tfrac{f_{BB}}{\Lambda^2}\mathcal{O}_{BB} + \tfrac{f_{WW}}{\Lambda^2}\mathcal{O}_{WW} + \tfrac{f_B}{\Lambda^2}\mathcal{O}_B + \tfrac{f_W}{\Lambda^2}\mathcal{O}_W \\ &\quad + \tfrac{f_\tau}{\Lambda^2}\mathcal{O}_{e\Phi,33} + \tfrac{f_{\text{bot}}}{\Lambda^2}\mathcal{O}_{d\Phi,33}.\end{aligned} \tag{5.1}$$

In this section we discuss the results of the 7 and 8 TeV runs of the LHC. We have included in Appendix B projections for the next run of the LHC as well as for the proposed high luminosity LHC.

5.1.1 Bosonic Dimension–Six Operator Analysis

We begin by studying scenarios where NP in the EWSB sector does not lead to modifications of the Higgs couplings to fermions. In other words we neglect the fermionic Higgs operators (i.e. setting $f_{\rm bot} = f_\tau = 0$) and fit the available data treating the remaining six free bosonic operators as independent. Considering all Higgs collider (ATLAS, CMS, and Tevatron) data we find $\chi^2_{\rm min} = 66.8$ for the combined analysis and the SM lays at $\chi^2_{\rm SM} = 68.1$, within the 3% confidence level region. The inclusion of TGV data has approximately no quantitative impact on the value of $\chi^2_{\rm min}$ and the confidence level of the SM. Adding EWPD increases $\chi^2_{\rm min(SM)}$ to 67.9 (69.9) so the SM lies in the full combined analysis at the 9% CL six–dimensional region in agreement with these combined results at the 0.1σ level.

The first column in Fig. 5.1 displays the chi–square ($\Delta\chi^2$) dependence on each of the six bosonic anomalous couplings after marginalizing over the other operator coefficients (i.e. minimizing with respect to the other 5 degrees of freedom). In this figure the solid red line represents the results from the analysis of all Higgs collider data, while the TGV data is included with the dashed purple line, and both TGV and EWPD are included in the dotted blue line. For inclusion of EWPD throughout this dissertation we always use the value $\Lambda = 10$ TeV (see Eq. (2.35)).

From the figure we infer:

- In general we find that the best fit for all coefficients lies near the SM prediction $f_i = 0$.

- One exception is f_g since we notice that $\Delta\chi^2$ as a function of f_g exhibits two degenerate minima. This is the result of the interference between the SM and anomalous contributions which possess exactly the same momentum dependence, so around the second minimum the anomalous contribution is approximately minus twice the SM value. The gluon fusion Higgs production cross section is too depleted for f_g values between the minima causing the intermediate barrier.

- Additionally as f_B and f_W are the only operator coefficients which modify the triple gauge vertices at tree level they show the largest impact of the inclusion of TGV data. f_W is the most constrained parameter by

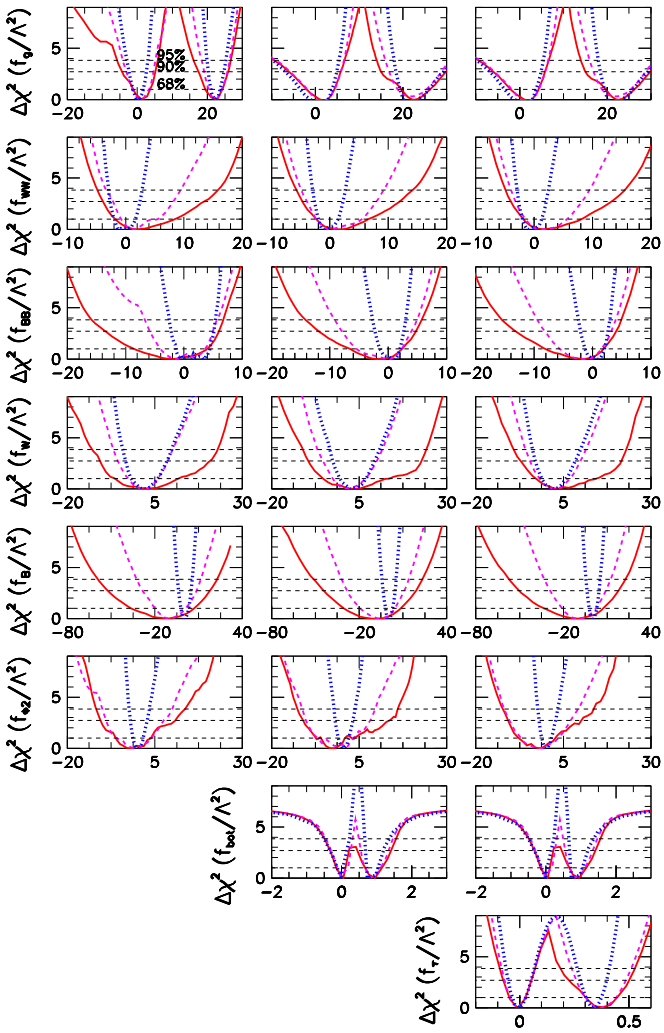

Figure 5.1: $\Delta\chi^2$ dependence on the fit parameters considering all Higgs collider (ATLAS, CMS and Tevatron) data (solid red line), Higgs collider and TGV data (dashed purple line) and Higgs collider, TGV and EWP data (dotted blue line). The rows depict the $\Delta\chi^2$ dependence with respect to the fit parameter shown on the left of the row with the anomalous couplings f/Λ^2 given in TeV^{-2}. In the first column we use f_g, f_{WW}, f_{BB}, f_W, f_B, and $f_{\Phi,2}$ as fit parameters with $f_{\text{bot}} = f_\tau = 0$. In the second column the fitting parameters are f_g, $f_{WW} = -f_{BB}$, f_W, f_B, $f_{\Phi,2}$, and f_{bot} with $f_\tau = 0$. In the panels of the right column we fit the data in terms of f_g, $f_{WW} = -f_{BB}$, f_W, f_B, $f_{\Phi,2}$, f_{bot}, and f_τ.

inclusion of TGV data as it corresponds to g_1^Z (see Eq. (2.38)) which is the most constrained of the two triple gauge couplings considered (see Eq. (4.13)).

- Adding EWPD greatly reduces the available parameter space for the bosonic operators, f_W, f_B, f_{WW}, f_{BB}, and $f_{\Phi,2}$.

- We also see that, as expected, inclusion of TGV and EWPD has little impact on f_g.

It is instructive to project these results into the observable branching ratios and production cross sections. In Fig. 5.2 we show the $\Delta\chi^2$ dependence on these observables using the collider and TGV data. The top two panels illustrate that the SM predictions are within the 1σ range with the largest deviation coming from the $\gamma\gamma$ channel. We note that the precision with which the Higgs branching ratios are known is about 20% and that of the production cross sections is of the order 30%.

We include in Tab. 5.1 the best fit values and 90% CL allowed ranges for the couplings and observables in the combined analysis of Higgs collider and TGV data. We do not include in these final allowed ranges the constraints from EWPD. As mentioned above, the quantitative interpretation of these one–loop contributions is debatable. We have included them in some of the figures for illustration of their possible impact, but have chosen not to include them in the final combined results given in Tab. 5.1 nor in the remaining figures in this section.

The most important correlations between these ranges are shown in Figs. 5.3 and 5.4. Figure 5.3 shows the correlation between f_{WW} and f_{BB} after marginalizing over the remaining four parameters for collider data. We note the strong anti-correlation between the two operator coefficients. This is a result of their dominantly contributing to the Higgs branching fraction to two photons which is proportional to $f_{WW} + f_{BB}$ (see $H\gamma\gamma$ vertex in Eq. (2.19)). The 95% CL region forms two narrow islands in a similar fashion to the f_g degeneracy – one where only small contributions from the anomalous operators are made and one where they contribute twice the SM value with the opposite sign. This degeneracy is not exact as f_{WW} and f_{BB} also contribute to WW^* and ZZ^* branching ratios as well as Vh and VBF production mechanisms, but with

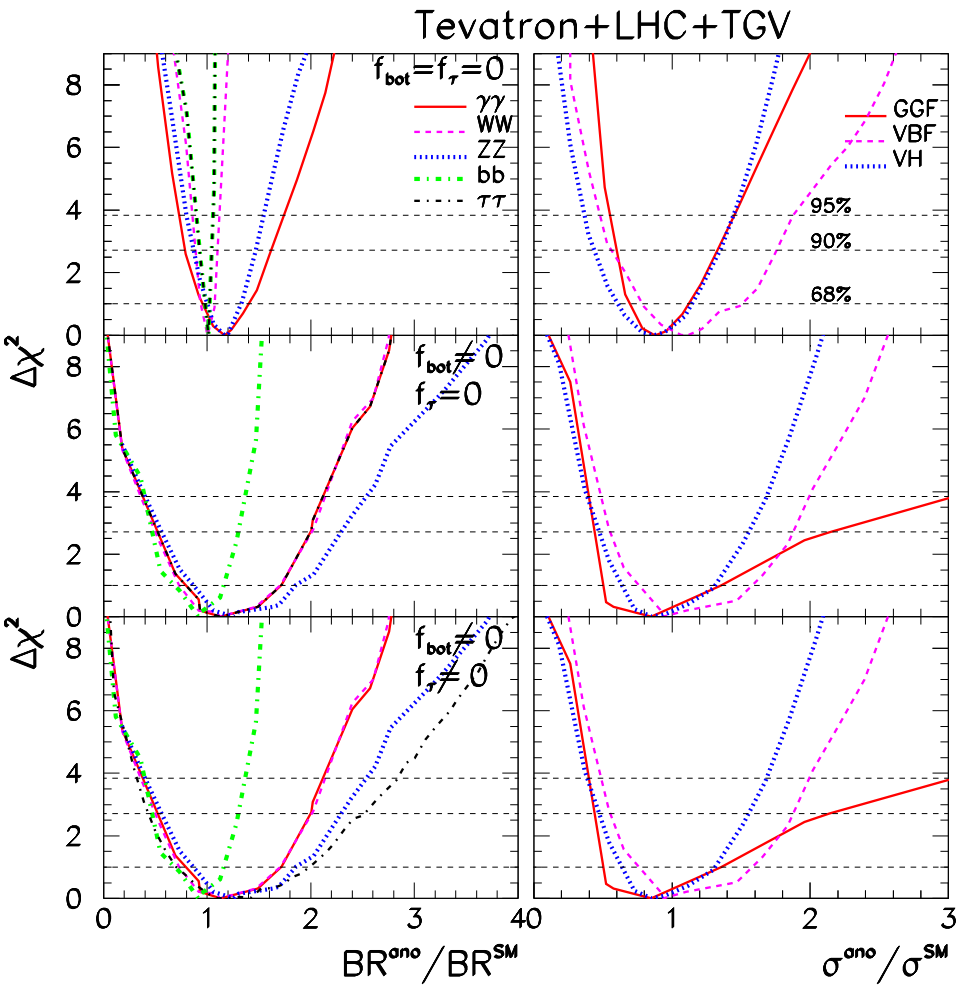

Figure 5.2: Chi–square dependence on the Higgs branching ratios (left panels) and production cross sections (right panels) when we consider all Higgs collider and TGV data. In the upper panels we have used f_g, f_{WW}, f_{BB}, f_W, f_B, and $f_{\Phi,2}$ as fitting parameters with $f_{\rm bot} = f_\tau = 0$, while in the middle panels the fit parameters are f_g, $f_{WW} = -f_{BB}$, f_W, f_B, $f_{\Phi,2}$, and $f_{\rm bot}$ with $f_\tau = 0$. In the lower row we parametrize the data in terms of f_g, $f_{WW} = -f_{BB}$, f_W, f_B, $f_{\Phi,2}$, $f_{\rm bot}$, and f_τ. The dependence of $\Delta\chi^2$ on the branching ratio to the fermions not considered in the analysis arises from the effect of the other parameters in the total decay width.

different coefficients. Comparing with the one–dimensional curves in Fig. 5.1 we see that marginalization over f_{WW} or f_{BB} results in two curves which are

	Fit with $f_{\rm bot} = f_\tau = 0$		Fit with $f_{\rm bot}$ and f_τ	
	Best fit	90% CL allowed range	Best fit	90% CL allowed range
f_g/Λ^2 (TeV^{-2})	1.1, 22	$[-3.3, 5.1] \cup [19, 26]$	2.1, 21	$[-5.3, 5.8] \cup [17, 22]$
f_{WW}/Λ^2 (TeV^{-2})	1.5	$[-3.2, 8.2]$	0.65	$[-4.2, 7.7]$
f_{BB}/Λ^2 (TeV^{-2})	-1.6	$[-7.5, 5.3]$	-0.65	$[-7.7, 4.2]$
f_W/Λ^2 (TeV^{-2})	2.1	$[-5.6, 9.6]$	1.7	$[-5.4, 9.8]$
f_B/Λ^2 (TeV^{-2})	-10	$[-29, 8.9]$	-7.9	$[-28, 11]$
$f_{\phi,2}/\Lambda^2$ (TeV^{-2})	-1.0	$[-10, 8.5]$	-1.3	$[-9.8, 7.5]$
$f_{\rm bot}/\Lambda^2$ (TeV^{-2})	—	—	0.01, 0.84	$[-0.28, 0.24] \cup [0.55, 1.3]$
f_τ/Λ^2 (TeV^{-2})	—	—	-0.01, 0.37	$[-0.07, 0.05] \cup [0.26, 0.49]$
$BR^{\rm ano}_{\gamma\gamma}/BR^{\rm SM}_{\gamma\gamma}$	1.2	[0.78, 1.7]	1.2	[0.55, 1.9]
$BR^{\rm ano}_{WW}/BR^{\rm SM}_{WW}$	1.0	[0.89, 1.1]	1.2	[0.51, 1.9]
$BR^{\rm ano}_{ZZ}/BR^{\rm SM}_{ZZ}$	1.2	[0.84, 1.5]	1.4	[0.6, 2.2]
$BR^{\rm ano}_{bb}/BR^{\rm SM}_{bb}$	1.0	[0.92, 1.1]	0.89	[0.46, 1.3]
$BR^{\rm ano}_{\tau\tau}/BR^{\rm SM}_{\tau\tau}$	1.0	[0.92, 1.1]	1.1	[0.42, 2.6]
$\sigma^{\rm ano}_{gg}/\sigma^{\rm SM}_{gg}$	0.88	[0.59, 1.3]	0.73	[0.38, 2.0]
$\sigma^{\rm ano}_{VBF}/\sigma^{\rm SM}_{VBF}$	1.1	[0.52, 1.9]	1.1	[0.58, 1.8]
$\sigma^{\rm ano}_{VH}/\sigma^{\rm SM}_{VH}$	0.82	[0.43, 1.4]	0.96	[0.47, 1.5]

Table 5.1: Best fit values and 90% CL allowed ranges for the combination of all available Tevatron and LHC Higgs data as well as TGV.

mirror images of one another. That is, to a good approximation the data favors $f_{WW} = -f_{BB}$, an approximation that we will make use of for our fits including fermionic operators.

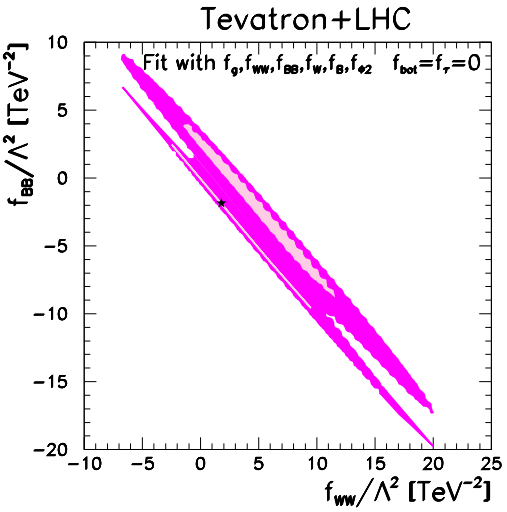

Figure 5.3: We display the 95% and 99% CL allowed regions in the plane $f_{WW} \times f_{BB}$ when we fit the Higgs collider data varying f_g, f_{WW}, f_{BB}, f_W, f_B, and $f_{\Phi,2}$. The star indicates the global minimum. We have marginalized over the undisplayed parameters.

In Fig. 5.4 we show the two–dimensional projection into the plane of $f_g \times f_{\Phi,2}$ after marginalizing over the remaining parameters. The results include both the Higgs collider and TGV data sets. Again we see two islands whose origin is the interference between anomalous and SM contributions to the Higgs coupling to two gluons. Whithin each island there is a clear anti-correlation between f_g and $f_{\Phi,2}$ coming from the fact the anomalous contribution to the gluon fusion production is proportional to $F_{gg}^{\rm SM} f_{\Phi,2} + 2 f_g$, where $F_{gg}^{\rm SM} \sim 0.7$ is the SM loop contribution to the Hgg vertex.

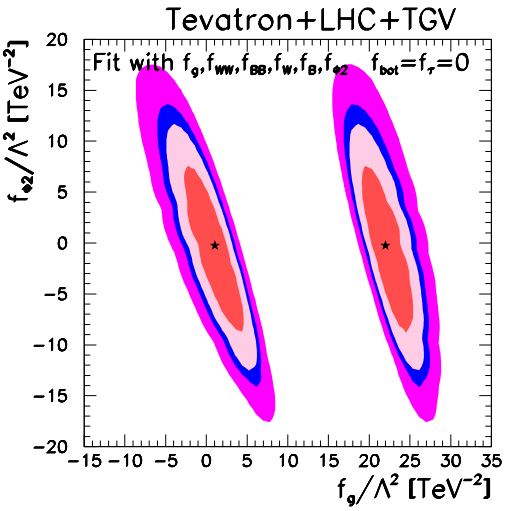

Figure 5.4: We present the 68%, 90%, 95%, and 99% CL allowed regions in the plane $f_g \times f_{\Phi,2}$ when we fit the Higgs collider and TGV data varying f_g, f_{WW}, f_{BB}, f_W, f_B, and $f_{\Phi,2}$. The stars indicate the global minima. We have marginalized over the undisplayed parameters.

Finally, in the left panel of Fig. 5.5 we show the correlations projected in the observables, in particular between the Higgs decay into photons and Higgs production via gluon fusion. These two quantities are anti–correlated because their product is the major source of Higgs events decaying into two photons, an increase in one requires a compensating decrease in the other to maintain the correct signal strength.

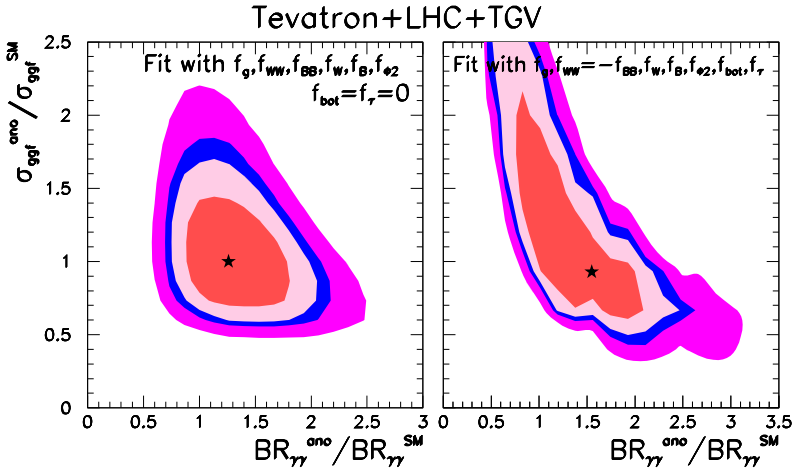

Figure 5.5: In the left (right) panel we present the 68%, 90%, 95%, and 99% CL allowed regions in the plane $\sigma_{gg}^{\rm ano}/\sigma_{gg}^{\rm SM} \times {\rm Br}(h \to \gamma\gamma)^{\rm ano}/{\rm Br}(h \to \gamma\gamma)^{\rm SM}$ when we fit the Higgs collider and TGV data varying f_g, f_{WW}, f_{BB}, f_W, f_B, and $f_{\Phi,2}$ (f_g, $f_{WW} = -f_{BB}$, f_W, f_B, $f_{\Phi,2}$, and $f_{\rm bot}$). The stars indicate the global minima. We have marginalized over the undisplayed parameters.

5.1.2 Including Fermionic Operators

We now consider the inclusion of fermionic operators. We begin by introducing $f_{\rm bot}$ to our parameter space. As mentioned above we take advantage of the strong anticorrelation between f_{WW} and f_{BB}, taking $f_{WW} = -f_{BB}$, to simplify the numerical analyses. The free parameters under consideration are now $\{f_g, f_W, f_B, f_{WW} = -f_{BB}, f_{\Phi,2}, f_{\rm bot}\}$.

The middle column of Fig. 5.1 shows the effects on the chi–square of the inclusion of $f_{\rm bot}$. We begin by noting that $\Delta\chi^2$ shows degenerate minima for $f_{\rm bot}$, one which represents a small correction to the SM Yukawa coupling, the other corresponding to a flip of the sign of the Hbb coupling. The parameter space being degenerate under the change of sign of the Hbb coupling indicates that experimental data does not favor one or the other sign at this time.

The allowed range for f_g is also opened dramatically by the inclusion of $f_{\rm bot}$. This is a reflection of the fact that $H \to bb$ is the dominant decay mode of the 125 GeV Higgs. Increases in $f_{\rm bot}$ push the Higgs branching ratio into a bottom pair to 1, and therefore the gluon fusion cross section must be enhanced to compensate the dilution of the Higgs decay in any other channel. This com-

pensation works because the data for the $H \to bb$ final state does not receive a contribution from gluon fusion production. We further illustrate this behavior in Fig. 5.6 where we plot the correlation between f_g and $f_{\rm bot}$. Additionally in the right panel of Fig. 5.5 we see that this correlation has opened the available range of the gluon fusion cross section, but at the necessity that the branching ratio to two photons be below the standard model to fit the observed $\gamma\gamma$ rate. Also from the middle column of Fig. 5.1 we see that inclusion of $f_{\rm bot}$ has a very small impact on the ranges of the Higgs coupling to electroweak gauge bosons (i.e. on the parameters $f_W,\ f_B,\ f_{WW} = -f_{BB},$ and $f_{\Phi,2}$).

The effect of including $f_{\rm bot}$ on the observables is also demonstrated in Fig. 5.2. We see that bounds on both the branching fractions and cross sections are weakened, with VH and VBF being the least affected channels. The gluon fusion cross section is the most effected, with its constraints being dramatically broadened, as expected from the previous discussion of f_g and $f_{\rm bot}$.

Finally we conclude with the inclusion of f_τ. Again we will constrain f_{WW} and f_{BB} such that our basis contains the free parameters $\{f_g,\ f_W,\ f_B,\ f_{WW} = -f_{BB},\ f_{\Phi,2},\ f_{\rm bot},\ f_\tau\}$. The right panels of Fig. 5.1 show the $\Delta\chi^2$ dependence of each of the free parameters while the lower panels of Fig. 5.2 show the allowed ranges of the branching ratios and cross sections given the addition of f_τ. We note that the introduction of f_τ does not result in any new strong correlations and the plots resemble those of the $(f_{\rm bot} \neq 0,\ f_\tau = 0)$ scenario with the exception of the f_τ branching ratio which is less constrained.

Again we see a degeneracy in the f_τ space similar to that of $f_{\rm bot}$ stemming from the fact the sign of the Yukawa is not constrained by current data. Additionally the analysis favors a slightly large $BR^{\rm ano}_{\tau\tau}/BR^{\rm SM}_{\tau\tau} \sim 1.1$ which accounts for the slight offset of the two minima for f_τ from the expected values of zero and the flip of sign in the Yukawa in Fig. 5.1.

Finally, Table 5.1 also includes the best fit points and the 90% CL range for branching ratios and production cross section for the fit including both fermionic operators using the Higgs collider and TGV data. The inclusion of fermionic operators maintains the agreement of the SM with the data at about the 9% CL.

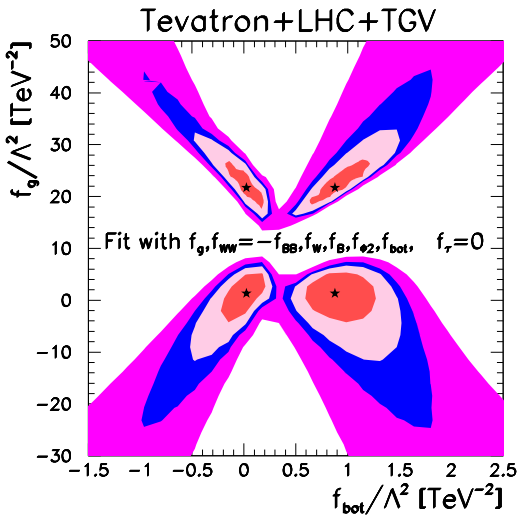

Figure 5.6: We present the 68%, 90%, 95%, and 99% CL allowed regions in the plane $f_{\rm bot} \times f_g$ from the Higgs collider and TGV data varying f_g, f_W, f_B, $f_{WW} = -f_{BB}$, $f_{\Phi,2}$, and $f_{\rm bot}$. The stars indicate the global minima. We have marginalized over the undisplayed parameters.

5.2 Implications for Triple Gauge Couplings

To date, LEP constraints on the triple gauge couplings (see Eq. (4.13)) are the most stringent bounds on deviations of the SM predictions of the TGV applicable to our effective lagrangian framework. LEP experiments were sensitive to anomalous TGCs through the W^+W^-, single γ, and W productions giving information on both the WWZ and $WW\gamma$ vertices [101]. Tevatron was also able to put constraints on the parameter space to a lesser extent through WW, WZ, and $W\gamma$ production in $p\bar{p}$ collisions, results from the detector at DØ can be found in [102] while those from CDF may be found in [103, 104][1].

Work at the LHC is beginning to constrain the parameter space as well, projections for the early LHC were made in [105]. In particular at ATLAS studies of TGCs in W^+W^- [106], WZ [107], and $W\gamma$ and $Z\gamma$ (fully leptonic) [108] have been made for 7 TeV with an integrated luminosity of 4.6 fb^{-1}. Additionally at 7 TeV for similar luminosities CMS has reported on the leptonic

[1]In the case of Tevatron a form factor of $1/(1 + s/\Lambda^2)$ with $\Lambda = 2$ TeV is used to unitarize the scattering amplitudes for high energy. Details on the divergence of amplitudes for anomalous operators are worked out in detail in Chapter 6.

WW channel [109], leptonic $W\gamma$ and $Z\gamma$ [110], and WW and WZ productions with two jets in final state [111].

In the previous section we have used these TGV results to impose additional constraints on the couplings of the Higgs boson. This is possible because both TGV and HVV sectors are related as seen in Eqs. (2.38) and (2.39), a relation which follows from the gauge invariance assumed in the construction of the low energy EFT.

Given these relations, it is interesting to ask if it is possible to instead constrain the TGCs in $\mathcal{L}_{WWV}$ using only the Higgs collider data. In order to use the Higgs observables to constrain the TGCs we employ our same chi–square framework, marginalized over all parameters which do not contribute to TGCs (i.e. $f_{WW},\ f_{BB},\ f_{\Phi,2},$ and f_g), and project the remaining f_W and f_B into the language of $\mathcal{L}_{WWV}$ via Eq. (2.39). Note that we leave $f_{\rm bot}$ and f_τ out of the fit, which is justified given our conclusions in Sec. 5.1 where we found the fermionic operators have a negligible effect on the parameter space of the bosonic operators.

In Fig. 5.7 we show 95% CL constraints (for two degrees of freedom) on the $\Delta\kappa_\gamma \times \Delta g_1^Z$ plane from the Higgs collider data (red contour). These bounds are obtained from Higgs data and are therefore independent of λ_γ and λ_Z. We note the strong correlation between $\Delta\kappa_\gamma$ and Δg_1^Z imposed by the tree level contribution of f_W and f_B to the $Z\gamma$ data. Additionally we have included the two–dimensional constraints from LEP (solid blue line), DØ (solid green), ATLAS WW (solid black), and ATLAS WZ (dashed black) where we have re-expressed these bounds on $\Delta\kappa_Z$ and Δg_1^Z in terms of $\Delta\kappa_\gamma$ and Δg_1^Z. In this case the bounds are obtained assuming $\lambda_\gamma = \lambda_\kappa = 0$

We are then able to put limits on $\Delta\kappa_\gamma$, $\Delta\kappa_Z$, and Δg_1^Z of which only two are independent. The 90% CL (for one degree of freedom) allowed ranges read:

$$\begin{aligned} -0.047 \leq \Delta g_1^Z \leq 0.089, \quad & -0.19 \leq \Delta\kappa_\gamma \leq 0.099 \\ \text{implying}: \quad & -0.019 \leq \Delta\kappa_Z \leq 0.083\,. \end{aligned} \tag{5.2}$$

Thus we find that the strength of the bounds derived from the analysis of the Higgs data are at the same precision level as the bounds derived from the direct TGV experimental measurements (see Eq. (4.13)).

In order to estimate the potential of a combination of all the data shown in

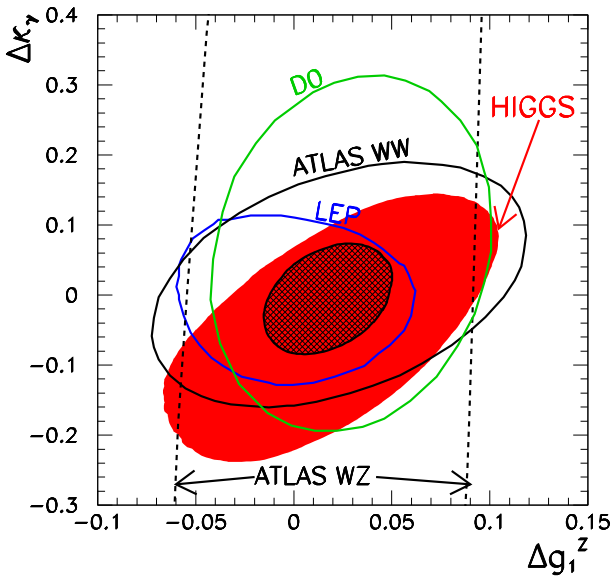

Figure 5.7: The 95% C.L. allowed regions (2 d.o.f.) on the plane $\Delta\kappa_\gamma \times \Delta g_1^Z$ from the analysis of the Higgs data from the LHC and Tevatron (filled region) together with the relevant bounds from different TGC studies from collider experiments as labeled in the figure. We also show the estimated constraints obtainable by combining these bounds (hatched region).

Fig. 5.7 we first reconstruct an approximate Gaussian $\chi^2_i(\Delta\kappa_\gamma, \Delta g_1^Z)$ reproducing the 95% CL regions for each contour from direct TGC data (i.e. we obtain the best fit point and two–dimensional covariance matrix from the condition $\chi^2 = 5.99$). Then define the total χ^2 as

$$\chi^2_{\rm comb} = \chi^2_H(\Delta\kappa_\gamma, \Delta g_1^Z) + \sum_i \chi^2_i(\Delta\kappa_\gamma, \Delta g_1^Z), \tag{5.3}$$

allowing us to project the combined result in the hashed region and find the one–dimensional limits to be:

$$\begin{aligned} -0.005 \leq \Delta g_1^Z \leq 0.040, \quad -0.058 \leq \Delta\kappa_\gamma \leq 0.047 \\ \text{implying}: \quad -0.004 \leq \Delta\kappa_Z \leq 0.040\,. \end{aligned} \tag{5.4}$$

5.3 Results in the Chiral Expansion

Next we apply our analysis framework to the operators in the chiral basis. For convenience we recall the applicable basis weighted by ξ relevant to the Higgs data:

$$\mathcal{P}_G, \quad \mathcal{P}_4, \quad \mathcal{P}_5, \quad \mathcal{P}_B, \quad \mathcal{P}_W, \quad \mathcal{P}_H, \quad \mathcal{P}_C \tag{5.5}$$

For the sake of simplification of the analysis we will categorize these operators into two sets of effectively six operators as a seven parameter fit is beyond the reach of this dissertation. We denote these sets as **Set A** and **Set B** which correspond to sets of the operator coefficients as defined in Eqs. (3.13) and (3.16). These sets are

$$\begin{aligned} &\textbf{Set A:} \quad a_G, \quad a_4, \quad a_5, \quad a_B, \quad a_W, \quad c_H, \quad 2a_C - c_C = 0, \\ &\textbf{Set B:} \quad a_G, \quad a_4, \quad a_5, \quad a_B, \quad a_W, \quad c_H = 2a_C - c_C. \end{aligned} \tag{5.6}$$

Additionally as mentioned in Chapter 3 we explore the sensitivity of the results to the sign of the h-fermion couplings by performing our analysis with both signs for the parameter $s_Y = \pm 1$.

Our choice of the relations between the operator coefficients relevant to $\mathcal{P}_H$ and $\mathcal{P}_C$ are not arbitrary. Recalling $\mathcal{P}_C$ induces universal shifts of the SM–like HVV couplings (See Tab. 3.1) and $\mathcal{P}_H$ induces shifts to all SM Higgs couplings we see that **Set A** corresponds to a scenario where we simultaneously shift the

SM HVV and Hff couplings while **Set B** corresponds to the Higgs–fermion coupling shifts being totally unrelated to the modification of the Higgs–vector couplings. The remaining operators are kept constant between the two sets, and correspond to Lorentz structures different from those of the SM.

Again employing our analysis framework of Chapter 4 we perform a chi–square test of the dependence of the six couplings for both sets and $s_Y = \pm 1$. Figure 5.8 displays the $\Delta\chi^2$ dependence of the sets in Eqs. (5.6) based on the collider (ATLAS, CMS, and Tevatron) data on Higgs couplings as compiled in Tabs. 4.1, 4.2, and 4.3. As with Fig. 5.1 for the linear case, we display the single parameter $\Delta\chi^2$ dependence while marginalizing over the unshown parameters.

We begin by noting that there is little difference between the two sets with the exception of a slight difference in the behavior of a_G, which we discuss in more detail below. The fit quality is approximately equally good for both sets with $|\chi^2_{\text{min,A}} - \chi^2_{\text{min,B}}| < 0.5$. We recall from Sec. 5.1 that $\chi^2_{SM} = 68.1$ which for the chiral basis corresponds to the 4% CL region for both sets.

Additionally the fit is equally good for both signs of s_Y, in fact $|\chi^2_{\text{min},+} - \chi^2_{\text{min},-}|$ is compatible with zero within numerical precision. However, for all couplings set to zero while keeping s_Y an open parameter there is a dramatic difference with $\chi^2_- - \chi^2_+ = 26$. This is a result of changing the sign of the interference between the W– and top–loop contributions to $h\gamma\gamma$ which is negative for the SM ($s_Y = +1$) and positive for $s_Y = -1$ which causes an increase $\text{BR}_-(h \to \gamma\gamma)/\text{BR}_{\text{SM}}(h \to \gamma\gamma) \sim 2.5$ which is strongly disfavored by the data. For the inclusion of the other operators (particularly $\mathcal{P}_B$ and $\mathcal{P}_W$ which give tree level contributions to $h\gamma\gamma$) we find both signs are equally favored.

As with the linear case of f_g we see two degenerate minima for a_G. Again these are due to the interference between the anomalous and SM contributions where the secondary minimum corresponds to the anomalous coupling accounting for twice that of the SM top–loop but with an opposite sign. Here we see a shifting of the two parameter spaces due to the sign $s_Y = \pm 1$ as this switches the sign of the top Yukawa and therefore reverses the location of the degenerate minimum. The slight shift in the minima for a_G between the two cases is a result of the behavior of c_H near the minima which shifts the contribution of the top–loop by a slightly different quantity in both analyses.

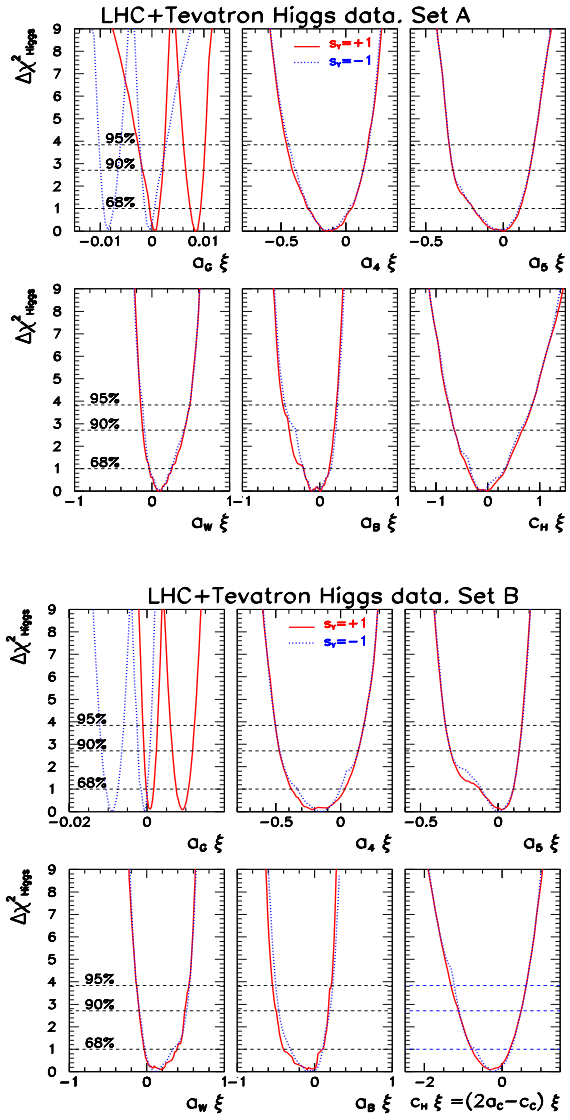

Figure 5.8: $\Delta\chi^2$ dependence on the coefficients of the seven bosonic operators in Eq. (5.6) from the analysis of all Higgs collider (ATLAS, CMS and Tevatron) data. In each panel, we have marginalized over the five undisplayed variables. The six upper (lower) panels corresponds to analysis with **Set A** (**B**). In each panel the red solid (blue dotted) line stands for the analysis with the discrete parameter $s_Y = +(-)1$.

We see that additionally for both cases a_W and a_B are almost mirror symmetric. As we saw in the linear case for f_{WW} and f_{BB}, this is due to the strong anticorrelation between these two coefficients as they are the dominant

contributions to the Higgs branching ratio to two photons which is proportional to $a_W + a_B$, see Tab. 3.1. Table 5.2 gives the 90% CL ranges for the six coefficients for both cases and signs of s_Y, except where the sign of s_Y or difference in set has an approximately negligible effect on the ranges.

Additionally we may constrain the coefficients c_2 and c_3 by applying the chi–square test of Eq. (4.16) as described in Sec. 4.2. We include these allowed ranges in Tab. 5.2 as well.

	Set A	Set B
$a_G\xi(\cdot 10^{-3})$	$s_Y = +1 : [-1.8, 2.1] \cup [6.5, 10]$ $s_Y = -1 : [-9.9, -6.5] \cup [-2.1, 1.8]$	$s_Y = +1 : [-0.78, 2.4] \cup [6.5, 12]$ $s_Y = -1 : [-12, -6.5] \cup [-2.3, 0.75]$
$a_4\xi$	$[-0.47, 0.14]$	
$a_5\xi$	$[-0.33, 0.17]$	
$a_W\xi$	$[-0.12, 0.51]$	
$a_B\xi$	$[-0.50, 0.21]$	
$c_H\xi$	$[-0.66, 0.66]$	$[-1.1, 0.49]$
$c_2\xi$	$[-0.12, 0.076]$	
$c_3\xi$	$[-0.064, 0.079]$	

Table 5.2: 90% CL allowed ranges of the coefficients of the operators contributing to Higgs data (a_G, a_4, a_5, a_W, a_B, and c_H) and TGV data (c_2 and c_3). For a_4, a_5, a_W, and a_B the range is almost the same for both sets and signs of s_Y.

5.4 Discriminating Signatures

In this section we quantify the present status for some of the signatures which we discussed in Sec. 3.4 which have potential to discriminate between the linear and chiral expansion.

5.4.1 (De)correlation Between HVV and TGV

As we discussed in Sec. 3.4.2 the relations between HVV and TGV differ between the two expansions and can be used to discriminate between them.

With the information on the allowed ranges of c_2, c_3, a_4, and a_5 obtained in the previous section we can consider the discriminating variables introduced in Eq. (3.29). We show in Fig. 5.9 the presently allowed ranges for $\Sigma_W \times \Sigma_B$ and $\Delta_W \times \Delta_B$. For simplicity we show the results for set A with $s_Y = +1$, however changes in set and/or s_Y have little impact on the figure. For the figure

on the left the sensor's departure from $(0,0)$ indicates possible NP without sensitivity to the choice of expansion, while departures from $(0,0)$ for the figure on the right indicate an underlying non-linear realization of EWSB. We see that within the present precision these variables neither signal a significant departure from the SM nor a preference for the chiral expansion.

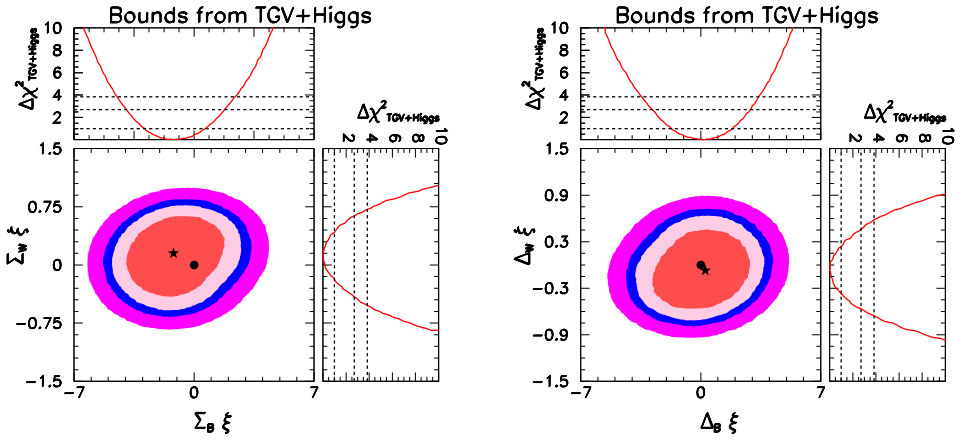

Figure 5.9: **Left**: A NP sensor insensitive to the type of expansion – constraints from TGV and Higgs data on the combinations $\Sigma_B = 4(2c_2 + a_4)$ and $\Sigma_W = 2(2c_3 - a_5)$, which converge to f_B and f_W in the linear $d = 6$ limit. The dot at $(0,0)$ signals the SM expectation. **Right**: A non–linear versus linear discriminator – constraints on the combinations $\Delta_B = 4(2c_2 - a_4)$ and $\Delta_W = 2(2c_3 + a_5)$, which would take zero values in the linear (order $d = 6$) limit (as well as in the SM), indicated by the dot at $(0,0)$. For both figures the lower left panel shows the two–dimensional allowed regions at 68%, 90%, 95%, and 99% CL after marginalization with respect to the other six parameters (a_G, a_W, a_B, c_H, Δ_B, and Δ_W) and (a_G, a_W, a_B, c_H, Σ_B, and Σ_W) respectively. The star corresponds to the best fit point of the analysis. The upper left and lower right panels give the corresponding one–dimensional projections over each of the two combinations.

If future data pointed to a departure from $(0,0)$ in the variables of the left panel it would indicate BSM physics irrespective of the linear or non–linear character of the underlying dynamics. Such a departure in the right panel would be consistent with a non–linear realization of EWSB instead.

5.4.2 ξ^2-weighted Couplings: LHC potential to study g_5^Z

As discussed in Sec. 3.4.1 one interesting property of the ξ^2–chiral Lagrangian is the presence of operator $\mathcal{P}_{14}(h)$ that generates a non-vanishing g_5^Z TGV, which is a C and P odd, but CP even operator (see Eq. (2.38)). Motivated by this fact we summarize here the study of the sensitivity to this coupling at the LHC which was presented in Ref. [76]

Presently, the best direct limits on this anomalous coupling come from the study of W^+W^- pairs and single W production at LEP II energies [112–114]. For example L3 limits imply [113] $-0.21 \leq g_5^Z \leq 0.2$ ($-0.12 \leq c_{14}\xi^2 \leq 0.11$) at 95% CL. Indirect (hence less robust) bounds can also be imposed from its contribution to Z physics at one-loop [115–117] which imply $-0.08 \leq g_5^Z \leq 0.04$ ($-0.04 \leq c_{14}\xi^2 \leq 0.02$) at 90% CL.

The LHC collaborations have presented some data analyses of anomalous TGV [107, 110, 111, 118, 119], but have not yet included the effects of g_5^Z. A preliminary study on the potential of LHC 7 to constrain this coupling was presented in Ref. [105] where it was shown that the LHC 7 with a very modest luminosity had the potential of probing g_5^Z at the level of the present indirect bounds. Reference [105] also discussed the use of some kinematic distributions to characterize the presence of a non–vanishing g_5^Z.

At the LHC, the anomalous coupling g_5^Z contributes to WW and WZ pair production, with the strongest limits originating from the latter channel [105]. Hence, our study is focused on the WZ production channel, where we consider only the leptonic decays of the gauge bosons for better background suppression:

$$pp \to \ell'^{\pm}\ell^+\ell^- E_T^{miss}\,, \tag{5.7}$$

where $\ell^{(\prime)} = e$ or μ. The main background for the g_5^Z analysis is the irreducible SM production of WZ pairs. There are further reducible backgrounds like W or Z production with jets, ZZ production followed by the leptonic decay of the Z's with one charged lepton escaping detection and $t\bar{t}$ pair production.

We simulated the signal and the SM irreducible background using an implementation of the anomalous operator g_5^Z in FeynRules [97] interfaced with MadGraph 5 [96] for event generation. In order to make the simulations more realistic, one can closely follow the TGV analysis performed by AT-

LAS [107]. Thus, the kinematic study of the WZ production starts with the usual detection and isolation cuts on the final state leptons. Muons and electrons are considered if their transverse momentum with respect to the collision axis z, $p_T \equiv \sqrt{p_x^2 + p_y^2}$, and pseudorapidity $\eta \equiv \frac{1}{2} \ln \frac{|\vec{p}|+p_z}{|\vec{p}|-p_z}$, satisfy $p_T^\ell > 15$ GeV , $|\eta^\mu| < 2.5$ and $|\eta^e| < 1.37$ or $1.52 < |\eta^e| < 2.47$.

To guarantee the isolation of muons (electrons), we required that the scalar sum of the p_T of the particles within $\Delta R \equiv \sqrt{\Delta\eta^2 + \Delta\phi^2} = 0.3$ of the muon (electron), excluding the muon (electron) track, is smaller than 15% (13%) of the charged lepton p_T. In the case where the final state contains both muons and electrons, a further isolation requirement has been imposed $\Delta R_{e\mu} > 0.1$

It was also required that at least two leptons with the same flavour and opposite charge are present in the event and that their invariant mass is compatible with the Z mass $M_{\ell^+\ell^-} \in [M_Z - 10, \quad M_Z + 10]$ GeV. A further constraint imposed is that a third lepton is present which passes the above detection requirements and whose transverse momentum satisfies $p_T^\ell > 20$ GeV . Moreover, with the purpose of suppressing most of the $Z +$ jets and other diboson production background, we required $E_T^{\rm miss} > 25$ GeV and $M_T^W > 20$ GeV, where $E_T^{\rm miss}$ is the missing transverse energy and the transverse mass is defined as $M_T^W = \sqrt{2 p_T^\ell E_T^{\rm miss} (1 - \cos(\Delta\phi))}$ with p_T^ℓ being the transverse momentum of the third lepton, and where $\Delta\phi$ is the azimuthal angle between the missing transverse momentum and the third lepton. Finally, it was required that at least one electron or one muon has a transverse momentum complying with $p_T^{e(\mu)} > 25 \;\; (20)$ GeV.

At the end the resulting Monte Carlo simulations have been tuned to the ATLAS ones [107], so as to incorporate more realistic detection efficiencies. We account for the different detection efficiencies by rescaling our simulation to the one done by ATLAS [107] for the study of $\Delta\kappa_Z$, g_1^Z, and λ_Z. Finally, the reducible backgrounds for the 7 TeV analysis were obtained from the simulations presented in the ATLAS search [107], and they were properly rescaled for the 8 TeV and 14 TeV runs.

After applying all the above cuts and efficiencies, the cross section for the

process (Eq. 5.7) in the presence of a non-vanishing g_5^Z can be written as[2]

$$\sigma \;=\; \sigma_{\rm bck} \;+\sigma_{\rm SM} \;+\; \sigma_{\rm int}\; g_5^Z \;+\; \sigma_{\rm ano}\; \left(g_5^Z\right)^2, \tag{5.8}$$

where $\sigma_{\rm SM}$ denotes the SM contribution to $W^{\pm}Z$ production, $\sigma_{\rm int}$ stands for the interference between this SM process and the anomalous g_5^Z contribution and $\sigma_{\rm ano}$ is the pure anomalous contribution. Furthermore, $\sigma_{\rm bck}$ corresponds to all background sources except for the SM EW $W^{\pm}Z$ production. We present in Tab. 5.3 the values of σ_{SM}, $\sigma_{\rm int}$ and $\sigma_{\rm ano}$ for center–of–mass energies of 7, 8 and 14 TeV, as well as the cross section for the reducible backgrounds.

COM Energy	$\sigma_{\rm bck}$ (fb)	$\sigma_{\rm SM}$ (fb)	$\sigma_{\rm int}$ (fb)	$\sigma_{\rm ano}$ (fb)
7 TeV	14.3	47.7	6.5	304
8 TeV	16.8	55.3	6.6	363
14 TeV	29.0	97.0	9.1	707

Table 5.3: Values of the cross section predictions for the process $pp \to \ell'^{\pm}\ell^{+}\ell^{-}E_T^{miss}$ after applying all the cuts described in the text. $\sigma_{\rm SM}$ is the SM contribution coming from EW $W^{\pm}Z$ production, $\sigma_{\rm int}$ is the interference between this SM process and the anomalous g_5^Z contribution, $\sigma_{\rm ano}$ is the pure anomalous contribution and $\sigma_{\rm bck}$ corresponds to all background sources except for the SM EW $W^{\pm}Z$ production.

As it was shown in Ref. [105] besides modifying the total number of events, g_5^Z modifies the kinematic distributions of the produced gauge bosons. We show in the left (right) panel of Fig. 5.10 the number of expected events with respect to the Z transverse momentum for the 7 (14) TeV run and an integrated luminosity of 4.64 (300) fb^{-1}. As illustrated by this figure, the existence of an anomalous g_5^Z contribution enhances the tail of the p_T^Z spectrum, signaling the existence of new physics.

Then, in order to enhance the sensitivity to this coupling we study the number of events with $p_T^Z > 90$ GeV. We perform a simple event counting analysis estimating the expected sensitivity by assuming that the number of

[2]We assumed in this study that all anomalous TGV vanish except for g_5^Z.

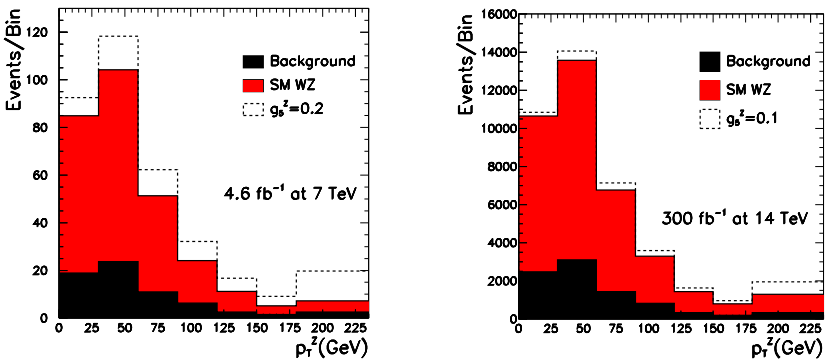

Figure 5.10: The left (right) panel displays the number of expected events as a function of the Z transverse momentum for a center–of–mass energy of 7 (14) TeV, assuming an integrated luminosity of 4.64 (300) fb^{-1}. The black histogram corresponds to the sum of all background sources except for the SM electroweak $pp \to W^{\pm}Z$ process, while the red histogram corresponds to the sum of all SM backgrounds, and the dashed distribution corresponds to the addition of the anomalous signal for $g_5^Z = 0.2$ ($g_5^Z = 0.1$). The last bin contains all the events with $p_T^Z > 180$ GeV.

observed events correspond to the SM prediction ($g_5^Z = 0$) and we look for the values of g_5^Z which lay at the 95% CL. We find that

$$\begin{aligned} &\text{with present LHC } 7+8 \text{ TeV Data} \quad -0.080 \leq g_5^Z \leq 0.072 \,, \\ &\text{adding expected LHC 14 TeV Data} \quad -0.033 \leq g_5^Z \leq 0.028 \,, \end{aligned} \tag{5.9}$$

where by expected LHC 14 TeV run we have considered an integrated luminosity of 300 fb^{-1}. In summary, we find that the LHC precision on g_5^Z will approach the percent level, clearly improving the present both direct and indirect bounds.

5.4.3 Anomalous Quartic Couplings

As shown in Sec. 3.4.3, in the chiral expansion several operators weighted by ξ or higher powers contribute to quartic gauge boson vertices without inducing any modification to TGVs. Therefore, their coefficients are much less constrained at present and one may still expect larger deviations on future studies of quartic vertices at LHC for large values of ξ.

Of the five operators giving rise to purely quartic gauge boson vertices, $\{\mathcal{P}_6(h), \mathcal{P}_{11}(h), \mathcal{P}_{23}(h), \mathcal{P}_{24}(h), \mathcal{P}_{26}(h)\}$, none modifies quartic vertices including photons while all generate the anomalous quartic vertex $ZZZZ$ that is not present in the SM. Moreover, all these operators but $\mathcal{P}_{26}(h)$ modify the ZZW^+W^- vertex, while only $\mathcal{P}_6(h)$ and $\mathcal{P}_{11}(h)$ also induce anomalous contributions to $W^+W^-W^+W^-$. Presently, the only bounds on the coefficients of these operators are indirect, from their one–loop contribution to the EWPD derived in Ref. [120].

At the LHC these anomalous quartic couplings can be directly tested in the production of three vector bosons or in vector boson fusion production of two gauge bosons [121]. At lower center–of–mass energies the best limits originate from the TGV processes, while the VBF channel dominates for the 14 TeV run [80, 121–124].

At the LHC with 14 TeV center−of−mass energy, the couplings c_6 and c_{11} can be constrained by combining their impact on the VBF channels,

$$pp \to jjW^+W^- \quad \text{and} \quad pp \to jj(W^+W^+ + W^-W^-)\,, \tag{5.10}$$

where j stands for a tagged jet and the final state Ws decay into electron or muon and a neutrino. It was shown in Ref. [80] that the attainable 99% CL limits on these couplings are

$$-12\times10^{-3} < c_6\,\xi < 10\times10^{-3}, \qquad \text{and} \qquad -7.7\times10^{-3} < c_{11}\,\xi^2 < 14\times10^{-3} \tag{5.11}$$

for an integrated luminosity of 100 fb^{-1}. Notice that the addition of the channel $pp \to jjZZ$ does not improve significantly the above limits [123].

5.5 Summary and Conclusions

In this chapter we have performed a fit to the relevant operator bases constructed in Chapters 2 and 3 using the framework introduced in Chapter 4. We have demonstrated that the present data is sufficient to support a robust data–driven analysis of the EFT extensions of the SM.

In Secs. 5.1 and 5.3 we discussed the parameter space of the operator coefficients for both the linear and chiral realizations, summarizing these main

results in 90% CL ranges with best fit points in Tabs. 5.1 and 5.2. Our analysis implies the SM is consistent with the data, laying well within the 1σ range of the data. In Sec. 5.2 we saw that the Higgs data constraints on TGCs is becoming competitive with the LEPII constraints. Noting that these constraints require the linear interpretation we also looked at discriminators between the linear and chiral realizations in Sec. 5.4. Here we explored the discriminating variables introduced in Eq. (3.29), as well as possible signals from the operator $\mathcal{P}_{14}$ which contributes to the g_5^Z TGC and operators which contribute to quartic gauge couplings. In the last two cases we also discussed projections for the Run 2 of the LHC, noting there is still potential for exciting NP in the gauge and Higgs sectors at the next run of the LHC. In the case of the linear basis, projections for Run 2 of the LHC and the proposed high luminosity LHC are reserved for Appendix B.

Chapter 6

Unitarity Considerations

In this chapter we consider constraints on the linear operator basis of Chapter 2 related to perturbative unitarity in electroweak gauge boson scattering. In Section 6.1 we will discuss the operators relevant to electroweak gauge boson scattering, in Section 6.2 we review the conditions of partial wave unitarity. We find all electroweak boson and Higgs scattering amplitudes which contribute to unitarity violation in Section 6.3, and finally in Section 6.4 we discuss the implications for each operator coefficient individually as well as in a six parameter search.

Previous works in the literature have studied similar unitarity bounds on some of the the dimension–six operators either considering only one non-vanishing coupling at a time, and/or they did not take into account coupled channels, or they worked in the framework of effective vertices [125–131]. Here we complete these previous analyses by considering the effects of coupled channels leading to the strongest constraints, including both elastic and inelastic channels. We also analyze the general six–dimensional parameter space of relevant anomalous couplings. We consider the contributions to order $1/\Lambda^2$ to apply systematically the effective field theory approach.

6.1 The Relevant Operator Basis

For the case of electroweak gauge boson scattering the relevant dimension–six operators in the linear (HISZ) basis are those in Eq. (2.2) with the exception of $\mathcal{O}_{GG}$ as it only involves gluons.

Again we will reduce the size of this basis by applying EWPD constraints. This allows us to remove $\mathcal{O}_{BW}$ and $\mathcal{O}_{\Phi,1}$, due to their contributions to the S and T parameters (see Eqs. (2.33) and (2.34)), respectively. Further as we will be discussing unitarity constraints we will be considering large center of mass energies (i.e. $\sqrt{s} \gg m_{W,Z,H}$), in this limit we find that the behavior of $\mathcal{O}_{\Phi,2}$ and $\mathcal{O}_{\Phi,4}$ is the same up to a sign. Therefore we will quantify their behavior by a single operator coefficient:

$$\frac{f_{\Phi 2,4}}{\Lambda^2} \equiv \frac{f_{\Phi,2} - f_{\Phi,4}}{\Lambda^2}. \tag{6.1}$$

One expects this behavior as the combination $\mathcal{O}_{\Phi,2} + \mathcal{O}_{\Phi,4}$ can be traded via the EOM (see Sec. 2.4 and Eq. (2.37)) by a combination of Yukawa-like operators which do not contribute to the $2 \to 2$ scattering processes we consider in this chapter.

Additionally we find $\mathcal{O}_{\Phi,3}$ modifies the Higgs self couplings and the relation between the Higgs mass, its vev, and its self coupling λ (for details see the discussions in Chapter 2 and Appendix A). These effects do not induce unitarity violation in the $2 \to 2$ scattering processes.

Then for this chapter we will consider the operator coefficients:

$$f_W, \quad f_B, \quad f_{WW}, \quad f_{BB}, \quad f_{WWW}, \quad \text{and} \quad f_{\Phi 2,4}. \tag{6.2}$$

6.2 Brief Review of Partial Wave Unitarity

We briefly review the requirements of partial wave unitarity. We begin by expanding an amplitude for the scattering of $(V_1,\ V_2)$ into $(V_3,\ V_4)$

$$V_{1\lambda_1} V_{2\lambda_2} \to V_{3\lambda_3} V_{4\lambda_4} \tag{6.3}$$

into its partial wave components as

$$\mathcal{M}(V_{1\lambda_1} V_{2\lambda_2} \to V_{3\lambda_3} V_{4\lambda_4}) =$$

$$16\pi \sum_J \left(J + \tfrac{1}{2}\right) \sqrt{1 + \delta^{V_{2\lambda_2}}_{V_{1\lambda_1}}} \sqrt{1 + \delta^{V_{4\lambda_4}}_{V_{3\lambda_3}}} d^J_{\lambda\mu}(\theta) e^{iM\phi} T^J(V_{1\lambda_1} V_{2\lambda_2} \to V_{3\lambda_3} V_{4\lambda_4}), \tag{6.4}$$

where λ_i is the helicity corresponding to the scattered state V_i, θ (ϕ) is the polar (azimuthal) scattering angle, and we have defined:

$$\lambda \equiv \lambda_1 - \lambda_2, \qquad \mu \equiv \lambda_3 - \lambda_4, \qquad \text{and} \qquad M \equiv \lambda_1 - \lambda_2 - \lambda_3 + \lambda_4 = \lambda - \mu. \tag{6.5}$$

d is the Wigner rotation matrix. In the case that one of the vector bosons is replaced by the Higgs we can still employ this expression by setting the corresponding λ to zero.

We will also consider the case of inelastic fermion scattering,

$$f_{1\sigma_1}\bar{f}_{2\sigma_2} \to V_{3\lambda_3}V_{4\lambda_4}\ . \tag{6.6}$$

here the decomposition takes the form,

$$\begin{aligned}\mathcal{M}(f_{1\sigma_1}\bar{f}_{2\sigma_2} \to V_{3\lambda_3}V_{4\lambda_4}) = \\ 16\pi \sum_J (J+\tfrac{1}{2})\delta_{\sigma_1,-\sigma_2} d^J_{\sigma_1-\sigma_2,\lambda_3-\lambda_4}(\theta) T^J(f_{1\sigma_1}\bar{f}_{2\sigma_2} \to V_{3\lambda_3}V_{4\lambda_4})\ ,\end{aligned} \tag{6.7}$$

where we have used our freedom to take $\phi = 0$. As these processes proceed via s-channel exchange of a vector $J = 1$ boson, in the limit of massless fermions the fermions must appear with opposite helicity states, made manifest in our decomposition by the $\delta_{\sigma_1,\sigma_2}$.

Next we consider the optical theorem where we will use $(ij \to kl)$ to denote $(V_{i\lambda_i}V_{j\lambda_j} \to V_{k\lambda_k}V_{l\lambda_l})$ with $ijkl$ denoting the various possible initial and final state particles,

$$\mathrm{Im}T^J(12 \to 34) = \sum_{12\to 1'2'} \frac{|\vec{p}_{1'2'}\,|}{\sqrt{s}} T^{J*}(12 \to 1'2') T^J(1'2' \to 34), \tag{6.8}$$

with

$$|\vec{p}_{ij}\,| = \frac{\sqrt{[s-(m_i+m_j)^2][s-(m_i-m_j)^2]}}{2\sqrt{s}}. \tag{6.9}$$

Taking $V_{3\lambda_3} = V_{1\lambda_1}$ and $V_{4\lambda_4} = V_{2\lambda_2}$ and separating out the part where the intermediate states are the same as the final we obtain:

$$\mathrm{Im}T^J(12 \to 12) = \frac{|\vec{p}_{12}|}{\sqrt{s}} \left|T^J(12 \to 12)\right|^2 + \sum_{1'2' \neq 12} \frac{|\vec{p}_{1'2'}|}{\sqrt{s}} \left|T^J(12 \to 1'2')\right|^2. \tag{6.10}$$

Then for only one intermediate channel we can conclude

$$\mathrm{Im}T^J(12 \to 12) = \frac{|\vec{p}_{12}|}{\sqrt{s}} |T^J(12 \to 12)|^2. \tag{6.11}$$

This implies a form of T^J,

$$T^J(12 \to 12) = \frac{\sqrt{s}}{|\vec{p}_{12}|} e^{i\delta} \sin\delta, \tag{6.12}$$

giving the condition for elastic scattering (with the limit representing $m_i \ll \sqrt{s}$):

$$|T^J(12 \to 12)| \leq \frac{\sqrt{s}}{|\vec{p}_{12}|} \to 2. \tag{6.13}$$

More stringent bounds can be obtained by diagonalizing T^J in the particle and helicity space and then applying the condition in Eq. (6.13) to each of the eigenvalues.

For unitarity constraints from fermion annihilation into gauge bosons we follow the procedure presented in Ref. [130] and obtain the unitarity bound on the inelastic production of gauge boson pairs in Eq. (6.6) by relating the corresponding amplitude to that of the elastic process

$$f_{1\sigma_1}\bar{f}_{2\sigma_2} \to f_{1\sigma_1}\bar{f}_{2\sigma_2} \ . \tag{6.14}$$

In this case the unitarity relation is

$$\begin{aligned} 2\mathrm{Im}[T^J(f_{1\sigma_1}\bar{f}_{2\sigma_2} \to f_{1\sigma_1}\bar{f}_{2\sigma_2})] \ &= \ \left|T^J(f_{1\sigma_1}\bar{f}_{2\sigma_2} \to f_{1\sigma_1}\bar{f}_{2\sigma_2})\right|^2 \\ &+ \sum_{V_{3\lambda_3}, V_{4\lambda_4}} \left|T^J(f_{1\sigma_1}\bar{f}_{2\sigma_2} \to V_{3\lambda_3}V_{4\lambda_4})\right|^2 \\ &+ \sum_{N} \left|T^J(f_{1\sigma_1}\bar{f}_{2\sigma_2} \to N)\right|^2 \ , \end{aligned} \tag{6.15}$$

where as before we take the limit $s \gg (M_{V_1} + M_{V_2})^2$. N represents any state into which $f_{1\sigma_1}\bar{f}_{2\sigma_2}$ can annihilate that does not consists of two gauge bosons. Denoting $f_{1\sigma_1}\bar{f}_{2\sigma_2}$ as 12 and $1'2'$ as all other final states (in particular gauge

boson pairs) and defining

$$T^J(12 \to 12) \equiv y + ix, \qquad d \equiv \sum_{1'2' \neq 12} \frac{|\vec{p}_{1'2'}|}{\sqrt{s}} \left|T^J(12 \to 1'2')\right|^2 , \tag{6.16}$$

we can rewrite Eq. (6.15) as

$$x = \frac{|\vec{p}_{12}|}{\sqrt{s}}(x^2 + y^2) + d. \tag{6.17}$$

Solving the quadratic equation, and requiring the terms under the radical be semi-positive definite (i.e. requiring x be real as required by Eq. (6.16)) gives the condition:

$$2 \sum_{1'2' \neq 12} \frac{|\vec{p}_{1'2'}|}{\sqrt{s}} \left|T^J(12 \to 1'2')\right|^2 \leq 1 \to \sum_{V_{3\lambda_3}, V_{4\lambda_4}} \left|T^J(f_{1\sigma_1}\bar{f}_{2\sigma_2} \to V_{3\lambda_3}V_{4\lambda_4})\right|^2 \leq 1 , \tag{6.18}$$

where again the limit comes from taking $\sqrt{s} \gg m_i$. We note this implies the strongest bound can be found by considering some optimized linear combination of states

$$|X\rangle = \sum_{f_1,\sigma_1} x_{f_2,\sigma_2} \, |f_{1\sigma_1}\bar{f}_{2\sigma_2}\rangle \, , \tag{6.19}$$

with the normalization condition $\sum_{f\sigma} |x_{f\sigma}|^2 = 1$, for which the amplitude $T^J(X \to V_{3\lambda_3}V_{4\lambda_4})$ is largest.

	$(\times \frac{f_{\Phi,2,4}}{\Lambda^2} \times s)$
$W^+W^+ \to W^+W^+$	-1
$W^+Z \to W^+Z$	$-\frac{1}{2}X$
$W^+H \to W^+H$	$-\frac{1}{2}X$
$W^+W^- \to W^+W^-$	$\frac{1}{2}Y$
$W^+W^- \to ZZ$	1
$W^+W^- \to HH$	-1
$ZZ \to HH$	-1
$ZH \to ZH$	$-\frac{1}{2}X$

Table 6.1: Unitarity violating (growing as s) terms of the scattering amplitudes $\mathcal{M}(V_{1\lambda_1}V_{2\lambda_2} \to V_{3\lambda_3}V_{4\lambda_4})$ for longitudinal gauge bosons generated by the operators $\mathcal{O}_{\Phi,2}$ and $\mathcal{O}_{\Phi,4}$ where $X = 1 - \cos\theta$ and $Y = 1 + \cos\theta$. The overall factor extracted from all amplitudes is given at the top of the table.

	$(\times e^2\frac{f_W}{\Lambda^2}\times s)$						
	0000	$00++$	$0+0-$	$0+-0$	$+00-$	$+0-0$	$++00$
$W^+W^+\to W^+W^+$	$-\frac{3}{4s_W^2}$	0	$\frac{1}{8s_W^2}X$	$-\frac{1}{8s_W^2}Y$	$-\frac{1}{8s_W^2}Y$	$\frac{1}{8s_W^2}X$	0
$W^+Z\to W^+Z$	$-\frac{3}{8s_W^2}X$	$-\frac{1}{8c_W}$	$\frac{c_W^2-s_W^2}{8s_W^2}X$	$-\frac{1}{16c_W}Y$	$-\frac{1}{16c_W}Y$	$\frac{1}{8c_W^2}X$	$-\frac{1}{8c_W}$
$W^+\gamma\to W^+\gamma$	–	–	$\frac{1}{4}X$	–	–	–	–
$W^+Z\to W^+\gamma$	–	$\frac{1}{8s_W}$	$\frac{(3c_W^2-s_W^2)}{16c_Ws_W}X$	–	$\frac{1}{16s_W}Y$	–	–
$W^+Z\to W^+H$	0	–	–	$-\frac{1}{16c_W}Y$	–	0	$\frac{1}{8c_W}$
$W^+\gamma\to W^+H$	–	–	–	$\frac{1}{16s_W}Y$	–	–	$-\frac{1}{8s_W}$
$W^+H\to W^+H$	$-\frac{3}{8s_W^2}X$	–	–	–	–	$\frac{1}{8s_W^2}X$	–
$W^+W^-\to W^+W^-$	$\frac{3}{8s_W^2}Y$	$-\frac{1}{4s_W^2}$	$\frac{1}{8s_W^2}X$	0	0	$\frac{1}{8s_W^2}X$	$-\frac{1}{4s_W^2}$
$W^+W^-\to ZZ$	$\frac{3}{4s_W^2}$	$\frac{s_W^2-c_W^2}{4s_W^2}$	$\frac{1}{16c_W}X$	$-\frac{1}{16c_W}Y$	$-\frac{1}{16c_W}Y$	$\frac{1}{16c_W}X$	$-\frac{1}{4s_W^2}$
$W^+W^-\to\gamma\gamma$	–	$-\frac{1}{2}$	–	–	–	–	–
$W^+W^-\to Z\gamma$	–	$\frac{1-4c_W^2}{8c_Ws_W}$	$-\frac{1}{16s_W}X$	–	$\frac{1}{16s_W}Y$	–	–
$W^+W^-\to ZH$	0	–	–	$-\frac{1}{16c_W}Y$	–	$-\frac{1}{16c_W}X$	0
$W^+W^-\to\gamma H$	–	0	–	$\frac{1}{16s_W}Y$	–	$\frac{1}{16s_W}X$	–
$W^+W^-\to HH$	$-\frac{3}{4s_W^2}$	–	–	–	–	–	$\frac{1}{4s_W^2}$
$ZZ\to ZZ$	0	$-\frac{1}{4s_W^2}$	$\frac{1}{8s_W^2}X$	$-\frac{1}{8s_W^2}Y$	$-\frac{1}{8s_W^2}Y$	$\frac{1}{8s_W^2}X$	$-\frac{1}{4s_W^2}$
$ZZ\to Z\gamma$	–	$-\frac{1}{8c_Ws_W}$	$\frac{1}{16c_Ws_W}X$	–	$-\frac{1}{16c_Ws_W}Y$	–	–
$ZZ\to HH$	$-\frac{3}{4s_W^2}$	–	–	–	–	–	$\frac{1}{4s_W^2}$
$Z\gamma\to ZZ$	–	–	$\frac{1}{16c_Ws_W}X$	$-\frac{1}{16c_Ws_W}Y$	–	–	$-\frac{1}{8s_Wc_W}$
$Z\gamma\to HH$	–	–	–	–	–	–	$\frac{1}{8s_Wc_W}$
$ZH\to ZH$	$-\frac{3}{8s_W^2}X$	–	–	–	–	$\frac{1}{8s_W^2}X$	–
$ZH\to\gamma H$	–	–	–	–	–	$\frac{1}{16c_Ws_W}X$	–

Table 6.2: Unitarity violating (growing as s) terms of the scattering amplitudes $\mathcal{M}(V_{1\lambda_1}V_{2\lambda_2}\to V_{3\lambda_3}V_{4\lambda_4})$ for gauge bosons with the helicities $\lambda_1\lambda_2\lambda_3\lambda_4$ listed on top of each column, generated by the operator $\mathcal{O}_W$. Notation as previous Table.

6.3 The Unitarity Violating Amplitudes

First we consider all two−to−two Higgs and electroweak gauge–boson scattering processes. We have calculated the amplitudes for all possible combinations of particles and helicites generated by the effective field theory to dimension–six discussed in Sec. 6.1. We keep terms only to linear order in the dimension–six operators as use of the dimension–six operators at quadratic and higher order requires the inclusion of dimension–eight and higher operators. That is we assume that the new physics occurs at a sufficiently high energy scale that it is sufficient to truncate the effective Lagrangian expansion at dimension–six.

We note that to linear order in the anomalous operator coefficients no amplitude diverges as s^2, this is a result of gauge invariance enforcing that the corresponding triple and quartic vertices satisfy the requirements for the cancellation for the s^2 terms to take place [132].

In total we find 26 processes (in particle space) which yield some helicity amplitude that grows as s for at least one of the dimension–six operators. The

	$(\times e^2 \frac{f_B}{\Lambda^2}) \times s$						
	0000	$00++$	$0+0-$	$0+-0$	$+00-$	$+0-0$	$++00$
$W^+W^+ \to W^+W^+$	$-\frac{3}{4c_W^2}$	0	0	0	0	0	0
$W^+Z \to W^+Z$	0	$-\frac{1}{8c_W}$	$\frac{s_W^2-c_W^2}{8c_W^2}X$	$-\frac{1}{16c_W}Y$	$-\frac{1}{16c_W}Y$	0	$-\frac{1}{8c_W}$
$W^+\gamma \to W^+\gamma$	–	–	$\frac{1}{4}X$	–	–	–	–
$W^+Z \to W^+\gamma$	–	$\frac{1}{8s_W}$	$\frac{c_W^2-3s_W^2}{16s_Wc_W}X$	–	$\frac{1}{16s_W}Y$	–	–
$W^+Z \to W^+H$	$-\frac{2+Y}{8c_W^2}$	–	–	$-\frac{1}{16c_W}Y$	–	0	$\frac{1}{8c_W}$
$W^+\gamma \to W^+H$	–	–	–	$\frac{1}{16s_W}Y$	–	–	$-\frac{1}{8s_W}$
$W^+W^- \to W^+W^-$	$\frac{3}{8c_W^2}Y$	0	0	0	0	0	0
$W^+W^- \to ZZ$	0	$\frac{c_W^2-s_W^2}{4c_W^2}$	$\frac{1}{16c_W}X$	$-\frac{1}{16c_W}Y$	$-\frac{1}{16c_W}Y$	$\frac{1}{16c_W}X$	0
$W^+W^- \to \gamma\gamma$	–	$-\frac{1}{2}$	–	–	–	–	–
$W^+W^- \to Z\gamma$	–	$\frac{3-4c_W^2}{8c_Ws_W}$	$-\frac{1}{16s_W}X$	–	$\frac{1}{16s_W}Y$	–	–
$W^+W^- \to ZH$	$\frac{1-Y}{4c_W^2}$	–	–	$-\frac{1}{16c_W}Y$	–	$-\frac{1}{16c_W}X$	0
$W^+W^- \to \gamma H$	–	0	–	$\frac{1}{16s_W}Y$	–	$\frac{1}{16s_W}X$	–
$ZZ \to ZZ$	0	$-\frac{1}{4c_W^2}$	$\frac{1}{8c_W^2}X$	$-\frac{1}{8c_W^2}Y$	$-\frac{1}{8c_W^2}Y$	$\frac{1}{8c_W^2}X$	$-\frac{1}{4c_W^2}$
$ZZ \to Z\gamma$	–	$\frac{1}{8c_Ws_W}$	$-\frac{1}{16c_Ws_W}X$	–	$\frac{1}{16c_Ws_W}Y$	–	–
$ZZ \to HH$	$-\frac{3}{4c_W^2}$	–	–	–	–	–	$\frac{1}{4c_W^2}$
$Z\gamma \to ZZ$	–	–	$-\frac{1}{16c_Ws_W}X$	$\frac{1}{16c_Ws_W}Y$	–	–	$\frac{1}{8s_Wc_W}$
$Z\gamma \to HH$	–	–	–	–	–	–	$-\frac{1}{8s_Wc_W}$
$ZH \to ZH$	$-\frac{3}{8c_W^2}X$	–	–	–	–	$\frac{1}{8c_W^2}X$	–
$ZH \to \gamma H$	–	–	–	–	–	$-\frac{1}{16c_Ws_W}X$	–

Table 6.3: Same as Tab. 6.2 for the operator $\mathcal{O}_B$.

remainder are constant or vanishing for $m_{W,Z,H} \ll \sqrt{s}$.

Table 6.1 contains the $f_{\Phi 2,4}$ divergent amplitudes. We note unitarity violation only occurs in the purely longitudinal modes for the operators $\mathcal{O}_{\Phi,2}$ and $\mathcal{O}_{\Phi,4}$. This behavior is expected as these operators do not generate higher derivative terms beyond those already present in the SM in the triple and quartic couplings. Table 6.2 (6.3) show the unitarity violating amplitudes for $\mathcal{O}_W$ ($\mathcal{O}_B$), the results for operators $\mathcal{O}_{WW}$ and $\mathcal{O}_{BB}$ are in Tab. 6.4 and those for $\mathcal{O}_{WWW}$ are in Tab. 6.5. Contrary to the case of $f_{\Phi 2,4}$ we see that these operators do introduce amplitudes which grow as s for helicity combinations beyond purely longitudinal. It is interesting to note all amplitudes which grow with s generated by $\mathcal{O}_{\Phi,2}$, $\mathcal{O}_{\Phi,4}$, $\mathcal{O}_W$, $\mathcal{O}_B$, $\mathcal{O}_{WW}$, and $\mathcal{O}_{BB}$ have only $J = 0$ or $J = 1$ partial-wave projections. $\mathcal{O}_{WWW}$ leads to violation of unitarity in helicity amplitudes with projections over $J \geq 2$. However, as bounds are weakened for increasing J, we compute our constraints using only the $J = 0$ and $J = 1$ partial waves.

We will also consider fermionic scattering into two vectors, $f\bar{f}' \to VV'$. Here only operators contributing to triple gauge vertices will contribute, as vertices involving the Higgs will be proportional to the fermion mass which

	$(\times e^2\frac{f_{WW}}{\Lambda^2}\times s)$						$(\times e^2\frac{f_{BB}}{\Lambda^2})\times s$					
	$00++$	$0+0-$	$0+-0$	$+00-$	$+0-0$	$++00$	$00++$	$0+0-$	$0+-0$	$+00-$	$+0-0$	$++00$
$W^+W^+\to W^+W^+$	0	$-\frac{1}{4s_W^2}X$	$\frac{1}{4s_W^2}Y$	$\frac{1}{4s_W^2}Y$	$-\frac{1}{4s_W^2}X$	0	0	0	0	0	0	0
$W^+Z\to W^+Z$	0	$-\frac{c_W^2}{4s_W^2}X$	0	0	$-\frac{1}{4s_W^2}X$	0	0	$-\frac{s_W^2}{4c_W^2}X$	0	0	0	0
$W^+\gamma\to W^+\gamma$	–	$-\frac{1}{4}X$	–	–	–	–	–	$-\frac{1}{4}X$	–	–	–	–
$W^+Z\to W^+\gamma$	0	$-\frac{c_W}{4s_W}X$	–	0	–	–	0	$\frac{s_W}{4c_W}X$	–	0	–	–
$W^+H\to W^+H$	–	–	–	–	$-\frac{1}{4s_W^2}X$	–	–	–	–	–	0	–
$W^+W^-\to W^+W^-$	$\frac{1}{2s_W^2}$	$-\frac{1}{4s_W^2}X$	0	0	$-\frac{1}{4s_W^2}X$	$\frac{1}{2s_W^2}$	0	0	0	0	0	0
$W^+W^-\to ZZ$	$\frac{c_W^2}{2s_W^2}$	0	0	0	0	$\frac{1}{2s_W^2}$	$\frac{s_W^2}{4c_W^2}$	0	0	0	0	0
$W^+W^-\to\gamma\gamma$	$\frac{1}{2}$	–	–	–	–	–	$\frac{1}{2}$	–	–	–	–	–
$W^+W^-\to Z\gamma$	$\frac{c_W}{2s_W}$	0	–	0	–	–	$-\frac{s_W}{2c_W}$	0	–	0	–	–
$W^+W^-\to HH$	–	–	–	–	–	$-\frac{1}{2s_W^2}$	–	–	–	–	–	0
$ZZ\to ZZ$	$\frac{c_W^2}{2s_W^2}$	$-\frac{c_W^2}{4s_W^2}X$	$\frac{c_W^2}{4s_W^2}Y$	$\frac{c_W^2}{4s_W^2}Y$	$-\frac{c_W^2}{4s_W^2}X$	$\frac{c_W^2}{2s_W^2}$	$\frac{s_W^2}{2c_W^2}$	$-\frac{s_W^2}{4c_W^2}X$	$\frac{s_W^2}{4c_W^2}Y$	$\frac{s_W^2}{4c_W^2}Y$	$-\frac{s_W^2}{4c_W^2}X$	$\frac{s_W^2}{2c_W^2}$
$ZZ\to\gamma\gamma$	$\frac{1}{2}$	–	–	–	–	–	$\frac{1}{2}$	–	–	–	–	–
$ZZ\to Z\gamma$	$\frac{c_W}{2s_W}$	$-\frac{c_W}{4s_W}X$	–	$\frac{c_W}{4s_W}Y$	–	–	$-\frac{s_W}{2c_W}$	$\frac{s_W}{4c_W}X$	–	$-\frac{s_W}{4c_W}Y$	–	–
$ZZ\to HH$	–	–	–	–	–	$-\frac{c_W^2}{2s_W^2}$	–	–	–	–	–	$-\frac{s_W^2}{2c_W^2}$
$Z\gamma\to ZZ$	–	$-\frac{c_W}{4s_W}X$	$\frac{c_W}{4s_W}Y$	–	–	$\frac{c_W}{2s_W}$	–	$\frac{s_W}{4c_W}X$	$-\frac{s_W}{4c_W}Y$	–	–	$-\frac{s_W}{2c_W}$
$Z\gamma\to Z\gamma$	–	$-\frac{1}{4}X$	–	–	–	–	–	$-\frac{1}{4}X$	–	–	–	–
$Z\gamma\to HH$	–	–	–	–	–	$-\frac{c_W}{2s_W}$	–	–	–	–	–	$\frac{s_W}{2c_W}$
$\gamma\gamma\to HH$	–	–	–	–	–	$-\frac{1}{2}$	–	–	–	–	–	$-\frac{1}{2}$
$ZH\to ZH$	–	–	–	–	$-\frac{c_W^2}{4s_W^2}X$	–	–	–	–	–	$-\frac{s_W^2}{4c_W^2}X$	–
$\gamma H\to\gamma H$	–	–	–	–	$-\frac{1}{4}X$	–	–	–	–	–	$-\frac{1}{4}X$	–
$ZH\to\gamma H$	–	–	–	–	$-\frac{c_W}{4s_W}X$	–	–	–	–	–	$\frac{s_W}{4c_W}X$	–

Table 6.4: Same as Tab. 6.2 for the operators $\mathcal{O}_{WW}$ and $\mathcal{O}_{BB}$.

	$(\times 2e^4\frac{f_{WWW}}{\Lambda^2}\times s)$							
	$00++$	$0+0-$	$0+-0$	$+00-$	$+0-0$	$++00$	$+++-$ $+--\,-$ $+-+\,+$ $++-+$	$++--$
$W^+W^+\to W^+W^+$	0	$-\frac{3(2+Y)}{32s_W^4}$	$\frac{3(2+X)}{32s_W^4}$	$\frac{3(2+X)}{32s_W^4}$	$-\frac{3(2+Y)}{32s_W^4}$	0	$-\frac{3}{4s_W^4}$	$\frac{3}{2s_W^4}$
$W^+Z\to W^+Z$	$\frac{3(Y-X)c_W}{32s_W^4}$	0	$\frac{3(X+2)c_W}{32s_W^4}$	$\frac{3(X+2)c_W}{32s_W^4}$	0	$\frac{3(Y-X)c_W}{32s_W^4}$	$-\frac{3c_W^2}{8s_W^4}X$	$\frac{3c_W^2}{4s_W^4}X$
$W^+\gamma\to W^+\gamma$	–	0	–	–	–	–	$-\frac{3}{8s_W^2}X$	$\frac{3}{4s_W^2}X$
$W^+Z\to W^+\gamma$	$-\frac{3(Y-X)}{32s_W^3}$	0	–	$\frac{3(X+2)}{32s_W^3}$	–	–	$-\frac{3c_W}{8s_W^3}X$	$\frac{3c_W}{4s_W^3}X$
$W^+Z\to W^+H$	–	–	$\frac{3(X+2)c_W}{32s_W^4}$	–	$\frac{3(2+Y)}{32s_W^4}$	$-\frac{3(Y-X)c_W}{32s_W^4}$	–	–
$W^+\gamma\to W^+H$	–	–	$\frac{3(X+2)}{32s_W^3}$	–	–	$-\frac{3(Y-X)}{32s_W^3}$	–	–
$W^+W^-\to W^+W^-$	$\frac{3(Y-X)}{32s_W^4}$	$\frac{3(2+Y)}{32s_W^4}$	0	0	$\frac{3(2+Y)}{32s_W^4}$	$\frac{3(Y-X)}{32s_W^4}$	$\frac{3}{8s_W^4}Y$	$-\frac{3}{4s_W^4}Y$
$W^+W^-\to ZZ$	0	$\frac{3(2+Y)c_W}{32s_W^4}$	$-\frac{3(X+2)c_W}{32s_W^4}$	$-\frac{3(X+2)c_W}{32s_W^4}$	$\frac{3(2+Y)c_W}{32s_W^4}$	0	$\frac{3c_W^2}{4s_W^4}$	$-\frac{3c_W^2}{2s_W^4}$
$W^+W^-\to\gamma\gamma$	0	–	–	–	–	–	$\frac{3}{4s_W^2}$	$-\frac{3}{2s_W^2}$
$W^+W^-\to Z\gamma$	0	$\frac{3(2+Y)}{32s_W^3}$	–	$-\frac{3(2+X)}{32s_W^3}$	–	–	$\frac{3c_W}{4s_W^3}$	$-\frac{3c_W}{2s_W^3}$
$W^+W^-\to ZH$	–	–	$-\frac{3(2+X)c_W}{32s_W^4}$	–	$-\frac{3(2+Y)c_W}{32s_W^4}$	$\frac{3(Y-X)}{32s_W^4}$	–	–
$W^+W^-\to\gamma H$	–	–	$-\frac{3(X+2)}{32s_W^3}$	–	$-\frac{3(2+Y)}{32s_W^3}$	–	–	–

Table 6.5: Same as Tab. 6.2 for the operator $\mathcal{O}_{WWW}$.

is taken to be small relative to $\sqrt{s}$. Therefore we need only consider the operators f_W, f_B, and f_{WWW}. The relevant unitarity violating amplitudes for these inelastic processes are compiled in Tab. 6.6. Notice the effects of the operator $\mathcal{O}_{WWW}$ occur for different helicity amplitudes than for $\mathcal{O}_W$ and $\mathcal{O}_B$ as a result of the different Lorentz structure of the operator.

Process	$\sigma_1, \sigma_2, \lambda_3, \lambda_4$	Amplitude
$e^+e^- \to W^-W^+$	$-+00$	$-\frac{ig^2 s\sin\theta}{8}\frac{c_W^2 f_W + s_W^2 f_B}{c_W^2\Lambda^2}$
	$+-00$	$-\frac{ig^2 s\sin\theta}{4}\frac{s_W^2 f_B}{c_W^2\Lambda^2}$
	$-+--$	$-\frac{3ig^4 s\sin\theta}{8}\frac{f_{WWW}}{\Lambda^2}$
	$-++-$	$-\frac{3ig^4 s\sin\theta}{8}\frac{f_{WWW}}{\Lambda^2}$
$\nu\bar{\nu} \to W^-W^+$:	$-+00$	$\frac{ig^2 s\sin\theta}{8}\frac{c_W^2 f_W - s_W^2 f_B}{c_W^2}$
	$+-00$	0
	$-+--$	$\frac{3ig^4 s\sin\theta}{8}\frac{f_{WWW}}{\Lambda^2}$
	$-++-$	$\frac{3ig^4 s\sin\theta}{8}\frac{f_{WWW}}{\Lambda^2}$
$u\bar{u} \to W^-W^+$	$-+00$	$\frac{ig^2 N_c s\sin\theta}{8}\frac{3c_W^2 f_W + s_W^2 f_B}{3c_W^2}$
	$+-00$	$\frac{ig^2 N_c s\sin\theta}{6}\frac{s_W^2}{c_W^2} f_B$
	$-+--$	$\frac{3ig^4 N_c s\sin\theta}{8}\frac{f_{WWW}}{\Lambda^2}$
	$-++-$	$\frac{3ig^4 N_c s\sin\theta}{8}\frac{f_{WWW}}{\Lambda^2}$
$d\bar{d} \to W^-W^+$	$-+00$	$-\frac{ig^2 N_c s\sin\theta}{8}\frac{3c_W^2 f_W - s_W^2 f_B}{3c_W^2}$
	$+-00$	$-\frac{ig^2 N_c s\sin\theta}{12}\frac{s_W^2 f_B}{c_W^2\Lambda^2}$
	$-+--$	$-\frac{3ig^4 N_c s\sin\theta}{8}\frac{f_{WWW}}{\Lambda^2}$
	$-++-$	$-\frac{3ig^4 N_c s\sin\theta}{8}\frac{f_{WWW}}{\Lambda^2}$
$e^+\bar{\nu} \to W^+Z$	$-+00$	$\frac{ig^2 s\sin\theta}{4\sqrt{2}}\frac{f_W}{\Lambda^2}$
	$+-00$	0
	$-+--$	$\frac{3ic_W g^4 s\sin\theta}{4\sqrt{2}}\frac{f_{WWW}}{\Lambda^2}$
	$-++-$	$\frac{3ic_W g^4 s\sin\theta}{4\sqrt{2}}\frac{f_{WWW}}{\Lambda^2}$
$e^+\bar{\nu} \to W^+A$:	$-+00$	0
	$+-00$	0
	$-+--$	$\frac{3is_W g^4 s\sin\theta}{4\sqrt{2}}\frac{f_{WWW}}{\Lambda^2}$
	$-++-$	$\frac{3is_W g^4 s\sin\theta}{4\sqrt{2}}\frac{f_{WWW}}{\Lambda^2}$

Table 6.6: Unitarity violating (growing as s) terms of the scattering amplitudes $\mathcal{M}(f_{1\sigma_1}\bar{f}_{2\sigma_2} \to V_{3\lambda_3}V_{4\lambda_4})$ for fermions and gauge bosons with the helicities $\sigma_1\sigma_2\lambda_3\lambda_4$ given in the second column.

6.4 Constraints from Perturbative Unitarity

With Tabs. 6.1, 6.2, 6.3, 6.4, and 6.5 in mind we proceed to build the T^0 and T^1 amplitude matrices in particle and parameter space. These matrices are formed of the s–divergent amplitudes corresponding to all combinations of gauge and Higgs boson pairs for each total charge ($Q = 2, 1, 0$) and partial

wave J as follows:

(Q,J)	States					Total
$(2,0)$	$W^+_\pm W^+_\pm$	$W^+_0 W^+_0$				3
$(2,1)$	$W^+_\pm W^+_\pm$	$W^+_\pm W^+_0$	$W^+_0 W^+_\pm$			6
$(1,0)$	$W^+_\pm Z_\pm$	$W^+_0 Z_0$	$W^+_\pm \gamma_\pm$	$W^+_0 H$		6
$(1,1)$	$W^+_0 Z_0$	$W^+_\pm Z_0$	$W^+_0 Z_\pm$	$W^+_\pm Z_\pm$		
	$W^+_0 \gamma_\pm$	$W^+_\pm \gamma_\pm$	$W^+_0 H$	$W^+_\pm H$		14
$(0,0)$	$W^+_\pm W^-_\pm$	$W^+_0 W^-_0$	$Z_\pm Z_\pm$	$Z_0 Z_0$		
	$Z_\pm \gamma_\pm$	$\gamma_\pm \gamma_\pm$	$Z_0 H$	HH		12
$(0,1)$	$W^+_0 W^-_0$	$W^+_\pm W^-_0$	$W^+_0 W^-_\pm$	$W^+_\pm W^-_\pm$	$Z_\pm Z_0$	
	$Z_0 Z_\pm$	$Z_0 \gamma_\pm$	$Z_0 H$	$Z_\pm H$	$\gamma_\pm H$	18

(6.20)

Where the upper index indicates charge, lower indices indicate helicity, and we have taken advantage of the relation:

$$T^J(V_{1\lambda_1}V_{2\lambda_2} \to V_{3\lambda_3}V_{4\lambda_4}) = (-1)^{\lambda_1-\lambda_2-\lambda_3+\lambda_4} T^J(V_{1-\lambda_1}V_{2-\lambda_2} \to V_{3-\lambda_3}V_{4-\lambda_4}) \tag{6.21}$$

In the right–most column of Eq. (6.20) we give the dimensionality of the corresponding T^J matrix. For example, for $Q = 2$, T^0 in the basis $(W^+_+W^+_+, W^+_0W^+_0, W^+_-W^+_-)$ we have the 3×3 matrix[1]

$$\frac{s}{8\pi}\begin{pmatrix} 0 & 0 & \frac{3}{s^2_{\rm W}}e^4 f_{WWW} \\ 0 & -\frac{3}{8c^2_{\rm W}}e^2 f_B - \frac{3}{8s^2_{\rm W}}e^2 f_W - \frac{1}{2}f_{\Phi,2} & 0 \\ \frac{3}{s^2_{\rm W}}e^4 f_{WWW} & 0 & 0 \end{pmatrix}. \tag{6.22}$$

To obtain the most stringent bounds on the operator coefficients, f_n/Λ^2 we diagonalize the six T^J matrices and impose the constraint from Eq. (6.13). Considering only one operator different from zero at a time we find the strongest

[1]We note in Eq. (6.4) we have included explicitly the symmetry factors $\sqrt{1+\delta^{V_{2\lambda_2}}_{V_{1\lambda_1}}}$ and $\sqrt{1+\delta^{V_{4\lambda_4}}_{V_{3\lambda_3}}}$. Therefore we need not include these explicitly in our matrix. Other conventions include this in the definition of the two equal gauge boson states.

constraints arise from the following eigenvalues:

$$\begin{aligned}
\left|\frac{3}{16\pi}\frac{f_{\Phi 2,4}}{\Lambda^2}s\right| &\leq 2 \quad\Rightarrow\quad \left|\frac{f_{\Phi 2,4}}{\Lambda^2}s\right| \leq 33 \ , \\
\left|1.4\frac{g^2}{8\pi}\frac{f_W}{\Lambda^2}s\right| &\leq 2 \quad\Rightarrow\quad \left|\frac{f_W}{\Lambda^2}s\right| \leq 87 \ , \\
\left|\frac{g^2 s_{\rm W}(\sqrt{9+7c_{\rm W}^2}+3s_{\rm W})}{128c_{\rm W}^2\pi}\frac{f_B}{\Lambda^2}s\right| &\leq 2 \quad\Rightarrow\quad \left|\frac{f_B}{\Lambda^2}s\right| \leq 617 \\
\left|\sqrt{\frac{3}{2}}\frac{g^2}{8\pi}\frac{f_{WW}}{\Lambda^2}s\right| &\leq 2 \quad\Rightarrow\quad \left|\frac{f_{WW}}{\Lambda^2}s\right| \leq 99 \ , \\
\left|.20\frac{g^2}{8\pi}\frac{f_{BB}}{\Lambda^2}s\right| &\leq 2 \quad\Rightarrow\quad \left|\frac{f_{BB}}{\Lambda^2}s\right| \leq 603 \ , \\
\left|(1+\sqrt{17-16c_{\rm W}^2 s_{\rm W}^2})\frac{3g^4}{32\pi}\frac{f_{WWW}}{\Lambda^2}s\right| &\leq 2 \quad\Rightarrow\quad \left|\frac{f_{WWW}}{\Lambda^2}s\right| \leq 82 \ .
\end{aligned} \tag{6.23}$$

Inclusion of the amplitudes for fermions scattering into gauge boson pairs requires the use of the constraint from Eq. (6.18). In summing over amplitudes we choose $|X\rangle$ such that we will have the largest values for the $Q=0$ and $Q=1$ cases. We find the strongest bounds come from the $Q=0$ (i.e. $VV=W^+W^-$) combination with the states:

$$|x1\rangle = \frac{1}{\sqrt{24}}\,|N_f\left(-e_-^-e_+^+ + \nu_{e-}\bar{\nu}_{e+} + N_c u_-\bar{u}_+ - N_c d_-\bar{d}_+\right)\rangle \ , \tag{6.24}$$

$$|x2\rangle = \frac{1}{\sqrt{21}}\,|N_f\left(-e_+^-e_-^+ + N_c u_+\bar{u}_- - N_c d_+\bar{d}_-\right)\rangle \ , \tag{6.25}$$

Where we have used N_f (N_c) to denote the number of flavors (colors). These two combinations of states give the bounds

$$\begin{aligned}
\frac{1}{24}\left[\left|6\frac{g^4}{8\pi}\frac{f_{WWW}}{\Lambda^2}s\right|^2 + \left|1.41\frac{g^2}{8\pi}\frac{f_W}{\Lambda^2}s\right|^2\right] \leq 1 \quad&\Rightarrow\quad \left|\frac{f_{WWW}}{\Lambda^2}s\right| \leq 122, \\
&\text{and} \quad \left|\frac{f_W}{\Lambda^2}s\right| \leq 211, \\
\frac{1}{21}\left|\sqrt{2}\frac{s_w^2}{c_w^2}\frac{g^2}{8\pi}\frac{f_B}{\Lambda^2}s\right|^2 = \left|0.053\frac{g^2}{8\pi}\frac{f_B}{\Lambda^2}s\right|^2 \leq 1 \quad&\Rightarrow\quad \left|\frac{f_B}{\Lambda^2}s\right| \leq 664,
\end{aligned} \tag{6.26}$$

respectively.

As we have no UV model to guide our choice of basis and parameters $f_i s/\Lambda^2$, we must consider the case of more than one parameter non–zero. Therefore we search for the largest allowed value of a given parameter while varying over others. We obtain general bounds for our basis of six operator coefficients from searching a six–dimensional grid and recording the largest range of the parameters which satisfy both the elastic and inelastic partial–wave unitarity constraints. This search yields the bounds:

$$\begin{aligned}
\left|\frac{f_{\Phi 2,4}}{\Lambda^2}s\right| &\leq 105 \ , \\
\left|\frac{f_W}{\Lambda^2}s\right| &\leq 205 \ , \\
\left|\frac{f_B}{\Lambda^2}s\right| &\leq 640 \ , \\
\left|\frac{f_{WW}}{\Lambda^2}s\right| &\leq 200 \ , \\
\left|\frac{f_{BB}}{\Lambda^2}s\right| &\leq 880 \ , \\
\left|\frac{f_{WWW}}{\Lambda^2}s\right| &\leq 82 \ .
\end{aligned} \tag{6.27}$$

We note that these constraints do not indicate the largest ranges which may be realized for each parameter simultaneously, rather the most conservative constraints on a given parameter allowing for all possible cancellations with the others in the scattering amplitudes.

Also the comparison of Eq. (6.27) with Eqs. (6.26) and (6.23) indicates that searching the six–dimensional space results in weaker constraints, but not substantially. Therefore even when allowing for all possible cancellations between the contribution of the relevant dimension–six operators, partial–wave unitarity still imposes constraints on their range of validity.

The bounds in Eq. (6.27) must be understood as providing the maximum center of mass energy ($\sqrt{s}$) for which unitarity holds for a given value of f_i/Λ^2. One may argue that for not−too−small values of f_i the bounds in Eq. (6.27) correspond to $s_{\rm max}$ approximately or larger than Λ^2 for which the quadratic contribution of dimension–six operators to the scattering amplitudes at order $f_i^2(s/\Lambda^2)^2$ can be sizeable and could substantially change the bounds. At such

an order, however, one must consider linear contributions from dimension–eight operators. Thus the results in Eq. (6.27) can be interpreted as the bounds that partial wave unitarity imposes on the effects of the dimension–six operators uniquely, irrespective of possible cancellations due to higher–order contributions. The interpretation of the perturbative unitarity bounds is that one expects the appearance of some new state or a strongly interacting phase at the bound. In this respect we may also interpret $\sqrt{s_{\max}}$ as a generous upper limit for the validity of the description provided by the lowest order of the EFT.

We can now compare these unitarity constraints in Eq. (6.27) with the bounds from the global analysis in Chapter 5 in Tab. 5.1. We map the 90% CL ranges of the six–dimensional space from the analysis in Chapter 5, Tab. 5.1, onto the unitarity constraints derived here to identify the lowest energy for which presently allowed values of the coefficients of operators affecting Higgs physics would lead to unitarity violation. For the operator $\mathcal{O}_{WWW}$, which is not included in the Higgs data analysis, we make use of the presently allowed range of ${\lambda_\gamma}^2$ from the PDG [57], $\lambda_\gamma = -0.022 \pm 0.019$. Altogether we obtain:

$$\begin{aligned}
-10 \leq \frac{f_{\Phi,2}}{\Lambda^2}(\text{TeV}^{-2}) \leq 8.5 \quad &\Rightarrow \quad \sqrt{s} \leq 3.2 \text{ TeV} , \\
-5.6 \leq \frac{f_W}{\Lambda^2}(\text{TeV}^{-2}) \leq 9.6 \quad &\Rightarrow \quad \sqrt{s} \leq 4.6 \text{ TeV} , \\
-29 \leq \frac{f_B}{\Lambda^2}(\text{TeV}^{-2}) \leq 8.9 \quad &\Rightarrow \quad \sqrt{s} \leq 4.7 \text{ TeV} , \\
-3.2 \leq \frac{f_{WW}}{\Lambda^2}(\text{TeV}^{-2}) \leq 8.2 \quad &\Rightarrow \quad \sqrt{s} \leq 4.9 \text{ TeV} , \\
-7.5 \leq \frac{f_{BB}}{\Lambda^2}(\text{TeV}^{-2}) \leq 5.3 \quad &\Rightarrow \quad \sqrt{s} \leq 11 \text{ TeV} , \\
-15 \leq \frac{f_{WWW}}{\Lambda^2}(\text{TeV}^{-2}) \leq 3.9 \quad &\Rightarrow \quad \sqrt{s} \leq 2.4 \text{ TeV} .
\end{aligned} \tag{6.28}$$

6.5 Summary

In this chapter we briefly put together the operator basis relevant to gauge boson scattering and reviewed the conditions of partial wave unitarity from both elastic and inelastic gauge boson scattering. We evaluate the amplitudes

[2]From Eq. (2.39) we recall $\lambda_\gamma = \lambda_Z = \frac{3g^2 M_W^2}{2\Lambda^2} f_{WWW}$.

which violate perturbative unitarity, allowing us to finally constrain the operators in the relevant basis of Eq. (6.2). We considered the constraints for individual operators in the case of elastic and inelastic fermion scattering and also combined them in a six–parameter search, noting that the constraints were not affected to a large degree by such a search.

Finally we included the results from the discussion of the linear basis in Sec. 5.1 allowing us to put lower bounds on the energies at which perturbative unitarity may be violated. In particular in Eq. (6.28) we have shown that for operators affecting Higgs couplings the present 90% CL constraints from Sec. 5.1 are such that perturbative unitarity is not violated for $\sqrt{s} \leq 3.2$ TeV. For the purely gauge–boson operator $\mathcal{O}_{WWW}$ our naive translation of the triple gauge boson constraints indicated that for the allowed 90% range perturbative unitarity can be violated for $f\bar{f}' \to VV'$ at $\sqrt{s} \geq 2.4$ TeV.

In the next chapter we summarize the discussions and results contained in this dissertation.

Chapter 7

Conclusions

In this dissertation we have used the exciting discovery of a Higgs–like particle at the Large Hadron Collider to motivate the use of effective field theories to quantify deviations from the predicted Standard Model behavior of the observed state. We began in Chapter 2 by introducing the Hagiwara, Ishihara, Szalapski, and Zeppenfeld basis of dimension–six operators for a CP–even Higgs requiring that baryon and lepton number be conserved. We noted that this was the relevant expansion under the assumption that the Higgs is a fundamental scalar doublet of the $SU(2)_L$ symmetry of the Standard Model. We proceeded to consider the Lorentz–structures implied by the new operators, many of which are not induced in the SM at tree level. From there we considered the correlations between the triple gauge vertices and Higgs–gauge interactions. We then reduced the size of our basis from the equations of motion and precision data taking care not to introduce blind directions.

Chapter 3 repeated the themes of Chapter 2, however this time we looked at the Higgs as a pseudo–Goldstone boson of some new global symmetry realized at a new high energy scale and for which electroweak symmetry breaking is assumed to be non–linearly realized in the low energy Lagrangian and hence a more appropriate expansion is that provided by chiral perturbation theory. We wrote the effective Lagrangian for such composite–like Higgs to order four derivatives. We organized the leading order operators in terms of the parameter $\xi = (v/f)^2$ where f is the characteristic scale of the Godstone boson while v is the scale set by the EW gauge boson mass. This parameter helped us to relate the chiral operators to those in the linear expansion, with ξ indicating

the lowest order at which each operators' effects would be induced in the linear expansion. From these relations we concluded that the correlations between the Higgs to gauge bosons and triple gauge boson couplings discussed for the linear expansion no longer existed for the chiral expansion, instead allowing for triple gauge vertices to be independently tuned from the Higgs–gauge vertices. This allowed for the formulation of discriminators between the two expansions. Together Chapters 2 and 3 motivated us to put together an analysis framework in Chapter 4 which would allow for quantifying the present status on the determination of the coefficients and correlations in these expansions to be drawn in Chapter 5.

Desiring data–driven discussions of the expansions we formed chi–square statistics from the three main sources of data. The first and most direct being the Higgs Collider data from the LHC and Tevatron. Here we formulated a method for incorporating the state of the art calculations with the anomalous corrections from the operator expansions of Chapters 2 and 3, accounting for correlations in theoretical uncertainties via the pulls method, and incorporating the weights of various production channels for the sometimes convoluted cuts made by the different experiments (in particular for the $H \to \gamma\gamma$ channel). We additionally put together a way to incorporate the LEP data on the triple gauge boson couplings into our chi–square structure, allowing us to consider the implications of triple gauge vertex measurements on the correlated structures between Higgs–gauge and triple gauge couplings in the linear expansion. Finally we formulated a similar system for the inclusion of the one–loop effects on electroweak precision data induced by the new operators. Thus, after completing Chapter 4 we were left with a framework to analyze the effective operator bases put together in the previous two chapters.

In Chapter 5 we put our framework to use, first by analyzing the free parameter space of the operator coefficients in the linear expansion. Our analysis implies that the Standard Model is consistent with the data, laying well within the 1σ uncertainties. Furthermore this quantification allowed us to consider first the implications of the triple gauge coupling data from LEP as constraints on the Higgs parameter space, and then to turn the argument around and constrain the triple gauge couplings using the results of the analysis of the Higgs data. We found that Higgs data driven constraints on triple gauge

boson couplings are becoming competitive with those from direct measurement of those couplings, and showed the potential for future combination of these two types of measurements.

Next we analyzed the parameter space of the chiral operator coefficients and the uncorrelated triple gauge couplings. This led to a discussion of discriminating between the two expansions, and we placed constraints on four variables, $\Sigma_{W,B}$ and $\Delta_{W,B}$ introduced in Chapter 3, which measure deviations from the Standard Model predictions and deviations from the behavior of the linear expansion respectively. All constraints at this point were found to be consistent with the Standard Model predictions, but Appendix B indicates that the next run of the LHC and the possible future high luminosity LHC both have the potential to vastly improve on these measurements. We then moved on to potential new physics signals from the chiral operator $\mathcal{P}_{14}$ which induced a new Lorentz-form in the triple gauge coupling differing from the Standard Model and from those induced by dimension–six operators in the linear expansion. Here we were able to place limits on c_{14}, or in the triple gauge vertex language g_5^Z, from the 7 and 8 TeV runs of the LHC, and projected the potential for study at the 14 TeV LHC. We finished our discussion with generic anomalous quartic gauge couplings (unrelated to triple gauge boson vertices) which appear to the lowest order in the chiral expansion unlike in the linear case, and quantify the potential limits on two such operators at the 14 TeV LHC where probing quartic gauge couplings directly will become possible.

In Chapter 6 we consider constraints on the linear operator basis arising from perturbative unitarity in electroweak gauge boson scattering from the conditions of partial wave unitarity for both the elastic and inelastic scattering processes involving gauge boson pairs. In order to do so we computed the divergent amplitudes for all the relevant processes in particle and helicity space. We used those to place limits on each operator individually, and by searching the six operator coefficient space to bound all operator coefficients simultaneously. Using these constraints we were able to project the bounds we had derived from the Higgs and triple gauge coupling data analyses onto the minimum energy at which perturbative unitarity may be violated, indicating the possible onset of new physics, which we found to be $\sqrt{s} \sim 2.4$ TeV.

In summary the LHC 7 and 8 TeV runs have served to establish the existence of a new particle which appears to be related to the electroweak symmetry breaking mechanism, opening the possibility of directly testing the symmetry breaking sector. From the analyses of the Higgs, triple gauge boson vertices, and precision data we have concluded that there are no hints so far for deviations with respect to the Standard Model in this sector. This fact added to the many experimental exclusion bounds on a large variety of new expected states in several beyond the Standard Model extensions set the current picture: after the first LHC runs the Standard Model with a minimal Higgs mechanism is still a valid picture of particle physics.

The quantification presented, however, also shows the present, sometimes poor, precision with which this conclusion stands. Large room for deviations is still allowed which will be within reach at the coming runs of LHC keeping open the possibility of new descoveries.

Appendix A

Anomalous Interactions in the Linear Expansion

In this Appendix we proceed to identify the coefficients of the different Lorentz structures generated by the dimension-six operators in the linear expansion for the remaining 3 and 4 point vertices relevant to our discussion in Chapter 6. Chapter 2 contains the effects of dimension-six effective operators which give rise to HVV and TGV interactions, see Eqs. (2.18) and (2.19), and Eqs. (2.20) and (2.21) respectively.

Quartic vertices involving Higgs and gauge bosons read:

$$\begin{aligned}
\mathcal{L}_{\text{eff}}^{HHV_1V_2} &= g^{(1)}_{HHWW} H^2 W^+_{\mu\nu} W^{-\mu\nu} + g^{(2)}_{HHWW} H(\partial_\nu H)(W^-_\mu W^{+\mu\nu} + \text{h.c.}) \\
&+ g^{(3)}_{HHWW} H^2 W^+_\mu W^{-\mu} + g^{(1)}_{HHZZ} H^2 Z_{\mu\nu} Z^{\mu\nu} \\
&+ g^{(2)}_{HHZZ} H Z_\nu (\partial_\mu H) Z^{\mu\nu} + g^{(3)}_{HHZZ} H^2 Z_\mu Z^\mu \\
&+ g^{(1)}_{HHZA} H(\partial_\mu H) Z_\nu A^{\mu\nu} + g^{(2)}_{HHZA} H^2 A_{\mu\nu} Z^{\mu\nu} \\
&+ g^{(1)}_{HHAA} H^2 A_{\mu\nu} A^{\mu\nu} \ ,
\end{aligned} \tag{A.1}$$

with

$$
\begin{aligned}
g^{(1)}_{HHWW} &= -\tfrac{g^2}{4\Lambda^2} f_{WW} \\
g^{(2)}_{HHWW} &= \tfrac{g^2}{4\Lambda^2} f_W \\
g^{(3)}_{HHWW} &= \tfrac{g^2}{4}\left[1+\tfrac{v^2}{2\Lambda^2}(5f_{\Phi,4}-f_{\Phi,1}-2f_{\Phi,2})\right] \\
&= M_W^2\sqrt{2}G_F\left[1+\tfrac{v^2}{2\Lambda^2}(5f_{\Phi,4}-f_{\Phi,1}-2f_{\Phi,2})\right] \\
g^{(1)}_{HHZZ} &= -\tfrac{g^2}{8c_{\rm W}^2\Lambda^2}(c_{\rm W}^4 f_{WW}+s_{\rm W}^4 f_{BB}+c_{\rm W}^2 s_{\rm W}^2 f_{BW}) \\
g^{(2)}_{HHZZ} &= -\tfrac{g^2}{4c_{\rm W}^2\Lambda^2}(c_{\rm W}^2 f_W+s_{\rm W}^2 f_B) \\
g^{(3)}_{HHZZ} &= \tfrac{g^2}{8c_{\rm W}^2}\left[1+\tfrac{v^2}{2\Lambda^2}(5f_{\Phi,1}+5f_{\Phi,4}-2f_{\Phi,2}-\tfrac{g^2g'^2}{(g^2+g'^2)}f_{BW})\right] \\
&= M_Z^2\sqrt{2}G_F\left[1+\tfrac{v^2}{2\Lambda^2}(4f_{\Phi,1}+5f_{\Phi,4}-2f_{\Phi,2})\right] \\
g^{(1)}_{HHZA} &= -\tfrac{g^2 s_{\rm W}}{4c_{\rm W}\Lambda^2}(f_W-f_B) \\
g^{(2)}_{HHZA} &= -\tfrac{g^2 s_{\rm W}}{4c_{\rm W}\Lambda^2}(c_{\rm W}^2 f_{WW}-s_{\rm W}^2 f_{BB}-\tfrac{1}{2}(c_{\rm W}^2-s_{\rm W}^2)f_{BW}) \\
g^{(1)}_{HHAA} &= -\tfrac{g^2 s_{\rm W}^2}{8\Lambda^2}(f_{WW}+f_{BB}-f_{BW}),
\end{aligned}
\tag{A.2}
$$

and

$$
\begin{aligned}
\mathcal{L}_{\rm eff}^{HV_1V_2V_3} &= g^{(1)}_{HZWW} H(W^-_\mu W^+_\nu - \text{h.c.})Z^{\mu\nu} + g^{(2)}_{HZWW} H Z_\mu (W^+_\nu W^{-\mu\nu} - \text{h.c.}) \\
&+ g^{(3)}_{HZWW}(\partial_\mu H) Z_\nu (W^{-\mu} W^{+\nu} - \text{h.c.}) \\
&+ g^{(1)}_{HAWW} H(W^-_\mu W^+_\nu - \text{h.c.})A_{\mu\nu} + g^{(2)}_{HAWW} H A_\nu (W^{+\nu}_\mu W^{-\mu} - \text{h.c.}) \\
&+ g^{(3)}_{HAWW}(\partial_\mu H) A_\nu (W^{-\mu} W^{+\nu} - \text{h.c.})\,,
\end{aligned}
\tag{A.3}
$$

with

$$
\begin{aligned}
g^{(1)}_{HZWW} &= \tfrac{ig^3 v}{8c_{\rm W}\Lambda^2}(c_{\rm W}^2 f_W - s_{\rm W}^2 f_B + 4c_{\rm W}^2 f_{WW} + 2s_{\rm W}^2 f_{BW}) \\
g^{(2)}_{HZWW} &= -\tfrac{ig^3 v}{4c_{\rm W}\Lambda^2}(f_W + 4c_{\rm W}^2 f_{WW}) \\
g^{(3)}_{HZWW} &= \tfrac{ig^3 v}{4c_{\rm W}\Lambda^2} s_{\rm W}^2 f_W \\
g^{(1)}_{HAWW} &= \tfrac{ig^3 v s_{\rm W}}{8\Lambda^2}(f_W + f_B + 4f_{WW} - 2f_{BW}) \\
g^{(2)}_{HAWW} &= -\tfrac{ig^3 s_{\rm W} v}{\Lambda^2} f_{WW} \\
g^{(3)}_{HAWW} &= -\tfrac{ig^3 v s_{\rm W}}{4\Lambda^2} f_W\,.
\end{aligned}
\tag{A.4}
$$

Quartic gauge boson vertices read:

$$\begin{aligned}
\mathcal{L}_{\text{eff}}^{WWV_1V_2} &= g^{(1)}_{WWWW} W^-_\mu W^+_\nu (W^{-\mu} W^{+\nu} - \text{h.c.}) \\
&+ g^{(2)}_{WWWW} W^+_{\mu\nu} W^{-\nu\rho} (W^{+\mu} W^-_\rho - W^+_\rho W^{-\mu}) \\
&+ g^{(1)}_{WWZZ} Z_\mu Z^\mu W^+_\nu W^-_\nu + g^{(2)}_{WWZZ} Z_\mu Z_\nu (W^+_\nu W^-_\mu + \text{h.c.}) \\
&+ g^{(3)}_{WWZZ} \left(W^+_{\mu\nu} Z_\rho{}^\mu (Z^\nu W^{-\rho} - Z^\rho W^{-\nu}) + \text{h.c.} \right) \\
&+ g^{(3)}_{WWAA} \left(W^+_{\mu\nu} A_\rho{}^\mu (A^\nu W^{-\rho} - A^\rho W^{-\nu}) + \text{h.c.} \right) \\
&+ g^{(1)}_{WWZA} W^-_\mu W^{+\mu} Z_\mu A^\mu + g^{(2)}_{WWZA} (W^-_\nu W^+_\mu + \text{h.c.}) A^\nu Z^\mu \\
&+ g^{(3)}_{WWZA} \left(W^+_{\mu\nu} Z_\rho{}^\mu (A^\nu W^{-\rho} - A^\rho W^{-\nu}) \right. \\
&\qquad \left. + W^+_{\mu\nu} A_\rho{}^\mu (Z^\nu W^{-\rho} - Z^\rho W^{-\nu}) + \text{h.c.} \right) , \qquad \text{(A.5)}
\end{aligned}$$

with

$$\begin{aligned}
g^{(1)}_{WWWW} &= \tfrac{e^2}{2s^2_{\text{W}}} + \tfrac{g^4 v^2}{8\Lambda^2} (f_W + 2\tfrac{s^2_{\text{W}}}{c_{2\text{W}}} f_{BW} - \tfrac{s^2_{2\text{W}}}{2c_{2\text{W}} e^2} f_{\Phi,1}) \\
g^{(2)}_{WWWW} &= \tfrac{-3g^4}{2\Lambda^2} f_{WWW} \\
g^{(1)}_{WWZZ} &= -e^2 \tfrac{c^2_{\text{W}}}{s^2_{\text{W}}} - \tfrac{g^4 v^2 \Lambda^2}{4c^2_{\text{W}}} (c^2_{\text{W}} f_W + \tfrac{2s^2_{2\text{W}}}{c_{2\text{W}}} f_{BW} - \tfrac{s^2_{2\text{W}} c^2_{\text{W}}}{2e^2 c_{2\text{W}}} f_{\Phi,1}) \\
g^{(2)}_{WWZZ} &= \tfrac{e^2 c^2_{\text{W}}}{2s^2_{\text{W}}} + \tfrac{g^4 v^2 \Lambda^2}{8c^2_{\text{W}}} (c^2_{\text{W}} f_W + \tfrac{s^2_{2\text{W}}}{2c_{2\text{W}}} f_{BW} - \tfrac{s^2_{2\text{W}} c^2_{\text{W}}}{2e^2 c_{2\text{W}}} f_{\Phi,1}) \\
g^{(3)}_{WWZZ} &= \tfrac{-3g^4 v^2 c^2_{\text{W}}}{2\Lambda^2} f_{WWW} \qquad \text{(A.6)} \\
g^{(3)}_{WWAA} &= -\tfrac{3g^4 v^2 s^2_{\text{W}}}{2\Lambda^2} f_{WWW} \\
g^{(1)}_{WWZA} &= -e^2 - \tfrac{g^4 v^2 s_{\text{W}}}{4c_{\text{W}} \Lambda^2} (f_W + 2\tfrac{s^2_{\text{W}}}{c_{2\text{W}}} f_{BW} - \tfrac{s^2_{2\text{W}}}{2c_{2\text{W}} e^2} f_{\Phi,1}) \\
g^{(2)}_{WWZA} &= \tfrac{e^2}{2} + \tfrac{g^4 v^2 s_{\text{W}}}{8c_{\text{W}} \Lambda^2} (f_W + 2\tfrac{s^2_{\text{W}}}{c_{2\text{W}}} f_{BW} - \tfrac{s^2_{2\text{W}}}{2c_{2\text{W}} e^2} f_{\Phi,1}) \\
g^{(3)}_{WWZA} &= \tfrac{-3g^4 s_{\text{W}} c_{\text{W}}}{2\Lambda^2} f_{WWW} \ .
\end{aligned}$$

Finally Higgs self interactions take the form:

$$\mathcal{L}_{\text{eff}}^{HHH} = g^{(1)}_{HHH} H^3 + g^{(2)}_{HHH} H (\partial_\mu H)(\partial^\mu H) \ , \qquad \text{(A.7)}$$

$$\qquad \text{(A.8)}$$

$$\mathcal{L}_{\text{eff}}^{HHHH} = g^{(1)}_{HHHH} H^4 + g^{(2)}_{HHHH} H^2 (\partial_\mu H)(\partial^\mu H) \ , \qquad \text{(A.9)}$$

where

$$
\begin{aligned}
g^{(1)}_{HHH} &= -\lambda v + \tfrac{v^3}{\Lambda^2}(\tfrac{3\lambda}{4} f_{\Phi,1} + \tfrac{5}{6} f_{\Phi,3} + \tfrac{3\lambda}{2} f_{\Phi,2} + \tfrac{3\lambda}{4} f_{\Phi,4}) \\
&= -\tfrac{M_H^2}{2}(\sqrt{2} G_F)^{1/2} \left[1 - \tfrac{v^2}{4\Lambda^2}(f_{\Phi,1} + 2 f_{\Phi,2} \tfrac{4}{3\lambda} f_{\Phi,3})\right] \\
g^{(2)}_{HHH} &= \tfrac{v}{\Lambda^2}(\tfrac{1}{2} f_{\Phi,1} + f_{\Phi,2} + \tfrac{1}{2} f_{\Phi,4}) \\
g^{(1)}_{HHHH} &= -\tfrac{\lambda}{4} + \tfrac{v^2}{4\Lambda^2}(\lambda f_{\Phi,1} + \tfrac{5}{2} f_{\Phi,3} + 2\lambda f_{\Phi,2} + \lambda f_{\Phi,4}) \\
&= -\tfrac{M_H^2}{8}(\sqrt{2} G_F) \left[1 + \tfrac{v^2}{2\Lambda^2}(f_{\Phi,1} + \tfrac{4}{\lambda} f_{\Phi,3} + f_{\Phi,2})\right] \\
g^{(2)}_{HHHH} &= \tfrac{1}{4\Lambda^2}(f_{\Phi,1} + 2 f_{\Phi,2} + f_{\Phi,4}).
\end{aligned}
\tag{A.10}
$$

Appendix B

Projections for LHC14

In this Appendix we summarize our contribution to the Energy Frontier working group on the Community Summer Study (Snowmass). In this study we assessed the impact of Higgs physics on the TGC determination at the LHC with a center−of−mass energy of 14 TeV and integrated luminosities of 300 fb^{-1} and 3000 fb^{-1}.

For the sake of simplicity we fit the ATLAS and CMS expected sensitivities [133, 134] for the Higgs signal strength using a reduced set of four independent operators $\{ \mathcal{O}_{GG} , \mathcal{O}_{WW} , \mathcal{O}_B , \mathcal{O}_W \}$ and setting the Yukawa couplings to their SM values. This simplified scenario captures most of the features of fits that we presented in Chapter 5 while keeping the analysis time efficient.

	68% CL allowed range		95% CL allowed range	
	300 fb^{-1}	3000 fb^{-1}	300 fb^{-1}	3000 fb^{-1}
f_g/Λ^2 (TeV^{-2})	$(-0.33, 0.31) \cup (22.40, 23.04)$	$(-0.17, 0.17) \cup (22.54, 22.88)$	$(-0.74, 0.86) \cup (21.85, 23.45)$	$(-0.33, 0.34) \cup (22.36, 23.04)$
f_{WW}/Λ^2 (TeV^{-2})	$(-0.043, 0.044)$	$(-0.023, 0.022)$	$(-0.093, 0.096) \cup (2.75, 2.82)$	$(-0.045, 0.044)$
f_W/Λ^2 (TeV^{-2})	$(-1.9, 2.5)$	$(-0.75, 0.83)$	$(-3.4, 9.1)$	$(-1.39, 1.82)$
f_B/Λ^2 (TeV^{-2})	$(-2.0, 2.5)$	$(-0.78, 0.85)$	$(-11.7, 7.5)$	$(-6.0, -4.1) \cup (-1.5, 1.8)$

Table B.1: 68% CL and 95% expected allowed ranges for 300 and 3000 fb^{-1} of integrated luminosity.

Figure B.1 displays $\Delta\chi^2$ as a function of the four fitting parameters for integrated luminosities of 300 fb^{-1} (upper row) and 3000 fb^{-1} (lower row). The corresponding 68% CL and 95% expected allowed ranges can be found

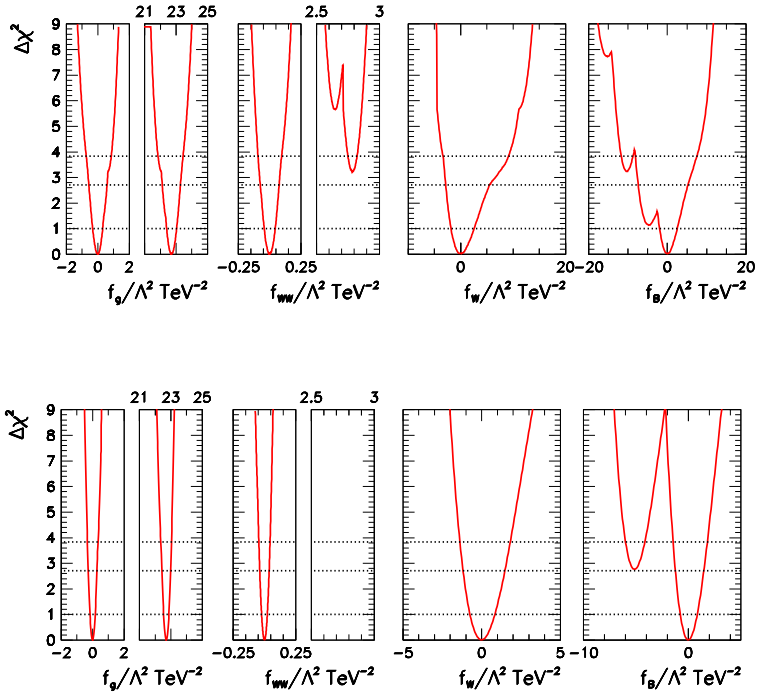

Figure B.1: $\Delta\chi^2$ as a function of f_g, f_{WW}, f_W, and f_B assuming $f_{\rm bot} = f_\tau = f_{\rm top} = 0$, after marginalizing over the three undisplayed parameters. The three horizontal dashed lines stand for the $\Delta\chi^2$ values associated with 68%, 90% and 95% from bottom to top respectively. The upper (lower) row was obtained for an integrated luminosity of 300 (3000) fb^{-1}.

in Tab. B.1. We observe in the upper and lower left panels that the $\Delta\chi^2$ as a function of f_g exhibits two degenerate minima due to the interference between SM and anomalous contributions to $gg \to H$ production, as was the case in Chapter 5. In the case of the χ^2 dependence on f_{WW} there is also an interference between anomalous and SM contributions to $H \to \gamma\gamma$, however, the degeneracy of the minima is lifted since the f_{WW} coupling contributes also to Higgs decays into WW^*, ZZ^* and γZ, as well as in Vh associated and vector boson fusion production mechanisms. Clearly larger statistics help to eliminate the degeneracy in f_{WW}. The interference between f_B and the SM contribution to $H \to \gamma Z$ is responsible for the two local minima with smaller $\Delta\chi^2$ while the additional minima in the upper right panel originate from the marginalization of f_{WW}. Comparing the upper and lower rows, we can see

that a larger integrated luminosity also helps to significantly reduce the errors in the determination of the anomalous couplings.

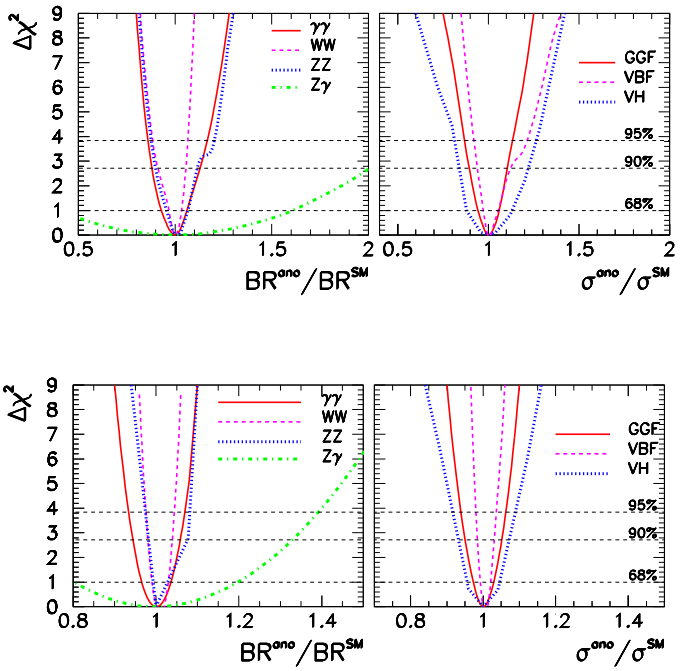

Figure B.2: $\Delta\chi^2$ as a function of branching ratios (left panels) and production cross sections (right panels) when we use only the expected ATLAS and CMS sensitivity on the Higgs signal strengths for integrated luminosities of 300 fb^{-1} (upper row) and 3000 fb^{-1} (lower row).

Figure B.2 depicts the χ^2 dependence on branching ratios and production cross sections for integrated luminosities of 300 fb^{-1} and 3000 fb^{-1}. As we can see these quantities can be determined with a precision better than 20% (5%) with 300 (3000) fb^{-1}. The only exception is the Higgs branching ratio into $Z\gamma$ that can be measured only within 20% with 3000 fb^{-1}. These results show the consistency of the extracted accuracies in the production cross sections and branching ratios in the dimension–six operator framework with those obtained by the experimental collaborations in their simulations [133, 134] assuming a shift of the SM couplings.

Next we focus our attention to the expected TGC bounds which can be derived from this analysis of the Higgs data. Eq. (2.20) allows us to translate

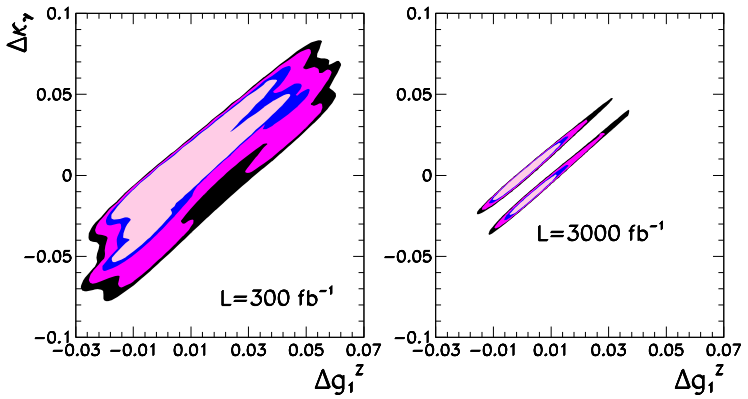

Figure B.3: We present the expected 90%, 95%, 99%, and 3σ allowed regions for the $\Delta\kappa_\gamma \otimes \Delta g_1^Z$ plane from the analysis of the Higgs data from LHC at 14 TeV with integrated luminosities of 300 fb^{-1} (left panel) and 3000 fb^{-1} (right panel).

the constraints on f_W and f_B coming from the Higgs measurements to bounds on $\Delta\kappa_\gamma$, $\Delta\kappa_Z$ and Δg_1^Z of which only two are independent. Fig. B.3 displays the results of this exercise where we plot the 90%, 95%, 99%, and 3σ CL allowed region in the plane $\Delta\kappa_\gamma \otimes \Delta g_1^Z$ after marginalizing over the other two parameters relevant to the Higgs analysis, i.e. f_g and f_{WW}. Notice that the two almost degenerate local minima in f_B lead to the appearance of two narrow disconnected regions due to the high precision achieved with 3000 fb^{-1}.

Clearly the analysis of the Higgs data alone can improve the present best bounds on TGCs which are still given by the LEP results. Further improvement will come from combining the Higgs results with those from direct studies of the TGCs which will be done once the results of the study of the capabilities of the LHC14 runs to constraints the TGCs from diboson production in this scenario are available.

Bibliography

[1] **ATLAS** Collaboration, *Observation of an excess of events in the search for the Standard Model Higgs boson in the gamma-gamma channel with the ATLAS detector*, .

[2] **ATLAS** Collaboration, *Measurements of the properties of the Higgs-like boson in the two photon decay channel with the ATLAS detector using 25* fb^{-1} *of proton-proton collision data*, .

[3] **CMS** Collaboration, V. Khachatryan *et al.*, *Observation of the diphoton decay of the Higgs boson and measurement of its properties*, *Eur.Phys.J.* **C74** (2014), no. 10 3076, [1407.0558].

[4] **CMS** Collaboration, S. Chatrchyan *et al.*, *Observation of a new boson at a mass of 125 GeV with the CMS experiment at the LHC*, *Phys.Lett.* **B716** (2012) 30–61, [1207.7235].

[5] **ATLAS** Collaboration, G. Aad *et al.*, *Observation of a new particle in the search for the Standard Model Higgs boson with the ATLAS detector at the LHC*, *Phys.Lett.* **B716** (2012) 1–29, [1207.7214].

[6] F. Englert and R. Brout, *Broken Symmetry and the Mass of Gauge Vector Mesons*, *Phys.Rev.Lett.* **13** (1964) 321–323.

[7] P. W. Higgs, *Broken Symmetries and the Masses of Gauge Bosons*, *Phys.Rev.Lett.* **13** (1964) 508–509.

[8] P. W. Higgs, *Broken symmetries, massless particles and gauge fields*, *Phys.Lett.* **12** (1964) 132–133.

[9] G. Guralnik, C. Hagen, and T. Kibble, *Global Conservation Laws and Massless Particles*, *Phys.Rev.Lett.* **13** (1964) 585–587.

[10] P. W. Higgs, *Spontaneous Symmetry Breakdown without Massless Bosons*, *Phys.Rev.* **145** (1966) 1156–1163.

[11] T. Kibble, *Symmetry breaking in nonAbelian gauge theories*, *Phys.Rev.* **155** (1967) 1554–1561.

[12] **CMS** Collaboration, V. Khachatryan *et al.*, *Constraints on the spin-parity and anomalous HVV couplings of the Higgs boson in proton collisions at 7 and 8 TeV*, 1411.3441.

[13] **ATLAS** Collaboration, G. Aad *et al.*, *Evidence for the spin-0 nature of the Higgs boson using ATLAS data*, *Phys.Lett.* **B726** (2013) 120–144, [1307.1432].

[14] **ATLAS** Collaboration, G. Aad *et al.*, *Measurement of Higgs boson production in the diphoton decay channel in pp collisions at center-of-mass energies of 7 and 8 TeV with the ATLAS detector*, *Phys.Rev.* **D90** (2014), no. 11 112015, [1408.7084].

[15] **CMS** Collaboration, S. Chatrchyan *et al.*, *Measurement of Higgs boson production and properties in the WW decay channel with leptonic final states*, *JHEP* **1401** (2014) 096, [1312.1129].

[16] **ATLAS** Collaboration, G. Aad *et al.*, *Observation and measurement of Higgs boson decays to WW^* with the ATLAS detector*, 1412.2641.

[17] **ATLAS** Collaboration, G. Aad *et al.*, *Measurements of Higgs boson production and couplings in the four-lepton channel in pp collisions at center-of-mass energies of 7 and 8 TeV with the ATLAS detector*, *Phys.Rev.* **D91** (2015), no. 1 012006, [1408.5191].

[18] **CMS** Collaboration, S. Chatrchyan *et al.*, *Measurement of the properties of a Higgs boson in the four-lepton final state*, *Phys.Rev.* **D89** (2014), no. 9 092007, [1312.5353].

[19] **CMS** Collaboration, S. Chatrchyan *et al.*, *Evidence for the 125 GeV Higgs boson decaying to a pair of τ leptons*, *JHEP* **1405** (2014) 104, [1401.5041].

[20] T. A. collaboration, *Evidence for Higgs boson Yukawa couplings in the $H \to \tau\tau$ decay mode with the ATLAS detector*, .

[21] A. C. Longhitano, *Low-Energy Impact of a Heavy Higgs Boson Sector*, *Nucl.Phys.* **B188** (1981) 118.

[22] T. Appelquist and C. W. Bernard, *Strongly Interacting Higgs Bosons*, *Phys.Rev.* **D22** (1980) 200.

[23] D. B. Kaplan and H. Georgi, *SU(2) x U(1) Breaking by Vacuum Misalignment*, *Phys.Lett.* **B136** (1984) 183.

[24] D. B. Kaplan, H. Georgi, and S. Dimopoulos, *Composite Higgs Scalars*, *Phys.Lett.* **B136** (1984) 187.

[25] T. Banks, *CONSTRAINTS ON SU(2) x U(1) BREAKING BY VACUUM MISALIGNMENT*, *Nucl.Phys.* **B243** (1984) 125.

[26] H. Georgi, D. B. Kaplan, and P. Galison, *Calculation of the Composite Higgs Mass*, *Phys.Lett.* **B143** (1984) 152.

[27] H. Georgi and D. B. Kaplan, *Composite Higgs and Custodial SU(2)*, *Phys.Lett.* **B145** (1984) 216.

[28] M. J. Dugan, H. Georgi, and D. B. Kaplan, *Anatomy of a Composite Higgs Model*, *Nucl.Phys.* **B254** (1985) 299.

[29] K. Agashe, R. Contino, and A. Pomarol, *The Minimal composite Higgs model*, *Nucl.Phys.* **B719** (2005) 165–187, [hep-ph/0412089].

[30] R. Contino, L. Da Rold, and A. Pomarol, *Light custodians in natural composite Higgs models*, *Phys.Rev.* **D75** (2007) 055014, [hep-ph/0612048].

[31] B. Gripaios, A. Pomarol, F. Riva, and J. Serra, *Beyond the Minimal Composite Higgs Model*, *JHEP* **0904** (2009) 070, [0902.1483].

[32] D. Marzocca, M. Serone, and J. Shu, *General Composite Higgs Models*, *JHEP* **1208** (2012) 013, [1205.0770].

[33] N. Arkani-Hamed, A. G. Cohen, and H. Georgi, *Electroweak symmetry breaking from dimensional deconstruction*, *Phys.Lett.* **B513** (2001) 232–240, [hep-ph/0105239].

[34] M. Schmaltz and D. Tucker-Smith, *Little Higgs review*, *Ann.Rev.Nucl.Part.Sci.* **55** (2005) 229–270, [hep-ph/0502182].

[35] R. Alonso, M. Gavela, L. Merlo, S. Rigolin, and J. Yepes, *The Effective Chiral Lagrangian for a Light Dynamical "Higgs Particle"*, *Phys.Lett.* **B722** (2013) 330–335, [1212.3305].

[36] K. Hagiwara, T. Hatsukano, S. Ishihara, and R. Szalapski, *Probing nonstandard bosonic interactions via W boson pair production at lepton colliders*, *Nucl.Phys.* **B496** (1997) 66–102, [hep-ph/9612268].

[37] K. Hagiwara, S. Ishihara, R. Szalapski, and D. Zeppenfeld, *Low-energy effects of new interactions in the electroweak boson sector*, *Phys.Rev.* **D48** (1993) 2182–2203.

[38] W. Buchmuller and D. Wyler, *Effective Lagrangian Analysis of New Interactions and Flavor Conservation*, *Nucl.Phys.* **B268** (1986) 621–653.

[39] B. Grzadkowski, M. Iskrzynski, M. Misiak, and J. Rosiek, *Dimension-Six Terms in the Standard Model Lagrangian*, *JHEP* **1010** (2010) 085, [1008.4884].

[40] I. Brivio, O. boli, M. Gavela, M. Gonzalez-Garcia, L. Merlo, *et al.*, *Higgs ultraviolet softening*, *JHEP* **1412** (2014) 004, [1405.5412].

[41] K. Hagiwara, R. Szalapski, and D. Zeppenfeld, *Anomalous Higgs boson production and decay*, *Phys.Lett.* **B318** (1993) 155–162, [hep-ph/9308347].

[42] M. Gonzalez-Garcia, *Anomalous Higgs couplings*, *Int.J.Mod.Phys.* **A14** (1999) 3121–3156, [hep-ph/9902321].

[43] F. de Campos, M. Gonzalez-Garcia, and S. Novaes, *Limits on anomalous coupling from Higgs boson production at the Tevatron collider*, *Phys.Rev.Lett.* **79** (1997) 5210–5213, [hep-ph/9707511].

[44] M. Gonzalez-Garcia, S. Lietti, and S. Novaes, *Search for nonstandard Higgs boson in diphoton events at p anti-p collisions*, *Phys.Rev.* **D57** (1998) 7045–7047, [hep-ph/9711446].

[45] O. J. Eboli, M. Gonzalez-Garcia, S. Lietti, and S. Novaes, *Bounds on Higgs and gauge boson interactions from LEP-2 data*, *Phys.Lett.* **B434** (1998) 340–346, [hep-ph/9802408].

[46] M. Gonzalez-Garcia, S. Lietti, and S. Novaes, *New Higgs couplings at e^+e^- and hadronic colliders*, *Phys.Rev.* **D59** (1999) 075008, [hep-ph/9811373].

[47] O. J. Eboli, M. Gonzalez-Garcia, S. . Lietti, and S. Novaes, *Probing intermediate mass Higgs interactions at the CERN Large Hadron Collider*, *Phys.Lett.* **B478** (2000) 199–207, [hep-ph/0001030].

[48] F. Bonnet, M. Gavela, T. Ota, and W. Winter, *Anomalous Higgs couplings at the LHC, and their theoretical interpretation*, *Phys.Rev.* **D85** (2012) 035016, [1105.5140].

[49] M. E. Peskin and T. Takeuchi, *A New constraint on a strongly interacting Higgs sector*, *Phys.Rev.Lett.* **65** (1990) 964–967.

[50] G. Altarelli, R. Barbieri, and F. Caravaglios, *Nonstandard analysis of electroweak precision data*, *Nucl.Phys.* **B405** (1993) 3–23.

[51] S. Alam, S. Dawson, and R. Szalapski, *Low-energy constraints on new physics revisited*, *Phys.Rev.* **D57** (1998) 1577–1590, [hep-ph/9706542].

[52] H. D. Politzer, *Power Corrections at Short Distances*, *Nucl.Phys.* **B172** (1980) 349.

[53] H. Georgi, *On-shell effective field theory*, *Nucl.Phys.* **B361** (1991) 339–350.

[54] C. Arzt, *Reduced effective Lagrangians*, *Phys.Lett.* **B342** (1995) 189–195, [hep-ph/9304230].

[55] H. Simma, *Equations of motion for effective Lagrangians and penguins in rare B decays*, *Z.Phys.* **C61** (1994) 67–82, [hep-ph/9307274].

[56] **ALEPH Collaboration, CDF Collaboration, D0 Collaboration, DELPHI Collaboration, L3 Collaboration, OPAL Collaboration, SLD Collaboration, LEP Electroweak Working Group, Tevatron Electroweak Working Group, SLD Electroweak and Heavy Flavour Groups** Collaboration, *Precision Electroweak Measurements and Constraints on the Standard Model*, 1012.2367.

[57] **Particle Data Group** Collaboration, K. Olive *et al.*, *Review of Particle Physics*, *Chin.Phys.* **C38** (2014) 090001.

[58] K. Hagiwara, S. Matsumoto, and R. Szalapski, *Constraints on new physics in the electroweak bosonic sector from current data and future experiments*, *Phys.Lett.* **B357** (1995) 411–418, [hep-ph/9505322].

[59] F. del Aguila and J. de Blas, *Electroweak constraints on new physics*, *Fortsch.Phys.* **59** (2011) 1036–1040, [1105.6103].

[60] F. del Aguila, J. de Blas, and M. Perez-Victoria, *Effects of new leptons in Electroweak Precision Data*, *Phys.Rev.* **D78** (2008) 013010, [0803.4008].

[61] A. De Rujula, M. Gavela, P. Hernandez, and E. Masso, *The Selfcouplings of vector bosons: Does LEP-1 obviate LEP-2?*, *Nucl.Phys.* **B384** (1992) 3–58.

[62] S. Kanemura, T. Ota, and K. Tsumura, *Lepton flavor violation in Higgs boson decays under the rare tau decay results*, *Phys.Rev.* **D73** (2006) 016006, [hep-ph/0505191].

[63] P. Paradisi, *Higgs-mediated tau ---> mu and tau ---> e transitions in II Higgs doublet model and supersymmetry*, *JHEP* **0602** (2006) 050, [hep-ph/0508054].

[64] E. Gabrielli and B. Mele, *Effective Yukawa couplings and flavor-changing Higgs boson decays at linear colliders*, *Phys.Rev.* **D83** (2011) 073009, [1102.3361].

[65] S. Davidson and G. J. Grenier, *Lepton flavour violating Higgs and tau to mu gamma*, *Phys.Rev.* **D81** (2010) 095016, [1001.0434].

[66] S. Davidson and P. Verdier, *LHC sensitivity to the decay $h \to \tau^{\pm} mu^{\mp}$*, *Phys.Rev.* **D86** (2012) 111701, [1211.1248].

[67] A. Goudelis, O. Lebedev, and J.-h. Park, *Higgs-induced lepton flavor violation*, *Phys.Lett.* **B707** (2012) 369–374, [1111.1715].

[68] G. Blankenburg, J. Ellis, and G. Isidori, *Flavour-Changing Decays of a 125 GeV Higgs-like Particle*, *Phys.Lett.* **B712** (2012) 386–390, [1202.5704].

[69] **D0, CDF** Collaboration, B. Tuchming, *Tevatron Higgs results*, *EPJ Web Conf.* **60** (2013) 02003, [1307.4873].

[70] **ATLAS** Collaboration, *Search for the Standard Model Higgs boson in H→ $\tau^+\tau^-$ decays in proton-proton collisions with the ATLAS detector*, .

[71] **CMS** Collaboration, V. Khachatryan *et al.*, *Search for lepton-flavour-violating decays of the Higgs boson*, 1502.07400.

[72] L. Susskind, *Dynamics of Spontaneous Symmetry Breaking in the Weinberg-Salam Theory*, *Phys.Rev.* **D20** (1979) 2619–2625.

[73] S. Dimopoulos and L. Susskind, *Mass Without Scalars*, *Nucl.Phys.* **B155** (1979) 237–252.

[74] E. Eichten and K. D. Lane, *Dynamical Breaking of Weak Interaction Symmetries*, *Phys.Lett.* **B90** (1980) 125–130.

[75] J. Callan, Curtis G., S. R. Coleman, J. Wess, and B. Zumino, *Structure of phenomenological Lagrangians. 2.*, *Phys.Rev.* **177** (1969) 2247–2250.

[76] I. Brivio, T. Corbett, O. Éboli, M. Gavela, J. Gonzalez-Fraile, *et al.*, *Disentangling a dynamical Higgs*, *JHEP* **1403** (2014) 024, [1311.1823].

[77] R. Alonso, I. Brivio, B. Gavela, L. Merlo, and S. Rigolin, *Sigma Decomposition*, *JHEP* **1412** (2014) 034, [1409.1589].

[78] R. Alonso, M. Gavela, L. Merlo, S. Rigolin, and J. Yepes, *Minimal Flavour Violation with Strong Higgs Dynamics*, *JHEP* **1206** (2012) 076, [1201.1511].

[79] R. Alonso, M. Gavela, L. Merlo, S. Rigolin, and J. Yepes, *Flavor with a light dynamical "Higgs particle"*, *Phys.Rev.* **D87** (2013), no. 5 055019, [1212.3307].

[80] O. Eboli, M. Gonzalez-Garcia, and J. Mizukoshi, *p p -> j j e+- mu+- nu nu and j j e+- mu-+ nu nu at O(alpha(em)**6) and O(alpha(em)**4 alpha(s)**2) for the study of the quartic electroweak gauge boson vertex at CERN LHC*, *Phys.Rev.* **D74** (2006) 073005, [hep-ph/0606118].

[81] **ATLAS** Collaboration, G. Aad *et al.*, *Determination of the off-shell Higgs boson signal strength in the high-mass ZZ and WW final states with the ATLAS detector*, 1503.01060.

[82] **CMS** Collaboration, C. Collaboration, *Constraints on the Higgs boson width from off-shell production and decay to ZZ to llll and llvv*, .

[83] T. A. collaboration, *Search for the bb decay of the Standard Model Higgs boson in associated W/ZH production with the ATLAS detector*, .

[84] **ATLAS** Collaboration, *Measurements of the properties of the Higgs-like boson in the four lepton decay channel with the ATLAS detector using 25 fb?1 of proton-proton collision data*, .

[85] **ATLAS** Collaboration, *Measurements of the properties of the Higgs-like boson in the $WW^{(*)} \to \ell\nu\ell\nu$ decay channel with the ATLAS detector using 25 fb^{-1} of proton-proton collision data*, .

[86] **ATLAS** Collaboration, *Search for the Standard Model Higgs boson in the $H \to Z\gamma$ decay mode with pp collisions at $\sqrt{s} = 7$ and 8 TeV*, .

[87] **CMS** Collaboration, S. Chatrchyan *et al.*, *Search for the standard model Higgs boson produced in association with a W or a Z boson and decaying to bottom quarks*, *Phys.Rev.* **D89** (2014), no. 1 012003, [1310.3687].

[88] **CMS** Collaboration, C. Collaboration, *Higgs to bb in the VBF channel*, .

[89] **CMS** Collaboration, *Update on the search for the standard model Higgs boson in pp collisions at the LHC decaying to W + W in the fully leptonic final state*, .

[90] **CMS** Collaboration, S. Chatrchyan *et al.*, *Search for a Higgs boson decaying into a Z and a photon in pp collisions at $\sqrt{s}$ = 7 and 8 TeV*, *Phys.Lett.* **B726** (2013) 587–609, [1307.5515].

[91] G. Fogli, E. Lisi, A. Marrone, D. Montanino, and A. Palazzo, *Getting the most from the statistical analysis of solar neutrino oscillations*, *Phys.Rev.* **D66** (2002) 053010, [hep-ph/0206162].

[92] M. Gonzalez-Garcia and M. Maltoni, *Phenomenology with Massive Neutrinos*, *Phys.Rept.* **460** (2008) 1–129, [0704.1800].

[93] **LHC Higgs Cross Section Working Group** Collaboration, S. Dittmaier *et al.*, *Handbook of LHC Higgs Cross Sections: 1. Inclusive Observables*, 1101.0593.

[94] F. Caola and K. Melnikov, *Constraining the Higgs boson width with ZZ production at the LHC*, *Phys.Rev.* **D88** (2013) 054024, [1307.4935].

[95] L. J. Dixon and Y. Li, *Bounding the Higgs Boson Width Through Interferometry*, *Phys.Rev.Lett.* **111** (2013) 111802, [1305.3854].

[96] J. Alwall, M. Herquet, F. Maltoni, O. Mattelaer, and T. Stelzer, *MadGraph 5 : Going Beyond*, *JHEP* **1106** (2011) 128, [1106.0522].

[97] N. D. Christensen and C. Duhr, *FeynRules - Feynman rules made easy*, *Comput.Phys.Commun.* **180** (2009) 1614–1641, [0806.4194].

[98] A. Pukhov, E. Boos, M. Dubinin, V. Edneral, V. Ilyin, *et al.*, *CompHEP: A Package for evaluation of Feynman diagrams and integration over multiparticle phase space*, hep-ph/9908288.

[99] **CompHEP Collaboration** Collaboration, E. Boos *et al.*, *CompHEP 4.4: Automatic computations from Lagrangians to events*, *Nucl.Instrum.Meth.* **A534** (2004) 250–259, [hep-ph/0403113].

[100] K. Arnold, J. Bellm, G. Bozzi, M. Brieg, F. Campanario, *et al.*, *VBFNLO: A Parton Level Monte Carlo for Processes with Electroweak Bosons – Manual for Version 2.5.0*, 1107.4038.

[101] T. L. collaborations and T. L. T. W. group.

[102] **D0 Collaboration** Collaboration, V. M. Abazov *et al.*, *Limits on anomalous trilinear gauge boson couplings from WW, WZ and $W\gamma$ production in $p\bar{p}$ collisions at $\sqrt{s} = 1.96$ TeV*, *Phys.Lett.* **B718** (2012) 451–459, [1208.5458].

[103] **CDF Collaboration** Collaboration, T. Aaltonen *et al.*, *Measurement of the WZ Cross Section and Triple Gauge Couplings in $p\bar{p}$ Collisions at $\sqrt{s} = 1.96$ TeV*, *Phys.Rev.* **D86** (2012) 031104, [1202.6629].

[104] **CDF Collaboration** Collaboration, T. Aaltonen *et al.*, *Measurement of the W^+W^- Production Cross Section and Search for Anomalous $WW\gamma$ and WWZ Couplings in $p\bar{p}$ Collisions at $\sqrt{s} = 1.96$ TeV*, *Phys.Rev.Lett.* **104** (2010) 201801, [0912.4500].

[105] O. Eboli, J. Gonzalez-Fraile, and M. Gonzalez-Garcia, *Scrutinizing the ZW+W- vertex at the Large Hadron Collider at 7 TeV*, *Phys.Lett.* **B692** (2010) 20–25, [1006.3562].

[106] **ATLAS** Collaboration, G. Aad *et al.*, *Measurement of W^+W^- production in pp collisions at $\sqrt{s}$=7 TeV with the ATLAS detector and limits on anomalous WWZ and $WW\gamma$ couplings*, *Phys.Rev.* **D87** (2013), no. 11 112001, [1210.2979].

[107] **ATLAS** Collaboration, G. Aad *et al.*, *Measurement of WZ production in proton-proton collisions at $\sqrt{s} = 7$ TeV with the ATLAS detector*, *Eur.Phys.J.* **C72** (2012) 2173, [1208.1390].

[108] **ATLAS** Collaboration, G. Aad *et al.*, *Measurements of $W\gamma$ and $Z\gamma$ production in pp collisions at $\sqrt{s}$=7 TeV with the ATLAS detector at the LHC*, *Phys.Rev.* **D87** (2013), no. 11 112003, [1302.1283].

[109] **CMS** Collaboration, S. Chatrchyan *et al.*, *Measurement of the W^+W^- Cross section in pp Collisions at $\sqrt{s} = 7$ TeV and Limits on Anomalous $WW\gamma$ and WWZ couplings*, *Eur.Phys.J.* **C73** (2013), no. 10 2610, [1306.1126].

[110] **CMS** Collaboration, S. Chatrchyan *et al.*, *Measurement of the $W\gamma$ and $Z\gamma$ inclusive cross sections in pp collisions at $\sqrt{s} = 7$ TeV and limits on anomalous triple gauge boson couplings*, *Phys.Rev.* **D89** (2014), no. 9 092005, [1308.6832].

[111] **CMS** Collaboration, S. Chatrchyan *et al.*, *Measurement of the sum of WW and WZ production with W+dijet events in pp collisions at $\sqrt{s} = 7$ TeV*, *Eur.Phys.J.* **C73** (2013), no. 2 2283, [1210.7544].

[112] **OPAL** Collaboration, G. Abbiendi *et al.*, *Measurement of charged current triple gauge boson couplings using W pairs at LEP*, *Eur.Phys.J.* **C33** (2004) 463–476, [hep-ex/0308067].

[113] **L3** Collaboration, P. Achard *et al.*, *Measurement of triple gauge boson couplings of the W boson at LEP*, *Phys.Lett.* **B586** (2004) 151–166, [hep-ex/0402036].

[114] **ALEPH** Collaboration, S. Schael *et al.*, *Improved measurement of the triple gauge-boson couplings gamma W W and Z W W in e+ e- collisions*, *Phys.Lett.* **B614** (2005) 7–26.

[115] O. J. Eboli, S. Lietti, M. Gonzalez-Garcia, and S. Novaes, *Epsilon(b) constraints on selfcouplings of vector bosons*, *Phys.Lett.* **B339** (1994) 119–126, [hep-ph/9406316].

[116] S. Dawson and G. Valencia, *Bounds on g5(Z) from precision LEP measurements*, *Phys.Lett.* **B333** (1994) 207–211, [hep-ph/9406324].

[117] O. J. Eboli, M. Gonzalez-Garcia, and S. Novaes, *Indirect constraints on the triple gauge boson couplings from $Z \to b\bar{b}$ partial width: An Update*, *Mod.Phys.Lett.* **A15** (2000) 1–8, [hep-ph/9811388].

[118] **ATLAS** Collaboration, G. Aad *et al.*, *Measurement of the WW cross section in $\sqrt{s} = 7$ TeV pp collisions with the ATLAS detector and limits on anomalous gauge couplings*, *Phys.Lett.* **B712** (2012) 289–308, [1203.6232].

[119] **ATLAS, CMS** Collaboration, V. Lombardo, *Diboson production cross section at LHC*, 1305.3773.

[120] A. Brunstein, O. J. Eboli, and M. Gonzalez-Garcia, *Constraints on quartic vector boson interactions from Z physics*, *Phys.Lett.* **B375** (1996) 233–239, [hep-ph/9602264].

[121] O. J. Eboli, M. Gonzalez-Garcia, S. Lietti, and S. Novaes, *Anomalous quartic gauge boson couplings at hadron colliders*, *Phys.Rev.* **D63** (2001) 075008, [hep-ph/0009262].

[122] O. Eboli, M. Gonzalez-Garcia, and S. Lietti, *Bosonic quartic couplings at CERN LHC*, *Phys.Rev.* **D69** (2004) 095005, [hep-ph/0310141].

[123] A. Belyaev, O. J. Eboli, M. Gonzalez-Garcia, J. Mizukoshi, S. Novaes, *et al.*, *Strongly interacting vector bosons at the CERN LHC: Quartic anomalous couplings*, *Phys.Rev.* **D59** (1999) 015022, [hep-ph/9805229].

[124] C. Degrande, J. Holzbauer, S. C. Hsu, A. Kotwal, S. Li, *et al.*, *Studies of Vector Boson Scattering And Triboson Production with DELPHES Parametrized Fast Simulation for Snowmass 2013*, 1309.7452.

[125] C. Bilchak, M. Kuroda, and D. Schildknecht, *On $W^{\pm}$, Z_0, γ Selfinteractions: High-energy Behavior and Tree Unitarity Bounds*, *Nucl.Phys.* **B299** (1988) 7.

[126] G. Gounaris, J. Layssac, and F. Renard, *Unitarity constraints for transverse gauge bosons at LEP and supercolliders*, *Phys.Lett.* **B332** (1994) 146–152, [hep-ph/9311370].

[127] G. Gounaris, J. Layssac, J. Paschalis, and F. Renard, *Unitarity constraints for new physics induced by dim-6 operators*, *Z.Phys.* **C66** (1995) 619–632, [hep-ph/9409260].

[128] G. Gounaris, F. Renard, and G. Tsirigoti, *Anomalous weak boson couplings: Suggestions from unitarity and dynamics*, *Phys.Lett.* **B350** (1995) 212–217, [hep-ph/9502376].

[129] C. Degrande, *BSM constraints from EW measurements*, *EPJ Web Conf.* **49** (2013) 14009, [1302.1112].

[130] U. Baur and D. Zeppenfeld, *Unitarity Constraints on the Electroweak Three Vector Boson Vertices*, *Phys.Lett.* **B201** (1988) 383.

[131] M. Dahiya, S. Dutta, and R. Islam, *Unitarizing VV Scattering in Light Higgs Scenarios*, 1311.4523.

[132] C. Csaki, C. Grojean, H. Murayama, L. Pilo, and J. Terning, *Gauge theories on an interval: Unitarity without a Higgs*, *Phys.Rev.* **D69** (2004) 055006, [hep-ph/0305237].

[133] **ATLAS** Collaboration, *Physics at a High-Luminosity LHC with ATLAS (Update)*, .

[134] **CMS Collaboration** Collaboration, *CMS at the High-Energy Frontier. Contribution to the Update of the European Strategy for Particle Physics*, Tech. Rep. CMS-NOTE-2012-006. CERN-CMS-NOTE-2012-006, CERN, Geneva, Oct, 2012.